Analysis of the Hull Structure of Sevan Arctic Mobile Offshore Drilling Unit subjected to accidental Ice Loads

Patrick Bratlie

Master Thesis, Spring 2015

for

Stud. Techn. Patrick Bratlie

Analysis of the Hull Structure of Sevan Arctic Mobile Offshore Drilling Unit subjected to accidental Ice Loads

Analyse av skrogkonstruksjonen på Sevan Arctic MODU utsatt for uforutsette islaster

A continuous development of structural design criteria for floating stationary units in Arctic areas is taking place. Within such a framework it is also important that adequate algorithms for analysis of non-linear structural behavior are available in order to quantify reserve strength properties in the case that damage to structural components might occur. The objective of the present project work is to address these issues in some detail.

The candidate shall address the following topics:

1. A summary is to be made of ice properties, ice mechanics and ice load formulations for floating hull structures.

2. Relevant loading conditions for the Sevan Arctic MODU unit are to be discussed with focus on local strength requirements (e.g. related to plate thickness and bending stiffeners). Corresponding methods for computation of linear and non-linear load-effects and the associated structural resistance as implemented in the computer program Abaqus are to be highlighted.

3. Local response calculations are performed for a particular part of the Sevan Arctic MODU by application of Abaqus. The example part selected based on discussion with the supervisor.

4. The degree of global platform motion due to ice impact is to be assessed. Alternative structural calculation models should be considered if found relevant.

5. Parameter studies are carried out to the extent that time allows. A corresponding matrix of parameter values for the different cases to be analyzed should be established prior to the analysis itself, and the matrix should also be discussed with the supervisor before the calculations are performed.

The work scope may prove to be larger than initially anticipated. Subject to approval from the supervisor, topics may be deleted from the list above or reduced in extent.

In the thesis the candidate shall present his personal contribution to the resolution of problems within the scope of the thesis work.

Theories and conclusions should be based on mathematical derivations and/or logic reasoning identifying the various steps in the deduction.

The candidate should utilise the existing possibilities for obtaining relevant literature.

The thesis should be organised in a rational manner to give a clear exposition of results, assessments, and conclusions. The text should be brief and to the point, with a clear language. Telegraphic language should be avoided.

The thesis shall contain the following elements: A text defining the scope, preface, list of contents, summary, main body of thesis, conclusions with recommendations for further work, list of symbols and acronyms, references and (optional) appendices. All figures, tables and equations shall be numbered.

The supervisor may require that the candidate, in an early stage of the work, presents a written plan for the completion of the work.

The original contribution of the candidate and material taken from other sources shall be clearly defined. Work from other sources shall be properly referenced using an acknowledged referencing system.

The thesis shall be submitted in 3 copies:

- Signed by the candidate
- The text defining the scope included
- In bound volume(s)
- Drawings and/or computer prints which cannot be bound should be organized in a separate folder.

Supervisor: Professor Bernt J. Leira
Deadline: June 24th 2015

Trondheim, January 15th 2015

Bernt J. Leira

Summary

Due to an increasing energy demand in the world, the interest of the Arctic region for offshore oil and gas exploration is increasing. The demand of structures capable of operating in the harsh Arctic environment is therefore expected to increase. Such structures need to overcome challenges like dealing with extremely low temperature and ice loads. The Sevan Arctic Mobile Offshore Drilling Unit (Sevan Arctic MODU) is an Arctic drilling unit concept developed by Sevan Marine. The main scope of the thesis has been to investigate how this structure are capable of dealing with large and unexpected ice loading.

Ice is a complicated material. When compressed, zones of high pressure forces may develop, accompanied by effects like spalling, splitting and recrystallization. Because of the complicated mechanical behaviour, the forces exerted from ice onto a structure are often simulated with a pressure-area relationship. However, using such a relationship in a collision analysis proves to be insufficient since it does not take into account local effects in a good way.

Abaqus has been used to model a part of the Sevan Arctic MODU. The model considered is a part of the platforms outer wall. The structural models have been used in non-linear finite elements analyses to investigate relevant loading conditions. The models have been used assess two topics concerning a collision between a small iceberg and a floating structure. The first topic was to see how the drilling unit reacts to high concentrated pressure loads which may be present in a collision. It was found that the structure is able to resist high forces without experience critical damage. It was also found that the impact location is less important in an iceberg collision than when the structure is subjected to level ice and smaller ice features. This is because the structure is designed with a sloping hull form in the ice draft, reducing the forces from incoming level ice by forcing the ice to fail in bending.

The second topic was to simulate a collision between the platform and an iceberg. The forces from the iceberg acting on the structure were calculated by considering the energy in the collision. In these calculations it was assumed that all of the kinetic energy in the collision was dissipated as crushing energy in the iceberg. The results from these energy considerations were implemented in Abaqus in terms of a pressure-area dependent load.

IV

Sammendrag

På grunn av en økende energietterspørsel er interessen for Arktis som et fremtidig område for offshore olje- og gassutvinning økende. Det vil dermed bli et behov for strukturer som kan operere i de tøffe arktiske områdene. Slike strukturer må takle utfordringene som ekstremt lave temperaturer og store islaster. Sevan Arctic Mobile Offshore Drilling Unit (Sevan Arctic MODU) er et konsept på en arktisk borerigg som er utviklet av Sevan Marine. Hovedoppgaven i dette arbeidet har vært å undersøke hvordan denne strukturen er i stand til å håndtere store og uventede islaster.

Is er et komplisert materiale. Når det komprimeres kan det dannes områder med veldig store trykk. På grunn av den kompliserte oppførsel til is simuleres ofte kreftene som utøves fra is på en struktur ved hjelp av trykk-areal relasjoner. Bruk av slike forenklede metoder tar derimot ikke hensyn til lokale effekter på en god måte og viser seg å være utilstrekkelig i en analyse av en kollisjon mellom isfjell og en flytende struktur.

Abaqus har blitt brukt til å modellere en del av skroget til Sevan Arctic MODU. Modellen er inkluderer en utvalgt del av plattforms yttervegg. Strukturmodellene har blitt brukt i ulineære elementanalyser for å undersøke relevante lastkondisjoner. Modellene har hovedsaklig blitt brukt for å analysere en kollisjon mellom et lite isfjell og en konstruksjon. To hovedtemaer har blitt sett nærmere på. Det første temaet har som hensikt å vurdere hvordan boreenheten reagerer på store, konsentrerte trykkbelastninger som kan forekomme i en kollisjon.

Det andre temaet har som hensikt å simulere og modellere en kollisjon mellom plattformen og et isfjell. Kreftene fra som virker på strukturen ble beregnet ved å se på energien i sammenstøtet. I disse beregningene ble det forutsatt at all den kinetiske energien i sammenstøtet ble tatt opp av isen. Resultatene fra disse beregningen ble implementert i Abaqus i form av et trykk-areaavhengig lasttilfelle.
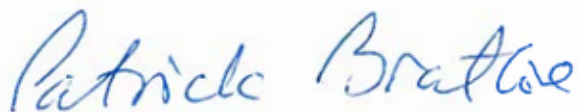
VI

Preface

This report is a Master Thesis in the field of marine structural engineering. The thesis was written at the Department of Marine Technology, Norwegian University of Technology and Science (NTNU), in Trondheim. The work was conducted during the spring semester 2015.

A large part of the time spent on the thesis work was used to make the models used in FE analyses. From before, I had little knowledge in using Abaqus, both in terms of making models and running analyses. Because this part turned out to be more time consuming than anticipated, the initial scope of work had to be changed during the semester. Nevertheless, I am pleased with how the end result turned out.

I would like to thank my supervisor, Professor Bernt Johan Leira, for guidance and support during the work process. I would also like to thank Hans Olav Sele and Einar Bernt Glomnes in Sevan Marine for providing information about the Sevan Arctic MODU and ice engineering in general. Lastly, I would like to thank fellow student Erlend Hopsdal Skjetne for the numerous discussions we have had regarding modeling and running analyses in Abaqus.

Patrick Bratlie
Trondheim, June 22nd 2015

VIII

Contents

List of Figures

List of Tables

Nomenclature

a_i	added mass of ice feature
a_s	added mass of structure
A	contact area
AR_B	load aspect ratio
b_B	height of design load patch
C	damage factor
CF_C	crushing failure class factor
CF_C	load patch class factor
CF_C	flexural failure class factor
d	water depth
D	accumulated damage
D_f	critical damage
D_i	diameter of iceberg
ex	pressure-area exponent
E	Young's modulus
E_{cr}	ice crushing energy
E_{kin}	kinetic energy
$E_{s,i}, E_{s,s}$	strain energy of ice and structure, respectively
fa_B	shape coefficient
F_B	impact force
h	draft of iceberg
h_ice	height of ice sheet
l_m	characteristic length of element
L_{wl}	ship length measured at ice waterline
m_i	mass of ice feature
m_s	mass of structure
mex	pressure-area exponent factor
F_n	normal force from ice
p	length of penetration
p_0	local design pressure factor
p_L	local design pressure
P	ice pressure
P_{avg}	average design patch pressure
PPF	peak pressure factor
Q_B	line load

r	radius of contact area
R	resistance
R_i	radius of iceberg
s	stiffener spacing
T	stress triaxiality
v_i	velocity of ice feature
v_s	velocity of structure
w	deformation depth
w_B	width of design load patch
x	distance from forward perpendicular to station under consideration

α_B	waterline angle
β'_B	normal frame angle
Δ_{tk}	ship displacement
ε	strain
ε_{cr}	critical average strain
ε_{eq}	effective plastic strain increment
ε_f	failure strain
ε_p	plastic strain
ε_y	yield strain
ν	Poisson number
ρ_i	density of ice
σ	stress
$\sigma_1, \sigma_2, \sigma_3$	principal stresses
σ_f	flexural strength of ice
σ_h	hydrostatic stress
σ_m	Mises stress
σ_y	yield stress

Abbreviations

ALIE	Abnormal-Level Ice Event
ALS	Accidental Limit State
DFS	Deformation Scale Factor
DNV	Det Norske Veritas
ELIE	Extreme-Level Ice Event
FE	Finite Element
FEM	Finite Element Method
FLS	Fatigue Limit State
HPZ	High Pressure Zone
ISO	International Organization for Standardization
IACS	International Association of Classification Society
MODU	Mobile Offshore Drilling Unit
NLFEA	Nonlinear finite-element analysis
NTNU	Norwegian University of Science and Technology
PC	Polar Class
SLS	Serviceability Limit State
S3R	Three-node shell element with reduced integration
S4	Four-node shell element
S4R	Four-node shell element with reduced integration
ULS	Ultimate Limit State
USGS	United States Geological Survey

Chapter 1

Introduction

1.1   Background and Motivation

In 2008 The United States Geological Survey (USGS) published an assessment where they presented their estimates of undiscovered oil and gas resources north of the Arctic circle. It states that about 30% of the world's undiscovered gas and 13% of the world's undiscovered oil is stored in the Arctic region (Gautier et al., 2009). Figure 1.1 shows the probability of the presence of at least one undiscovered oil and/or gas field with recoverable resources greater than 50 million barrels of oil equivalent.
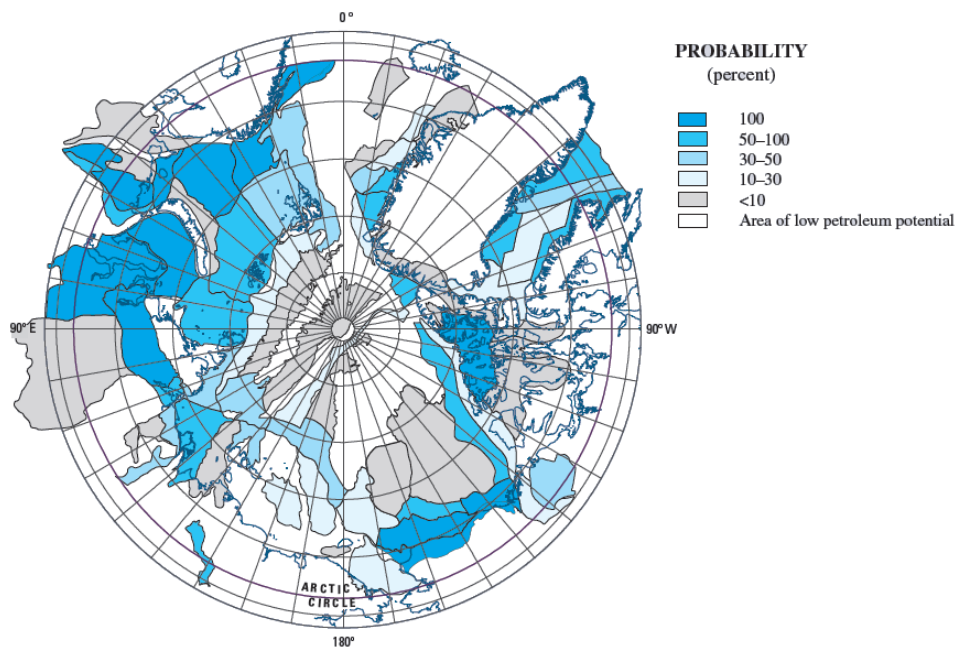
Figure 1.1: Assessment units (AUs) in the Circum-Arctic Resource Appraisal (CARA) color-coded by assessed probability of the presence of at least one undiscovered oil and/or gas field with recoverable resources greater than 50 million barrels of oil equivalent (MMBOE) (USGS, 2008).

1

Due to an increasing energy demand and easier accessibility of the region, activities related to exploration of offshore oil and gas in the Arctic have seen an uprise in recent years. Oil companies began development in the Arctic as early as the 1980s, but exploration of the region is said to still be in the early stages. In addition to more extensive mapping of the region, technological and environmental challenges need to be solved before the region can be fully concurred. One of the fundamental problems in ice engineering is the determination of ice actions and which effects these have on ships and offshore structures. In addition to the activity related to the petroleum industry, transportation using the north-east and north-west passage are expected to increase due to decreasing extent of the sea ice cover and ice free seasons.

It is a known fact that the climate change and increasing temperatures are contributing to melting of sea ice both in the Arctic and the Antarctic. This melting process leads to new water areas being seasonal ice free. However, the accelerating melting of glaciers also causes an increase in production of icebergs and other large ice features. A collision between a structure and a large ice feature may potentially be disastrous, both in terms of loss of life and equipment and damage of important ecosystems. Due to their size, large icebergs are easily observed on radar systems or spotted with the naked eye. They are therefore not considered to be the biggest problem. Ships can maneuver to avoid them, and for fixed structures (like an drilling rig) a disconnection possibility gives the ability to avoid leave the site if needed. A potentially greater risk is an impact with a smaller iceberg. These can be difficult to detect and may cause huge damage on the hull of a ship or an other structure. .

1.2 Iceberg Collisions with Marine Structures

Due to the increasing interest for the Arctic (both from the maritime and petroleum industry) there is a need for standardizations and regulations regarding structures operating in ice-infested waters. The most recently published standard for structures intended for operation in ice-infested waters is the ISO 19906 Arctic Offshore Structures (ISO, 2010). Rules for ships have existed longer than for offshore structures, and years of experience have helped in the development and understanding of the actions and the corresponding action effects on ships. Most of the research done on collisions between icebergs and marine structures are in relation with exploration of oil and gas fields in Arctic and sub-Arctic areas.

1.3 Outline of the Thesis

The primary objective of this thesis is to investigate how an ice-strengthened drilling concept unit designed be Sevan Marine deals with large ice loads. Relevant loading conditions are discussed. A partcilar part of the structure is modeled and analysed in Abaqus, which is a powerful numerical FEM tool.

The thesis includes the following chapters:

- *Chapter 1 - Introduction.*

- *Chapter 2 - Factors Governing Ice Action.* Relevant theory regarding ice mechanics and the field of Arctic engineering is presented.

- *Chapter 3 - Sevan Arctic MODU.* Presentation of the Arctic drilling design analysed in the thesis.

- *Chapter 4 - Calculation of Ice Action.* Presentation of different existing method for estimating ice action. The chapter also includes calculation of the design loads that the scantlings of the Sevan Arctic MODU is based on.

- *Chapter 5 - Impact Design.* Presentation of different design principles and methodologies relevant for collision analysis between a structure and ice features. A calculation example for some relevant collision scenarios is presented.

- *Chapter 6 - Finite Element Method.* The chapter gives an overview of relevant theory regarding the finite element method.

- *Chapter 7 - Modeling and Setup of Analyses.* The models used in the analyses are presented, including applied mesh, boundary conditions and material properties.

- *Chapter 8 - Main Results.* Presentation of results from the main analyses. This includes the IACS design load condition, a capacity analysis and a analysis where the load is determined from a pressure-area relationship.

- *Chapter 9 - General Conclusions.*

- *Chapter 10 - Recommendations for Further Work.*

Chapter 2

Factors Governing Ice Action

Sea ice occur in many different forms. The actions from the ice on a structure depends on many factors. This chapter will present the main factors governing ice actions on marine structures. The theory is, where nothing else is stated, taken from Løset et al. (2006).
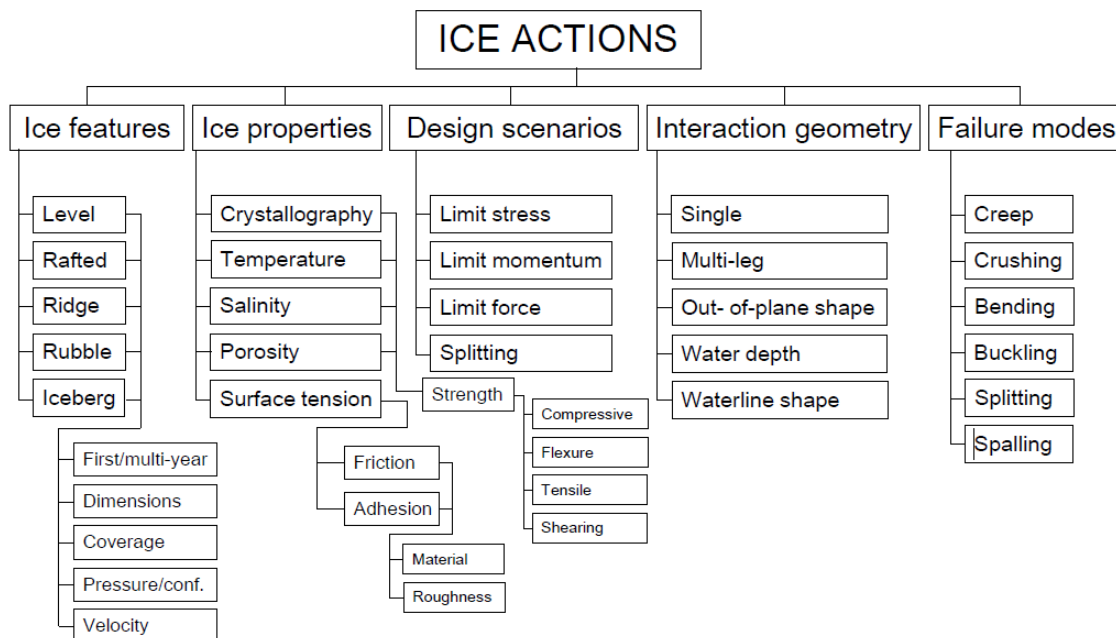
Figure 2.1: Major parameters affecting ice action (Løset et al., 2006).

2.1 Local and Global Action

When designing a structure against ice action, both local and global effects need to be taken into account. The global action is taken as the load exerted on the structure at any time instant.

These loads depend on the contact area between the structure and ice feature and the effective pressure. In addition to this, local stresses are exerted on smaller areas of the structure. The total ice action is dependent on many factors. In figure 2.1, a representation given by (Løset et al., 2006) of the major parameters affecting ice action is given.

2.2 Ice Features

Sea ice is found in different forms. The following are the most relevant ice features when dealing with ice actions on offshore structures.

- Level ice: Sea ice which is not affected by deformation, and with approximately the same thickness over a larger area.

- Rafted ice: Ice formation formed when one piece of ice slides over another.

- Ridge: Wall of broken ice formed by ice sheets pushing towards each other. Most of the ridge is submerged and is termed an ice keel. The part above water is called the sail of the ridge.

- Rubble: Piles of smaller pieces of ice in the form of a ridge or wall.

- Iceberg: Massive piece of ice which has broken off an glacier.

Large ice features are often categorized by size. In table 2.1 (Diemand, 2001) ice features are grouped into different types according to the mass range. The height given in the table for each group is a measure of the above waterline height of the ice feature. In this thesis, the term *iceberg* will be used when discussing all larger ice features.

Table 2.1: Categorization of ice features by mass range (Diemand, 2001).

Designation	Height	Mass range
Growler	< 1 m	m < 0.001 MT
Bergy bit	1-5 m	0.001 MT ≤ m < 0.01 MT
Small iceberg	5-15 m	0.01 MT ≤ m < 0.1 MT
Medium iceberg	16-45 m	0.1 MT ≤ m < 2 MT
Large iceberg	46-75 m	2 MT ≤ m < 10 MT
Very large iceberg	> 75 m	m ≥ 10 MT

2.3 Ice Properties

Several parameters affect the mechanical behavior of ice, the main being temperature, porosity, salinity, crystallography and surface tension. Sea ice is in general an inhomogeneous, anisotropic and nonlinear viscous material. It becomes weaker and softer with increasing temperature, porosity and grain size. The salinity also has an effect on the porosity. With lower temperatures,

the strength of the ice increases up to the point where brittle failure becomes dominant. The decreasing strength is due to small cracks starting to develop. The most important properties of sea ice are briefly described in the following.

2.3.1   Elastic Properties

The elastic properties of ice have been extensively studied. Kämäräinen (1993) presents some approximate values for different types of ice. These are given in table 2.2.

Table 2.2: Elastic properties of ice (Kämäräinen, 1993).

	Pure ice	Sea ice	Brackish ice
E [GPa]	9	4-6	4-6
ν [-]	0.3	0.3	0.3

2.3.2   Compressive Strength

The compressive strength of ice is often taken as the materials uniaxial strength. Sea ice has a columnar structure. The behavior of the ice depends on the orientation of the grains. Tests have shown that the horizontal and vertical compressive strengths range from 0.5-5 MPa and 0.5-10 MPa, respectively. Icebergs ice on the other hand is usually considered isotropic, having the same strength properties in all directions.

2.3.3   Tensile and Flexural Strength

Bending failure of ice depend on the flexural and tensile strength of the ice. The tensile strength of ice has been measured to be in the range of 0.1-2 MPa. As for the compressive strength, the tensile and flexural strengths are highly dependent on the grain orientation, in addition to the other parameters stated above.

2.4   Design Scenarios

In the design process of a structure, different interaction scenarios have to be considered (see figure 2.2.)

- Limit stress: If the stress in the ice reaches the bearing capacity of the ice, the ice will fail. If limit stress is the governing scenario (which is often the case), this stress level then decide the maximum action exerted on the structure. The ice is driven by wind and current.

- Limit momentum: If the kinetic energy from the ice is too small for the structure to penetrate it, the ice will come to a halt. This is often seen in ridge action on the structure.

- Limit force: If an ice sheet comes to rest in front of a wide structure, it can transmit actions from other surrounding ice features and also from wind and currents.

- Splitting: This scenario typically occurs if the corner of a structure is directed against the motion of the ice flow. The structure then works as a wedge on the ice, splitting the sheet in two or more pieces.
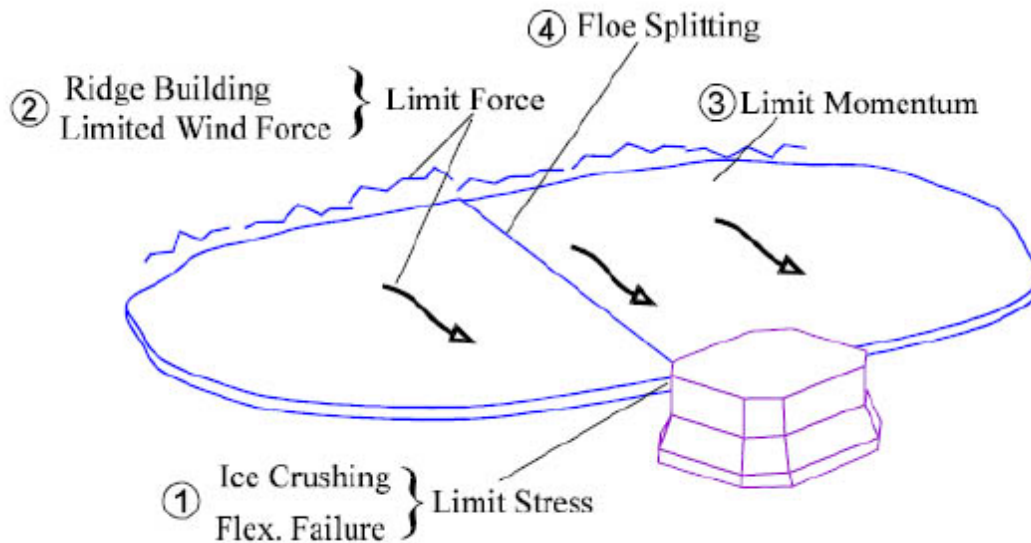
Figure 2.2: Ice action design scenarios (Løset et al., 2006).

2.5   Interaction Geometry

The geometry of the structure is one of the most important factors when calculating the ice action. A vertical wall is subjected to higher actions than a sloped wall subjected to the same ice actions. The structure size is also important, since this has a large impact on which design scenario that will be the dominant one (see section 2.4). From experiments it is found that the effective pressure is larger for a small/narrow structure than for a wide one.

The most used limit stress scenario is a thick level ice sheet moving towards a vertical (or close to vertical) structure. It has been seen that ice actions are significantly reduced if the structure has sloping sides. As seen in figure 2.3, for structures with sloped sides the ice will ride up along the structure and fail by repeated bending. For sloped structures, bending is the primary failure mode but crushing will occur locally as a part of the bending failure. This is important to take into account in local design. A sloped interaction surface is assumed to be favorable since the ice will fail at a lower load, due to the fact that the flexure strength of ice is lower than the compressive. However, the advantage of a sloping structure may diminish because of other factors. Due to the sloping face (either downward or upward sloping) there will be a accumulation of

rubble on and/or around the structure. The weight of the rubble is an addition to the total ice action. Friction forces will form due to ice moving along the structure.

a) Crushing failure (vertical structure)   b) Bending failure (sloping structure)
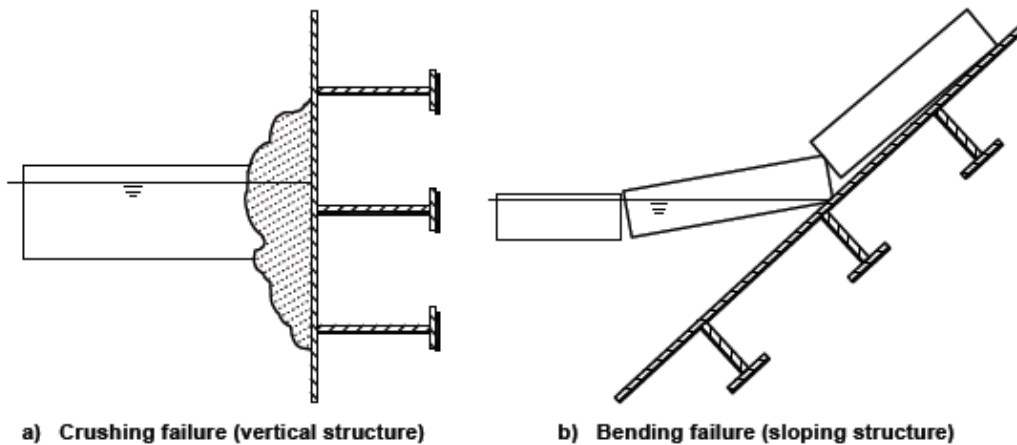
Figure 2.3: Bending and crushing failure (ISO, 2010).

2.6   Failure Modes

The pressure on the structure from the ice is highly related to the way the ice fails when it meets the structure. The way (modes) the ice fails in depends, among other factors, on size, thickness and velocity of the ice feature. From laboratory experiments, six main failure modes have been classified. These are illustrated in figure 2.4.

(a) Creep develops at very low indentation rates. We then have that the ice material yields and no cracks forms in the ice. This effect is only relevant for narrow structures. For wider structures and thick ice, other failure modes will be dominant before creep begins to develop.

(b) Radial cracking is connected to the tensile strength of the ice.

(c) Buckling is often found when thin ice interacts with a wide structure. This failure mode is often found in combination with radial and circumferential cracking.

(d) Circumferential cracking forms as a result of a out-of-plane bending moment or elastic buckling.

(e) Spalling from the ice sheet due to horizontal cracks may occur for different impact velocities.

(f) Crushing is found when the velocity of the ice is high. The crushed ice leaves the structure as a pulverized material. It is often the crushing process which is the most important of the failure modes.
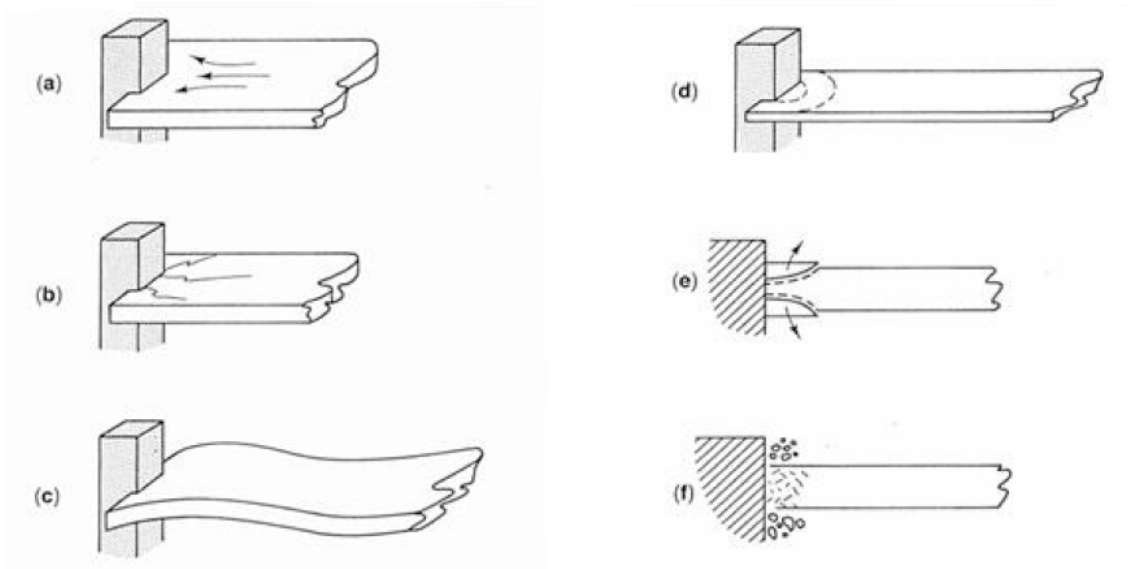
Figure 2.4: Ice failure modes (Løset et al., 2006).

Chapter 3

Sevan Arctic MODU

3.1 About the Design

The Sevan Arctic MODU is a design by Sevan Marine of a drilling unit intended for exploration of oil and gas in Arctic environments. Figure 3.1 shows the cross-section of the hull of the unit. It is designed as a moored cylindrical structure, similar to other Sevan platform designs. The platform has the form of a hexadecagon (sixteen-sided polygon). Sevan Marine has worked with several variations of the hull in the design phase. The design considered in this thesis has a 45 degrees downward sloping conical hull shape at the ice action draft. This shape provides the ability to mitigate ice actions as the approaching ice is failing in bending. This will, as described in section 2.5, lead to lower forces acting on the hull than if the hull side was vertical. In addition to the ice draft, the platform is designed to operate with a second draft, optimized for wave action. At this draft the hull is vertical. This makes it possible to operate in waters which is not ice-infested all year around. The main dimensions are given in table 3.1. More drawings of the hull are given in appendix B.

Table 3.1: Main dimensions of the Sevan Arctic MODU.

Parameter	Unit	Value
Main hull diameter	m	75
Main deck diameter	m	113.0
Double bottom height	m	3.5
Double side breadth	m	5.0
Main deck elevation	m	24.0
Draft, transit	m	10.0
Draft, ice operation	m	15.0
Waterline cone angle, ice condition	deg	45.0
Displacement, ice condition[1]	m^3	95000

---

[1]Displacement calculated based on drawings given in appendix B.
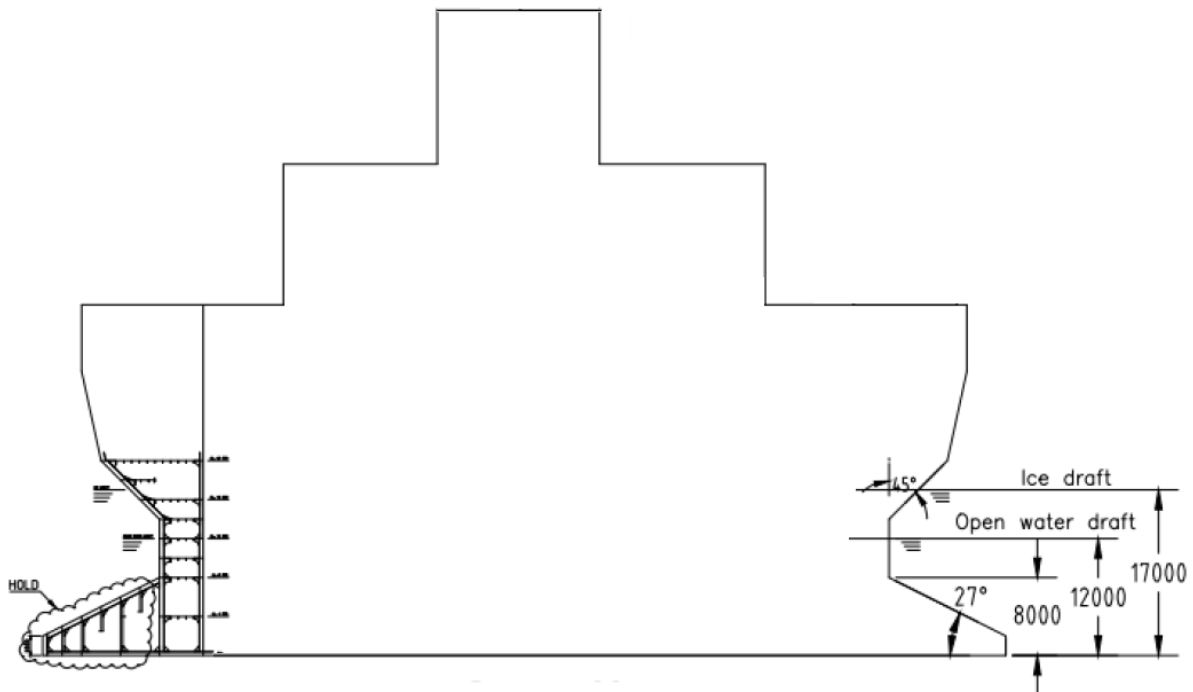
Figure 3.1: Cross section of the Sevan Arctic MODU (Haugen, 2014).

The hull is designed to withstand ice loads from any direction. It is designed according to Polar Class 4 (PC4) which is a class notation given by the International Association of Classification Society (IACS). This states that the structure should be designed with respect to operational capability and strength to handle year-round operation in thick first-year ice which may include old ice inclusions.

3.2 Experience from Similar Designs - The Kulluk Exploration Vessel

Drilling vessels were first used in ice-covered waters off the east cost of Canada and West Greenland in the early 1970s. The first operations mainly took place without permanent sea ice, but in the presence of icebergs which were towed away from the vessels. The Kulluk was a moored vessel used for exploration in Arctic waters. During its lifetime it operated in the Canadian Beaufort Sea and in the Gulf of Alaska. This makes it the only moored vessel that has been kept on station in a "near full range" of moving pack ice (Løset et al., 2006). In 2012, the vessel drifted while being towed to a drilling site around the northern coast of Alaska. This accident eventually led to the scrapping of the vessel due to too high cost of bringing it back in operation.

The Kulluk had a conical hull with a waterline diameter of about 70 m and a downward sloping hull of 30 degrees at the ice draft. It was equipped with a quick-release mooring system, making it possible to leave the site when unmanageable ice features were approaching. It was

typically supported by two icebreakers. The Kulluk is smaller than the Sevan Arcic MODU but the two vessels are similar when it comes to hull shape and intended areas of operation. Figure 3.2 shows the Kulluk operating in managed ice in the Canadian Beaufort Sea.

Figure 3.2: Kulluk in managed ice in the Canadian Beaufort Sea (Palmer and Croasdale, 2012).

Chapter 4

Calculation of Ice Action

When designing a structure intended for operations in Arctic waters, both local and global ice actions need to be considered. The global action is typically used in stability calculations, in mooring design and assessment of overall strength of the structure. The effect of local action needs to be included in design of small parts of the structure where the actions from the ice may be larger and more varying than the global action. This chapter will present some existing methods for calculating ice action and discuss how these methods are relevant for the Sevan Arctic MODU under different loading conditions.

4.1 ISO 19906

A common perception in the field of ice mechanics is that during an ice-structure interaction, the ice pressure decreases as the contact are increases. Masterson et al. (2007) combined pressure-area data from tests performed in the Beaufort Sea and used this to produce a pressure-area curve for local ice action. This curve is given in figure 4.1, together with the data points from which it is created. Based on the measured data, a upper bound pressure area curve was created, by taking the average value of the pressures at each area and adding three standard deviations. This resulted in the following relationship

$$p_L = 7.40 A^{-0.70}, A \leq 10 m^2$$
$$p_L = 1.48, A > 10 m^2$$

(4.1)

where p_L is the pressure expressed in mega pascals. The International Association of Classification Society (ISO) has in the ISO 19906 Arctic Structures Standard (ISO, 2010) adopted the Masterson pressure-area relationship for calculating local pressures for thick, massive ice features having a thickness in excess of 1.5 m. For areas above 10^2 the pressure has a constant value of 1.48 MPa.

In the data sets used to obtain the pressure-area relationship in figure 4.1, the highest pressure values were found from test where indenters where installed on the ice features used in the

15
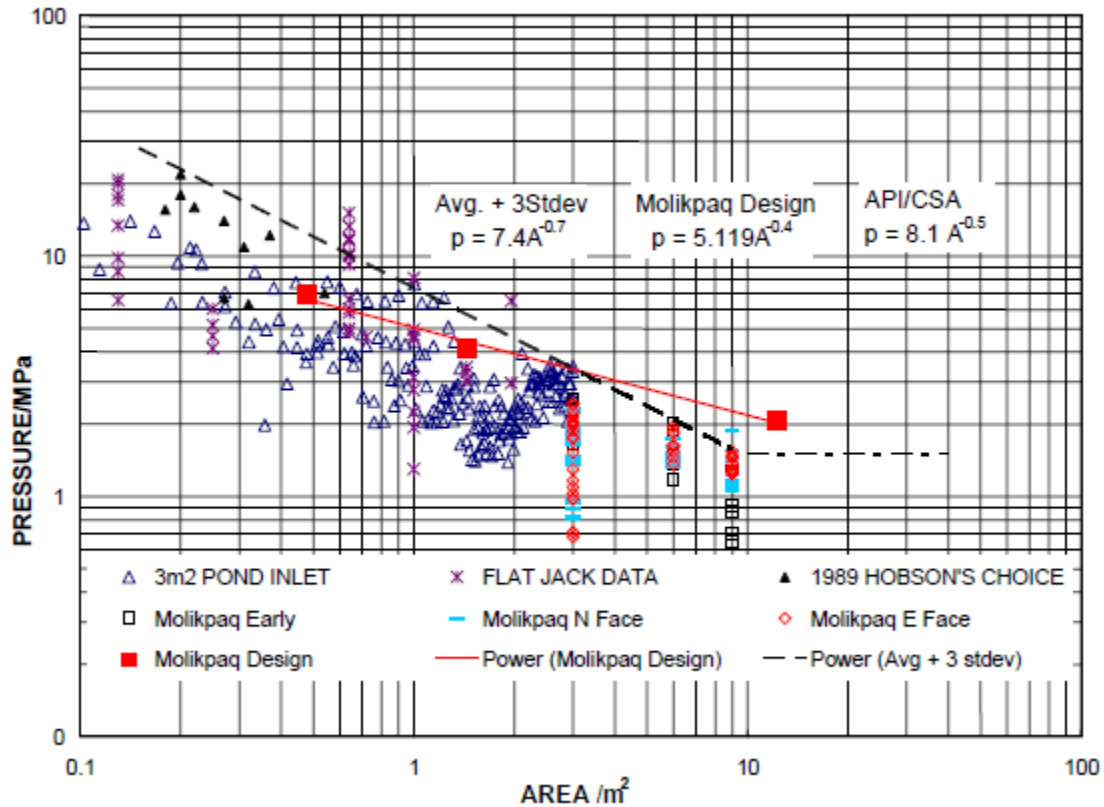
Figure 4.1: Pressure-area relationship for thick, massive ice features (Masterson et al., 2007).

testing. Palmer and Croasdale (2012) questions the fact that results from such test are compared and combined with test results from other types of impact tests. The data obtained from such tests may be appropriate to use when calculating actions from icebergs, multi-year floes and other large ice features. However, in general this may give to large actions. The problem of combining data from dissimilar test into one single curve is also brought up by Croasdale (2001). He also criticizes the use of logarithmic scales in the presentation, which makes the validity of the relationship much more convincing for unexperienced users.

4.2 Iceberg Ineraction Scenarios

Pressure-area relationships like the one discussed in section 4.1 model the ice pressure as uniform during the ice-crushing process. Experience has shown that this is not the case, and that areas of high pressures (High Pressure Zones, or HPZs) appear and disappear as the ice in small local areas fail and the load being picked up by other parts of the loaded area (Timco and Sudom, 2013). In such areas pressures of 20 MPa or more can exist on small areas of around 0.1 m^2, typically existing only fractions of a second (Croasdale, 2001). In analyses of ice-structure interactions, this effect can be included by implementing a more realistic ice material model.

Another concern with using a pressure-area curve (which show a decreasing ice pressure with

16

increasing area) is that where the aspect ratio of the ice (width divided by height of contact area) is reported, most data show a significant decrease in ice pressure with increasing aspect ratio (Croasdale, 2001). For a iceberg-structure interaction, the aspect ratio will be much lower than for an interaction scenario with level ice. Measurements where the aspect ratio is included often show that local ice pressures over a given area may be higher if the distance from the area to the free edge is greater (Croasdale, 2001). This is due to the larger degree of confinement in the center region. Croasdale (2001) proposes a scheme (alternative to the plain pressure-area) for iceberg impact crushing scenarios. The contact zone is assumed made up by two regions. An outer region where the ice is unconfined, where failure in the ice can propagate to the free edges, and an inner confined zone, where crushing gives rapid growth and decay of high pressure zones. This is illustrated in figure 4.2.
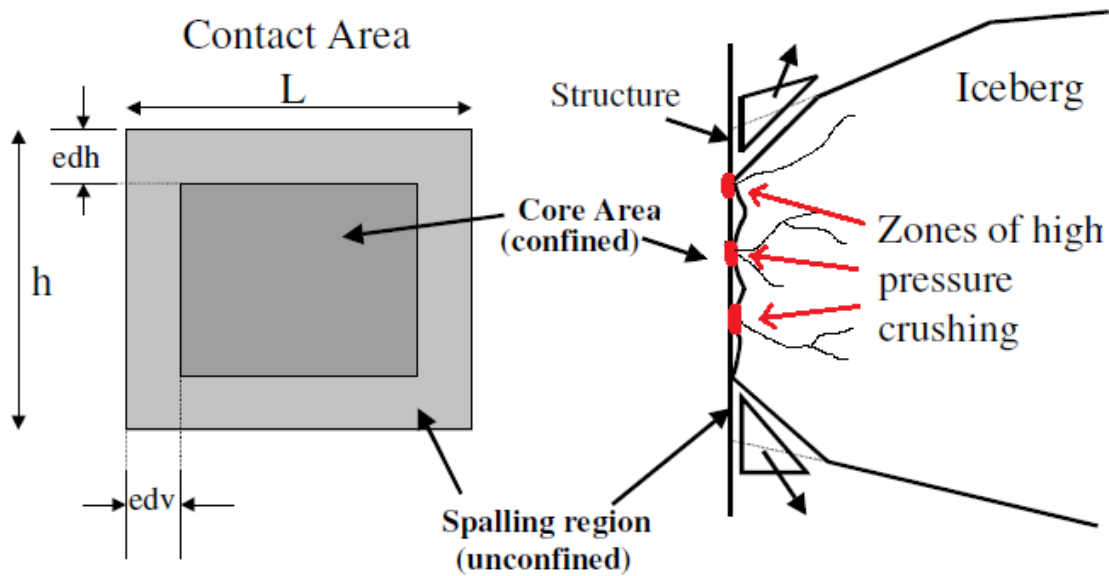
Figure 4.2: Crushing model concept (Croasdale, 2001).

4.3 Polar Class

The hull of the Sevan Arctic MODU is, as mentioned earlier, designed in accordance with IACS Polar Class which are given in IACS Unified Requirements (UR) for Polar Ships (IACS, 2011). They will here be presented in the way they are given in *Ships for navigation in ice* (DNV, 2013b).

The IACS UR for Polar Ships is the result of a work by several classification societies and nations to form one common standard. This standard apply to ships constructed of steel that are intended for navigation in ice-infested polar waters. It considers the hull of the ship, propulsion system, emergency systems etc. Here only the requirements concerning the hull structure will be presented.

The IACS UR are divided into seven polar classes (PC 1 - PC 7), where the different classes are

divided with respect to the length of the operational periods (year-round or seasonal) and the ice conditions the ship is expected to encounter. The Sevan Arctic MODU is designed according to PC 4. This class states that the vessel should be able to operate on a year-round basis in thick first-year ice which may include old ice inclusions. The complete list of the Polar Class descriptions is given in table A.1 in appendix A.

The requirements concerning the hull is dependent on which area of the structure that is considered, reflecting the different magnitudes of action that are expected to act upon them. The Sevan Arctic MODU is not a ship shaped structure and is designed to be able to take on the same loads from all angles. In the IACS requirements, the bow of the ship is assumed to take on the largest action. This is because the calculations of the design load are based upon a glancing impact with an ice feature. Therefore, the whole outer hull structure of the Sevan Arctic MODU is defined as *bow* when calculating the design loads.

4.3.1 Design Load Calculation

The load acting on the hull is found as an average pressure, P_{avg}, which is working over an design load patch area defined by b_B and w_B, which are the height and width of the rectangular load patch, respectively. These three load parameters are functions of the force, F_B, load aspect ratio, AR_B, the line load, Q_B, and the pressure, P_B. These are determined from the following expressions.

$$F_B[MN] = fa_B \cdot CF_C \Delta_{tk}^{0.64} \tag{4.2}$$

$$AR_B[-] = 7.46 \cdot sin(\beta'_B) \geq 1.3 \tag{4.3}$$

$$Q_B[MN/m] = F_B^{0.61} \frac{CF_D}{AR_B^{0.35}} \tag{4.4}$$

$$P_B[MPa] = F_B^{0.22} CF_D^2 AR_B^{0.3} \tag{4.5}$$

where fa_B is a shape coefficient found from

$$
\begin{aligned}
fa_B[-] &= minimum(fa_{B,1}; fa_{B,2}; fa_{B,3}) \\
&\text{where} \\
fa_{B,1} &= \left(0.097 - 0.68\left(\frac{x}{L_{wl}} - 0.15\right)^2\right)\frac{\alpha_B}{(\beta'_B)^{0.5}} \\
fa_{B,2} &= \frac{1.2 \cdot CF_F}{(sin(\beta'_B) \cdot CF_C \cdot \Delta_{tk}^{0.64})} \\
fa_{B,3} &= 0.60
\end{aligned}
\tag{4.6}
$$

and where

- CF_C, CF_D and CF_F are class factors for the Polar Class considered, given in table A.2.

- x [m] is the distance from the forward perpendicular (FP) to the station under considera-
tion.

- L_{wl} [m] is the ship length measured at the ice waterline.

- Δ_{tk} [kt] is the ship displacement.

- β'_B [deg] is the normal frame angle.

- α_B [deg] is the waterline angle.

The distance x is set to 0 m and the length L_{wl} equal to the diameter of the hull in the ice draft
waterline. The hull angles β'_B and α_B are to be taken as defined in figure 4.3. In the case of the
Sevan Arctic MODU, β'_B is equal to 45 degrees (the slope of the hull in the ice waterline) and α_B
to 90 degrees.
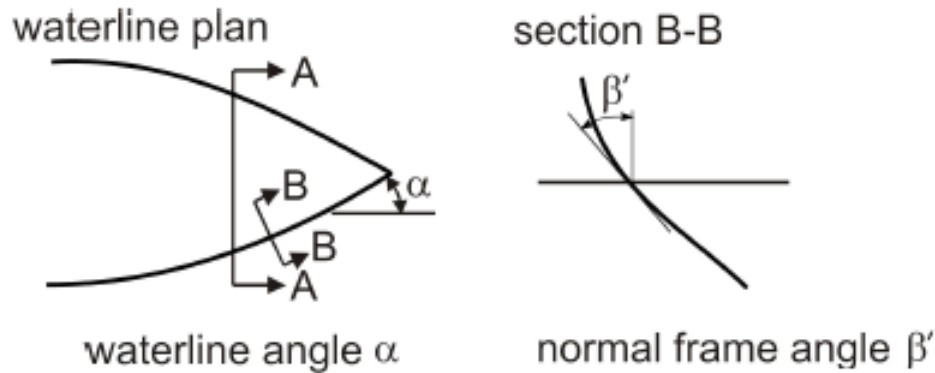
Figure 4.3: Definition of hull angles as used in Polar Class design load calculations (IACS, 2011).

The load patch area parameters w_B and b_B are found from

$$w_B = \frac{F_B}{Q_B} \tag{4.7}$$

$$b_B = \frac{Q_B}{P_B} \tag{4.8}$$

The average pressure, P_{avg} within the design load patch defined by w_B and b_B is given

$$P_{avg}[MPa] = \frac{F_B}{b_B \cdot w_B} \tag{4.9}$$

For the Sevan Arctic MODU, P_{avg} is calculated as 6.71 MPa, working over a design area of 2.83 m^2, defined by w_B = 4.24 m and h_B = 0.67 m. Additional values from the calculation of the design load are given in table A.3 in appendix A.

As the name of P_{avg} indicates, it is to be seen as the average pressure which is working over an area. Areas with higher and more concentrated pressures will exist within the load patch. This is taken into consideration by applying peak pressure factors (PPF) when calculating the scantlings of the structural members in the hull. These depends on the type of member under consideration and range from 1.0 to 2.0. For a transversely framed structure the PPF is given

$$PPF_p = (1.8 - s) \geq 1.2 \tag{4.10}$$

Figure 4.4 illustrates how the higher pressure works over a stiffener load area. With a stiffener spacing s = 0.4 m, the PPF_p = 1.4. Multiplying this with P_{avg} gives a stiffener design pressure of 9.39 MPa.
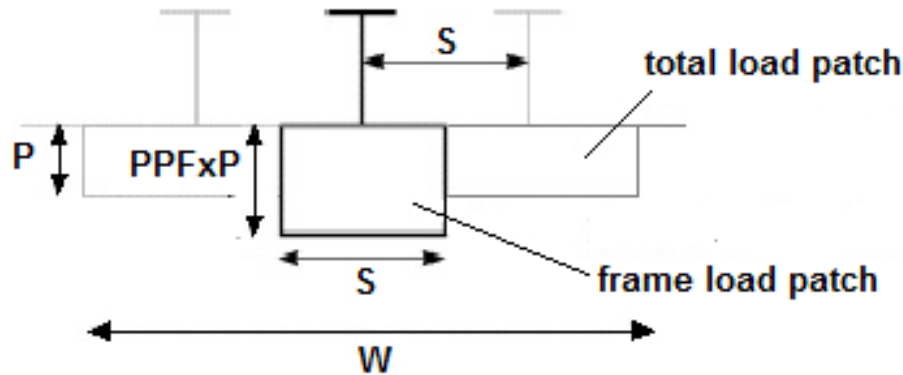
Figure 4.4: Location of frame load patch within total load patch area (Daley, 2000).

4.4 Numerical Modeling

Ice is a complicated material. Under a high compressive stress field, the ice behavior includes the development of HPZs that accompany the formation of a damage layer in the contact zone, including recrystallization, microcracking, rapid ejection of crushed ice, spalling, splitting, and pressure melting (Kim, 2014). Several numerical ice models have been developed to try to simulate the behavior of ice. In this section a model by Liu et al. (2010) will be briefly presented.

The material model proposed by Liu et al. (2010) is not intended to consider all scenarios of ice-structure interactions under all ice conditions. Instead it focuses on iceberg impact scenarios. The model is a simple, isotropic elastic perfect plastic model where the iceberg ice is idealized as an isotropic material. In a collision scenario, the contact area will include areas with confinement pressures close to the center while edge spalling are likely to occur closer to the edge (see section 2.6). Liu et al. (2010) states that as high pressures as 70 MPa can be found in HPZs in

such areas.

In Liu et al. (2011), an integrated analysis of a ship-iceberg collision is presented, in form of a non-linear finite element simulation where the deformation of both the ship and iceberg is taken into consideration. A spherical iceberg with a radius of 2 m was free to move towards the bow of the ship at a velocity of 4 m/s. Figure 4.5 shows the measured contact pressures on the ship outer hull at time 0.005 s and 0.15 s. The maximum contact pressure is in the beginning very high (in the range of 16-37 MPa (Liu et al., 2011)). At the second time step (t = 0.15 s) the maximum pressure is about 15.5 MPa (and still found in the center region), while other HPZs are distributed randomly within the contact surface. The higher pressure in the center of the contact area (compared to the outer region) is explained by the center area being well confined. This effect is also found in field measurements by Gagnon (2008), where contact pressures from ship collisions with small icebergs were measured using impact panels.

(a) t = 0.005 s   (b) t = 0.15 s
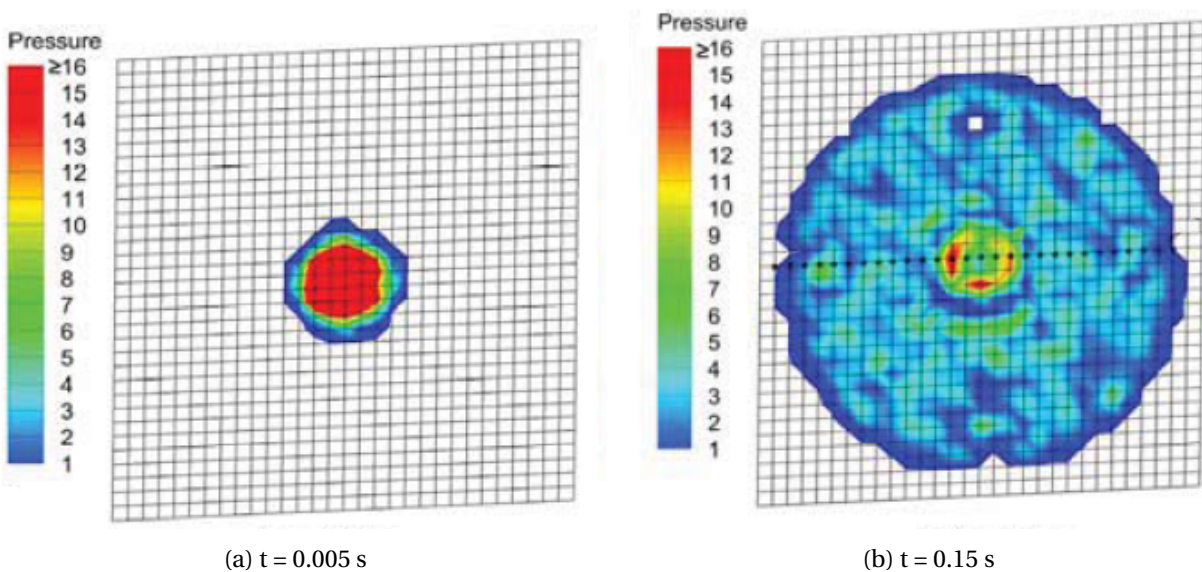
Figure 4.5: Contact pressure on ship outer hull in numerical analysis of iceberg collision with foreship structure (Liu et al., 2011).

The results from the numerical collision simulations were plotted against the Masterson pressure-area relationship (see equation 4.1). This is seen in figure 4.6. The results show that the maximum pressure found in the contact area decreases in the same manner as in the design curves.
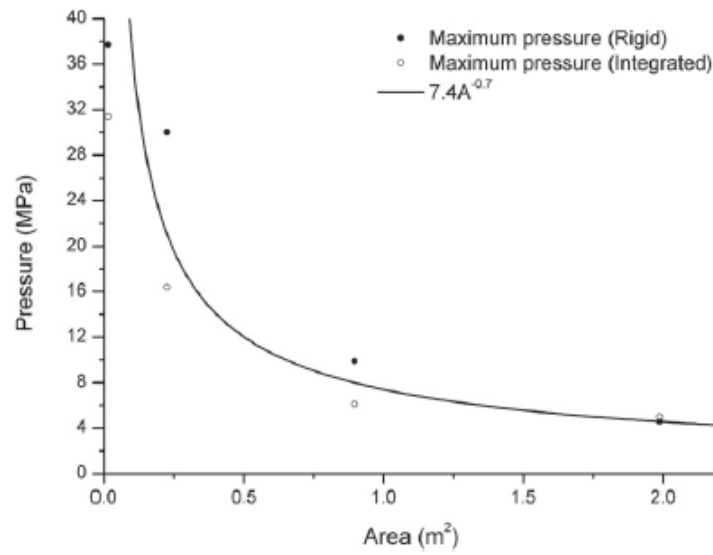
Figure 4.6: Pressure-area relationship recorded during rigid and integrated analysis (Liu et al., 2011).

Chapter 5

Impact Design

5.1 Design Principles

A collision action is characterized by the kinetic energy of the colliding bodies, which in tern are governed by the masses and velocities at the instant of impact. During the collision, parts of the kinetic energy is dissipated as strain energy in the two bodies (in this case the iceberg and the platform). Such events generally involve large plastic strains and significant structural damage. Depending on the dissipation of energy in the different bodies, which depends on their relative strength, design principles may be divided into three main categories. This is illustrated in figure 5.1. The figure shows energy dissipation in a ship-installation collision. However, the same division is relevant for a collision between a iceberg and platform (which in figure 5.1 is the denoted *installation*).
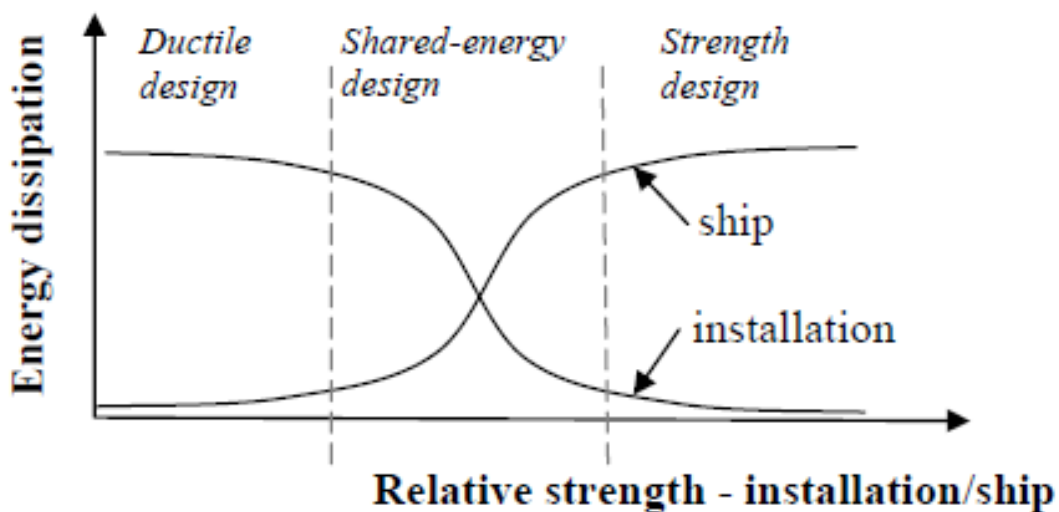
Figure 5.1: Energy dissipation for strength, ductile and shared-energy design (NORSOK, 2004).

- Strength design implies that the platform is strong enough to only suffer minor deformations, forcing the iceberg to dissipate the major part og the energy.

- Ductility design implies that it is the platform that dissipates the major part of the energy and therefore undergoes large plastic deformations.

- Shared-energy design implies that both the ice and the platform dissipate significant parts of the energy.

The strength and ductility design strategies are least computational demanding since the deformation of the softer body can be found by considering the geometry of the rigid (or close to rigid) structure. In the shared energy design approach the collision is coupled, meaning that the distribution and magnitude of the collision forces depend on the deformation of both bodies. The mechanics of such a interaction process makes the analysis more complex. In the analyses performed in the this, the ice action will be applied as constant (non-deformable) pressure forces, meaning that ductile design will be used.

5.2 Limit State Designs

In structural design, requirements are often linked to a limit state. The term *limit state* describes a condition where the structure (or a part of it) not any longer fulfills the design criteria and therefore is considered to be unsafe. The limit state is important when evaluating actions on a structure. The limit states are usually classified into four categories: *ultimate limit state* (ULS), *serviceability limit state* (SLS), *fatigue limit state* (FLS) and *accidental limit state* (ALS). The ULS corresponds to resistance to extreme applied actions. The SLS corresponds to the criteria governing normal functional use. The FLS corresponds to the reduction of the structures ultimate strength due to repetitive actions. The ALS corresponds to situations where the structure is subjected to unusual, extreme actions, typically leading to collapse of the structure.

According to ISO (2010), the ULS requirement ensures that no structural damage of significance occurs for actions that have an acceptably low probability of being exceeded during the structures design service lifetime. The ALS requirement is intended to ensure that a structure have sufficient reserve strength, displacement or dissipation capacity to sustain action without complete loss of integrity. Thus, two conditions are therefore considered in ALS design:

- the ALS condition, considering the structures ability to resist accidental event.

- the post-ALS condition, considering the damaged structures resistance to progressive collapse due to the damage and a continued exposure to actions.

The design principles described in section 5.1 may be linked to the limit states as shown in figure 5.2. The ULS approach is based on elastic response or limited plastic deformations of the structure, whereas the ALS approach allow larger deformations.
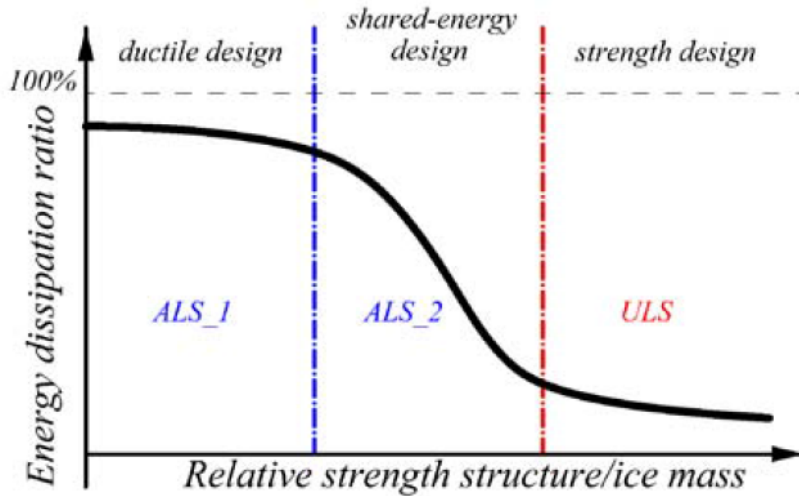
Figure 5.2: Energy dissipation ratio in structure-ice collisions (Kim, 2014).

In ISO (2010), the ALS condition for ice action include both Abnormal-Level Ice Event (ALIE) and Extreme-level Ice Events (ELIE). Local and global actions shall be considered. The value of the actions shall be determined based on an annual probability of exceedance not grater than 10^{-2} (event with 100-year return period) for ELIE and 10^{-4} (event with 10000-year return period) for ALIE. Figure 5.3 shows pressure-area relationships for small iceberg impact on a FPSO offshore New Foundland, showing that ALS actions may be substantially larger than ULS actions.
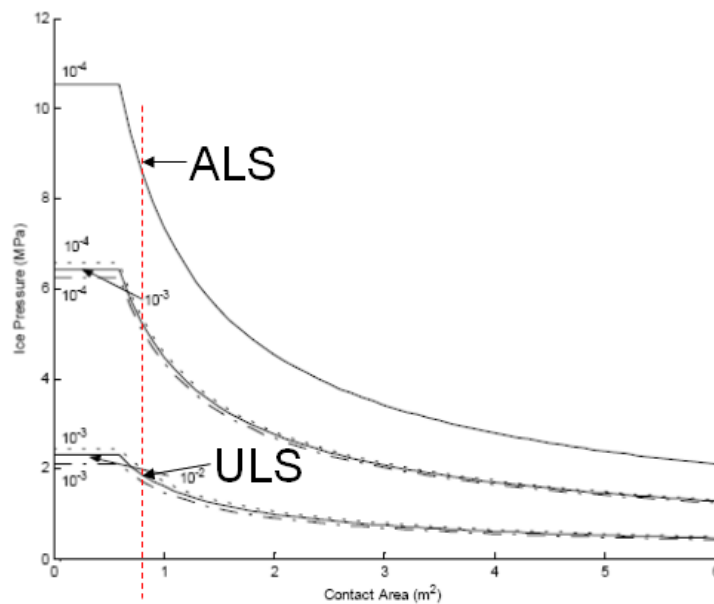
Figure 5.3: Pressure-area relationship for small iceberg impacts on FPSO for various probability levels (Amdahl, 2009).

5.2.1 Critial Values

The ALS requirement is intended to ensure that a structure has reserve strength, displacement or energy dissipation capacity to sustain large actions and other action effects in the inelastic region without complete loss of integrity. Some structural damage can therefore be allowed. NOR-SOK (2004) proposes a critical strain rate, ε_{cr}, equal to 0.15 for S355 construction steel, which is a commonly applied steel type in the maritime industry. Figure 5.4 shows typical critical strain rates applied with the ALS and ULS approaches.
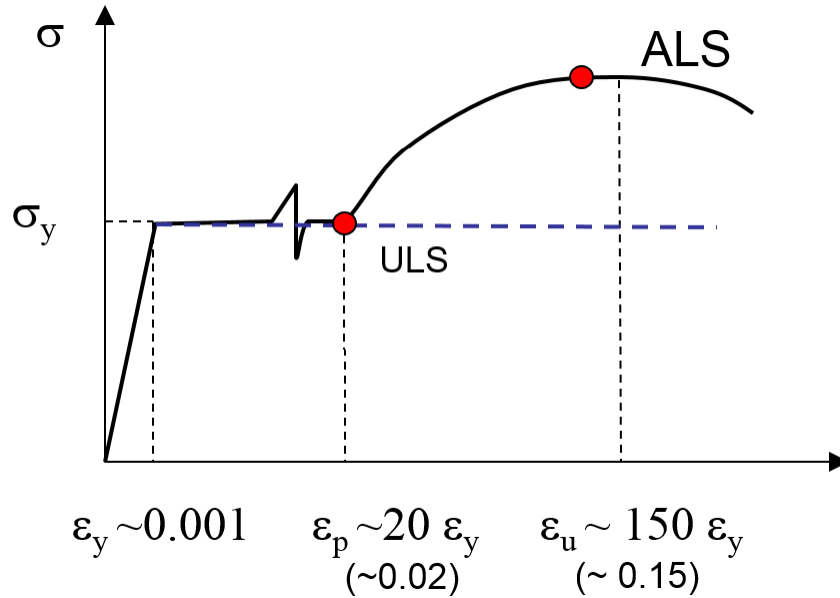
Figure 5.4: Acceptable strain levels for ULS and ALS design (Amdahl, 2009).

5.3 Collision Mechanics

A collision between an iceberg and a platform is characterized by the kinetic energy of the bodies. This energy is governed by mass and velocity of the iceberg at the instant of impact. The kinetic energy of the iceberg, E_{kin}, is found from

$$E_{kin} = \frac{1}{2}(m_i + a_i)v_i^2 \tag{5.1}$$

where m_i, a_i and v_i are the mass, added mass and velocity of the iceberg, respectively. The amount of the collision energy that is dissipated as strain energy, E_s, can be found from

$$E_s = \frac{1}{2}(m_i + a_i)v_i^2 \frac{(1 - \frac{v_s}{v_i})^2}{1 + \frac{m_i + a_i}{m_s + a_s}} \tag{5.2}$$

where m_s, a_s and v_s. are the mass, added mass and velocity of the platform, respectively. A common velocity for the iceberg and platform after the collision can be found from the equation for conservation of momentum, given as

$$(m_i + a_i)v_i + (m_p + a_p)v_p = (m_i + a_i + m_p + a_p)v_c \tag{5.3}$$

where v_c is the velocity of the system. If the initial velocity of the platform is assumed negligible, the system velocity can be found as

$$v_c = \frac{(m_i + a_i)v_i}{(m_i + a_i + m_p + a_p)} \tag{5.4}$$

In the above equation it is assumed that inertia forces are dominant, such that resistance from the mooring and hydrodynamic forces can be neglected. Equation 5.4 shows that system velocity is small if the mass of the platform is much bigger than that of the iceberg.

5.4 Calculation Example

5.4.1 Factors Governing Collision

When modeling a collision scenario, the speed, mass and shape of the iceberg need to be determined. McKenna (2005) assumes that a good representation for a shape of an iceberg is to model it as a sphere. In nature large ice masses are found in various sizes and shapes. The local shape of an iceberg at the impact zone has a large effect on the geometry of the contact area and the magnitude of the ice pressures exerted onto the structure. The mass of an iceberg is straightforward to find if the volume is known. The added mass however is more uncertain. Mc-Taggart and Isaacson (1990) presents a graph for determining the added mass for use in icebergs impacts (see figure 5.5). In the figure, h is the draft of the iceberg, d is the water depth and D_i is the diameter of the iceberg. The plot is made for vertical, circular cylinders but is in this thesis assumed applicable also for spherical shapes. When assuming large water depth relative to the draft ($\frac{h}{d} -> 0$) and having a draft relative to the iceberg diameter close to 1 ($\frac{h}{D_i} \approx 1$) the added mass coefficient is found as approximately $C_a = 0.7$.

The velocity of the iceberg plays an important role when predicting the loads from a iceberg onto a moored structure. The velocity depends on the mass of the iceberg, and wind, currents and the wave motion at the specific location. Raghuvanshi and Ehlers (2015) uses a drift velocity of 0.25 m/s in their assessment of iceberg loads on structures in the North Barents Sea. Brown and Daley (1999) uses iceberg drift velocities ranging from 0.5 to 2.0 m/s when simulating transverse collisions between stationary ships and spherical icebergs. According to Diemand (2001), the drift velocity of an iceberg will normally not exceed 1 m/s but the maximum instantaneous velocity of small icebergs and other ice masses in storm conditions may be 4-5 times larger than the hourly drift speed.
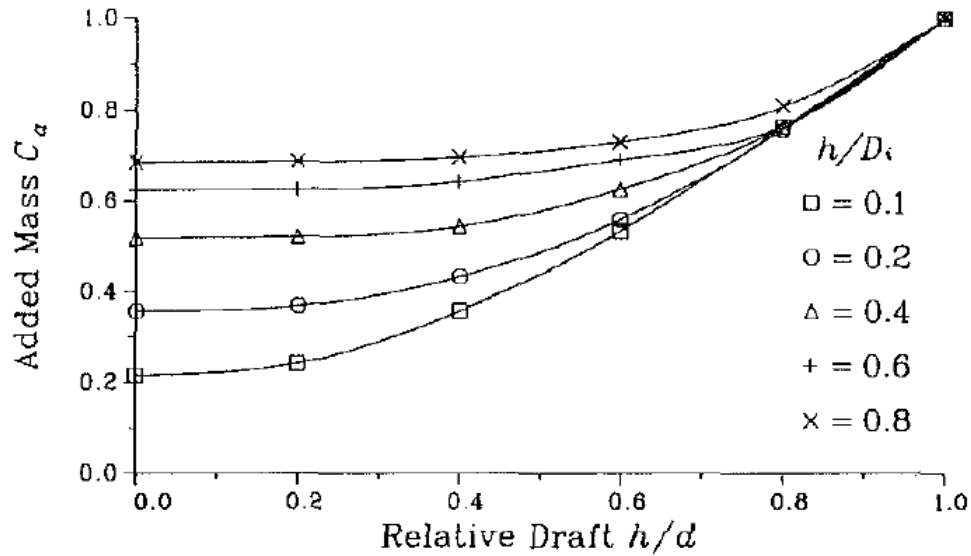
Figure 5.5: Added mass of ice features (McTaggart and Isaacson, 1990).

5.4.2 Dissipation of Energy

Table 5.1 present calculated values for the kinetic and strain energies for the three spherical icebergs sizes, for an impact velocity $v_i = 2.0 m/s$. It is seen that for all three icebergs, the main part of the kinetic energy is dissipated as strain energy. For the iceberg with radius 15 m, the calculated system velocity after the collision is found as 0.23 m/s. This is around 10 % of the initial velocity. Assuming that the platform is stationary after the collision can therefore be considered to be a good approximation.

Table 5.1: Energy calculation

Parameter	Unit	Radius 5 m	Radius 10 m	Radius 15 m
Volume	m^3	471	3770	12723
Effective mass	tons	801	6409	21630
Mass ratio	-	0.005	0.039	0.131
Kinetic energy	MJ	1.60	12.82	43.26
Strain energy	MJ	1.59	12.34	38.26
Absorption rate (%)	-	99.52	96.27	88.44
System velocity	m/s	0.01	0.07	0.23

5.4.3 Collision Force

Brown and Daley (1999) has developed a method for simulating transverse collisions between a stationary ship and a spherical iceberg moving with an constant initial velocity (see figure 5.6). The model is based on a collision where the collision force acts through the center of gravity

of the ship and ice. The ship is considerably more massive than the iceberg and the ship is therefore assumed to be stationary during the collision. The solution is found by equating the kinetic and crushing energy, assuming that all kinetic energy is dissipated as crushing energy by the iceberg.
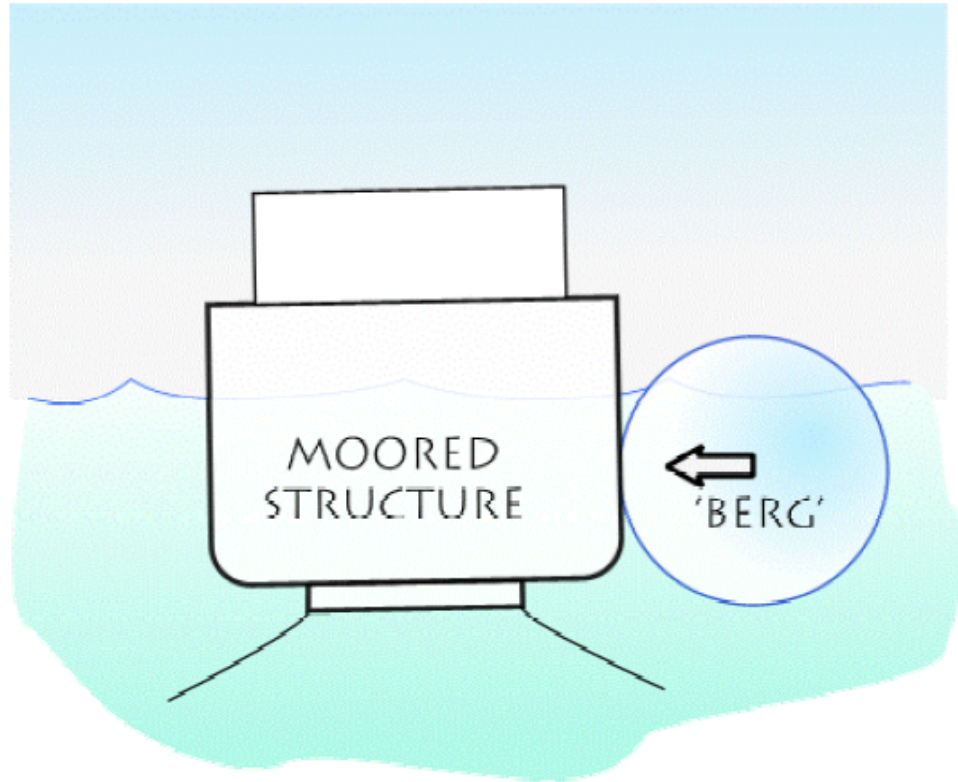
Figure 5.6: Iceberg-structure collision scenario (Brown and Daley, 1999).

A relation between the pressure and area is assumed on the form

$$P(A) = P_0 A^{ex} \tag{5.5}$$

where $P(A)$ is the average pressure over the contact area A, ex is a area exponent and P_0 is the ice pressure constant, given as the average pressure working over $1 \, \text{m}^2$. This is on the same form as the Masterson pressure-area relationship described in section 4.1. From this, the contact force acting on the hull, F, is found from

$$F = PA \rightarrow F = P_0 A^{ex} A = P_0 A^{(ex+1)} \tag{5.6}$$

For a spherical iceberg striking a flat plate the contact area will be circular. This area is determined from

$$A = \pi r^2 \tag{5.7}$$

where r is the radius of the contact area. Using basic geometry considerations, r is calculated as

$$r = \sqrt{2Rp - p^2} \tag{5.8}$$

where p is the length of penetration (as shown in figure 5.7) and R the radius of the iceberg. The contact area as a function of the penetration length is then given

$$A = \pi(2Rp - p^2) \tag{5.9}$$

Substituting equation 5.9 into equation 5.6 gives an expression for the contact force as a function of p. If it is further assumed that p is small compared to R, the expression for F can be written

$$F = P_0 A^{(ex+1)} = P_0 \pi (2Rp - p^2)^{(ex+1)} \rightarrow F_n = P_0(\pi(2Rp))^{(ex+1)} \tag{5.10}$$
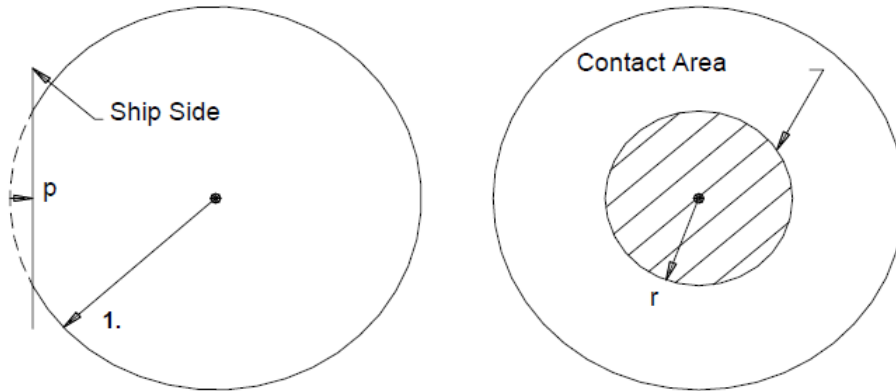
Figure 5.7: Definition of contact area in iceberg-structure collision (Brown and Daley, 1999).

The crushing energy, E_{crush}, is found by integrating the contact force over the penetration length.

$$E_{crush} = \int F_n dp = \frac{P_0(2R\pi)^{(1+ex)} p^{(2+ex)}}{(2+ex)} \tag{5.11}$$

By combining equations 5.1 and 5.11 and solve the expression for p

$$p = \left(\frac{(m_i + a_i) v_i^2 (2+ex)}{2P_0(2R\pi)^{(1+ex)}} \right)^{\frac{1}{(2+ex)}} \tag{5.12}$$

Finally, equation 5.12 is substituted into 5.10, giving a velocity dependent expression of the collision force.

$$F_n = P_O^{\frac{1}{(2+ex)}} (\pi R(m_i + a_i)(2+ex))^{mex} v_i^{mex} \tag{5.13}$$

where $mex = (1 + ex)/(2 + ex)$. In the calculations above it is important to remember that the resistance in the steel is not taken into account. In this sense the method may be considered as a strength design approach, since the ice dissipates all of the collision energy (see section 5.1). The contact force for the three icebergs sizes presented earlier are calculated for $v_i = 2.0 m/s$ and presented in table 5.2. In the calculations, the values of P_o and ex have been chosen as in the pressure-area relationship gien in ISO (2010) (see equation 4.1 in section 4.1).

Table 5.2: Collision force, penetration depth and impact area for iceberg-structure collision.

Parameter	Unit	Radius 5 m	Radius 10 m	Radius 15 m
Normel force	MN	13.56	25.72	37.40
Penetration	m	0.24	1.01	2.35
Impact area	m^2	7.36	60.38	204.11

In the calculation method presented above, the force increases until the movement stops. This may give a good approximation of the force acting on the hull during an idealized collision. However, since the calculation is based on the pressure-area relationship given in equation 5.5, the pressure acting on the hull will not exceed the value determined for the specific area. Including the velocity term will therefore not effect the maximum pressures, but instead the maximum total force acting on the hull. A larger velocity will give larger penetration length which means that the contact area also increases.

Since the calculations are based on the Masterson pressure-area relationship, the results are highly dependent on the values of P_0 and ex which are the parameters defining the strength of the ice. Brown and Daley (1999) gives no recommendations for which values to use. Figure 5.8 shows the maximum force plotted against the penetration depth for the iceberg with radius 10 m, plotted for three different values of the exponent ex. The largest total force if found for the lowest value of the exponent ($ex = -0.3$), but using this value also gives the smallest penetration depth. This is because the ice is stronger (compared to for example $ex = -0.5$) and therefore requires a larger pressure before it crushes. Because of this it dissipates more energy for the same penetration length. The highest pressures are however found by using $ex = -0.7$, for low contact areas. This is also seen from equation 5.5.
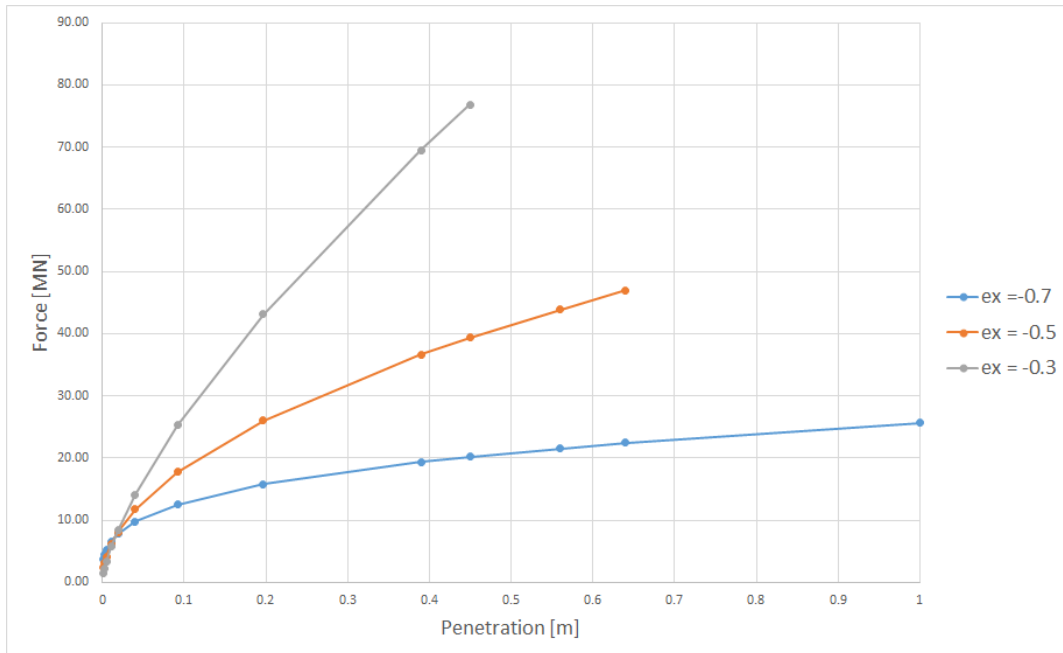
Figure 5.8: Force plotted against penetration depth for spherical iceberg with radius 10 m and a drift velocity of 2 m/s.

The effect of increasing velocity is presented in figure 5.9. The graph shows how the maximum force increases for an increasing velocity of the iceberg. The maximum force decreases when the value of ex is decreased because this weakens the ice.
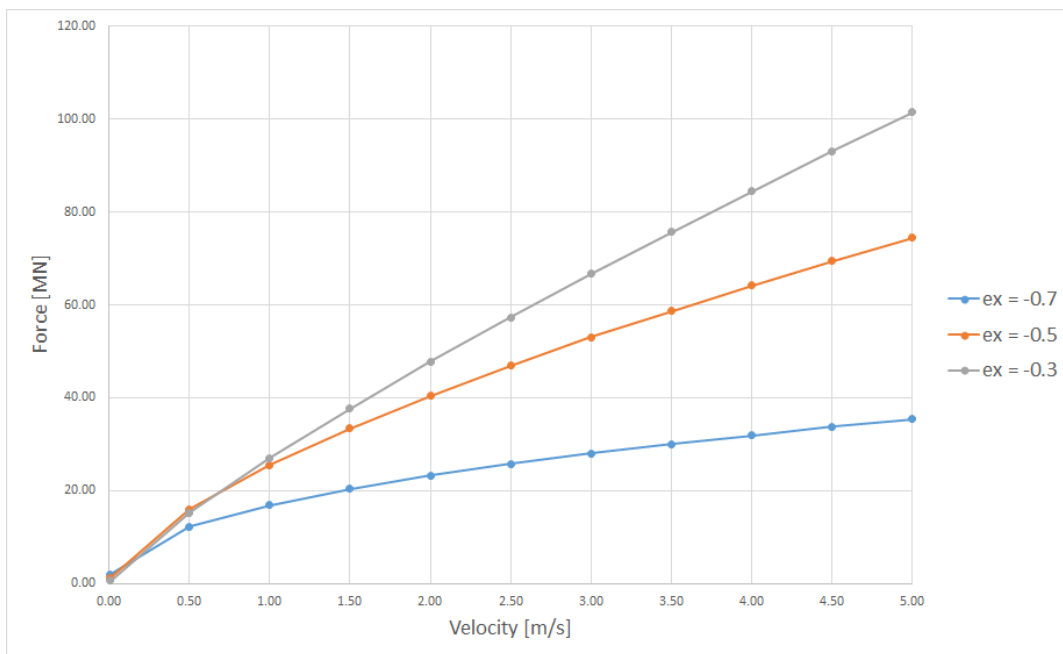
Figure 5.9: Force plotted against drift velocity for spherical iceberg with radius 10 m.

Chapter 6

Finite Element Method

In this chapter an overview of the Finite Element Method (FEM) will be given. This is a large subject so only the topics most relevant for the thesis will be presented. The following theory is taken from Moan (2003a), Moan (2003b) and Abaqus (2014).

6.1   General FEM Theory

The finite element method is a numerical solving procedure used for analysing structures and continua. The structures are discretized into finite elements connected via nodes. The accuracy of the results obtained from the method depends on the number of equations solved. Applying more elements and more exact element definitions will make the analysis result converge towards the exact solution.

FEM is, as for structural analysis in general, based on the following three principles.

- Equilibrium in stresses
- Kinematic compatibility of strains
- Stress-strain relationship

A normal analysis of a structure using FEM can be divided into some distinctive steps.

(a) Discretization: The structure is divided into elements, connected together with nodes.

(b) Element analysis: Establishing the element stiffness relationship, expressing the displacement within the elements while maintaining equilibrium and compatibility (stress-strain relationship).

$$S = k \cdot v + S^0 \tag{6.1}$$

where S is the generalized nodal point forces, k the element stiffness matrix, v the nodal point displacements and S_0 the nodal point forces from external loads.

(c) System analysis: A relationship between the load and nodal displacements is found by demanding equilibrium for all nodal points, giving

$$R = K \cdot r + R^0 \tag{6.2}$$

where R is the global load vector found from combining the nodal force matrices, K the system stiffness matrix found from combining the element matrices, r the global displacements and R_0 the nodal forces from external loads.

(d) Boundary conditions: Introduced into the system matrix by changing the stiffness and displacement matrices.

(e) Global displacements and stresses: The global displacements are found from solving the system matrix.

$$r = K^{-1} \cdot (R - R^0) \tag{6.3}$$

When the global displacements are known the element displacements can be found and used for obtaining the stresses in each element.

6.2 Shell and Plate Elements

For stiffened plate structures, shells are the most used element type. These elements provide both lateral and in-plane stresses, and they are therefore much more preferable than plate elements which only can produce bending stresses (plate elements are therfore not included in most of todays computer codes). For a stiffened panel, lateral loading will cause bending of both the plate and stiffeners, producing membrane stresses in both members. Thus, shell element will be the better choice.

Shell (and plate) elements can be divided into different categories, depending on the thickness ratio (thickness over characteristic length) of the element. In Moan (2003a), three plate theories are presented.

- Thin plate theory (Kirchhoff theory)

- Thick plate theory (Mindlin-Reissner theory)

- Three-domensional theory of elasticity (solid elements)

Abaqus offers three different shell element categories: thin, thick and general-purpose elements. Use of the thin and thick shell elements corresponds to the Kirchhoff theory and Mindlin-Reissner theory presented in sections 6.2.1 and 6.2.2. When general-purpose elements are applied, Abaqus uses an element definition which changes from thick shell elements (using Mindlin

Theory) to thin shell elements (using Kirchhoff theory) as the thickness decreases and the transverse shear deformations become very small. For most purposes the use of the general-purpose elements will be a good choice.

6.2.1 Kirchhoff Theory

In both thin and thick plate theory the transverse stress σ_z is considered negligible. Kirchhoff theory assumes Kirchhoff-Navier's hypothesis to be valid, stating that a straight line normal to the mid-surface remains straight and normal to the mid-surface also after deformation. Further, in addition to the transverse stress, the transverse shear strains γ_{xz} and γ_{yz} are considered negligible. The stress-strain relationship is given by the following expression.

$$\boldsymbol{\sigma} = \begin{bmatrix} \sigma_x \\ \sigma_y \\ \tau_{xy} \end{bmatrix} = \frac{E}{1-v^2} \begin{bmatrix} 1 & v & 0 \\ v & 1 & 0 \\ 0 & 0 & \frac{1}{2}(1-v) \end{bmatrix} \begin{bmatrix} \varepsilon_x \\ \varepsilon_y \\ \gamma_{xy} \end{bmatrix} = \boldsymbol{D}\boldsymbol{\varepsilon} \tag{6.4}$$

where $\sigma \, and \, \tau$ are the stresses, E is the material stiffness, v is the Poisson number, and ε and γ the strains.

6.2.2 Mindlin-Reissner Theory

In the Mindlin-Reissner theory it is assumed that a straight line normal to the mid-surface remains straight but not necessarily normal to the mid-surface after deformation. The transverse shear deformation components γ_{xz} and γ_{yz} are included in the solution of the problem. The stress-strain relationship is given by

$$\boldsymbol{\sigma} = \begin{bmatrix} \sigma_x \\ \sigma_y \\ \tau_{xy} \\ \tau_{xz} \\ \tau_{yz} \end{bmatrix} = \frac{E}{1-v^2} \begin{bmatrix} 1 & v & 0 & 0 & 0 \\ v & 1 & 0 & 0 & 0 \\ 0 & 0 & \frac{1}{2k}(1-v) & 0 & 0 \\ 0 & 0 & 0 & \frac{1}{2k}(1-v) & 0 \\ 0 & 0 & 0 & 0 & \frac{1}{2k}(1-v) \end{bmatrix} \begin{bmatrix} \varepsilon_x \\ \varepsilon_y \\ \gamma_{xy} \\ \gamma_{xz} \\ \gamma_{yz} \end{bmatrix} = \boldsymbol{D_{MI}}\boldsymbol{\varepsilon} \tag{6.5}$$

where k is a correction factor equal to 1.2 to ensure that the shear strain energy for the plate can be correctly represented by a uniform shear stress. When using Mindlin-Reissner theory the transverse shear stresses can be calculated directly from the transverse shear strains. The need of using thick element theory occurs when the thickness of the shell is more than 1/15 of the characteristic length of the surface of the shell (Abaqus, 2014).

6.2.3 Relevant Shell Elements

ABAQUS offers a wide range of element types. In this thesis only conventional stress/displacement shell elements have been applied. Shell elements are used to model structures where the thickness in one dimension is significantly smaller than in the two other dimensions. In the analyses performed in this thesis three element types have been applied. They will here be briefly presented.

S4R is a four-node, quadrilateral shell element with reduced integration and five degrees of freedom (dof) (three translations and two rotations) in each node. Abaqus recommends the S4R element when high strain gradients or large strains are expected (Abaqus, 2014). The element uses hourglass control to prevent shear locking (see section 6.4).

S4 is similar to the S4R element but does not use reduced integration. It can be desirable to use for problems where hour-glassing occurs or where in-plane bending is expected. Due to the full integration rule it is more computationally demanding than the S4R element. In general, higher order elements give more accurate stresses. This means that an analysis using S4R will require more elements to give the same accuracy in stresses as if the higher order S4 was used.

S3R is a three-node general purpose element. The element is a degenerated version of the S4R element and is fully compatible with it. A finer mesh (compared to the S4R) may be required to capture bending deformations or high strain gradients. This is due to how the element approximates bending and membrane strains. Triangular element types are useful to model the transitions in element meshes between areas with large and small stress gradients.

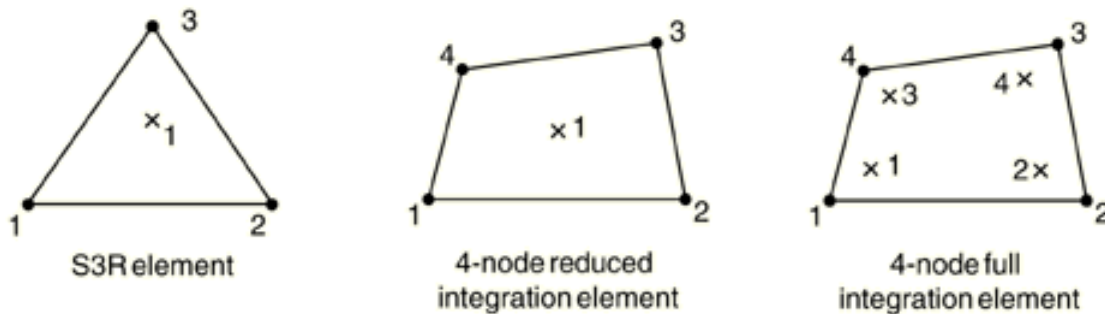Figure 6.1: The S3R, S4R and S4 shell elements with integration points (Abaqus, 2014).

Figure 6.1 shows the three above mentioned shell elements and the number of integration point in each element.

6.3 Nonlinear Theory

Linear analysis assume small displacements and linear-elastic material behavior. The equilibrium equations are then solved based on the initial conditions alone, and the strains are found

as linear functions of the displacement gradients. When the material reaches and exceeds the yield strength plastic deformations will be present. The assumptions of linear theory and small displacements are then no longer valid. Nonlinear theory is applied because of the presence of material, geometry and boundary condition nonlinear effects.

For many problems, running a nonlinear analysis is the obvious choice. However, a good practice is run a linear analysis first. The results from this can be helpful to see if and which nonlinear effect that may be important to consider, and where these effects occur.

6.3.1   Geometry Effects

When the shape of a structural member is subjected to high external loads the shape is changed to much for the initial stiffness matrix to be used throughout the analysis. Instead the stiffness needs to be re-calculated during the analysis. Figure 6.2 is an example where nonlinear geometrical effects is present, showing a panel being loaded until it "snaps through". As this happens, the stiffness becomes negative, followed by a regaining of positive stiffness shortly after.
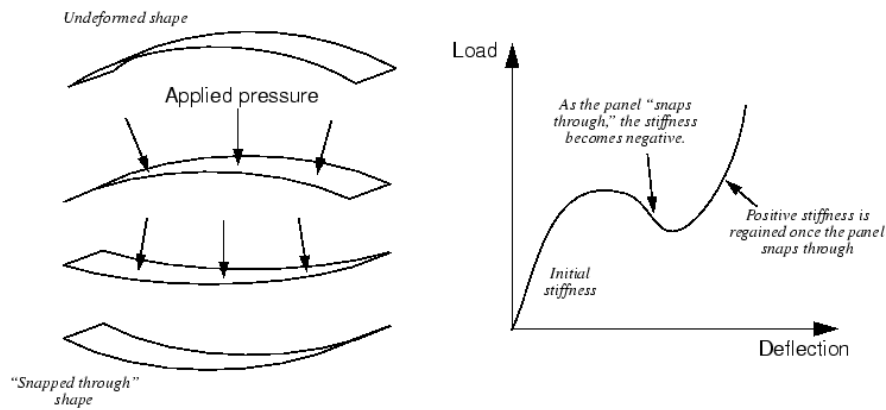
Figure 6.2: Geometry nonlinear effects (Abaqus, 2014).

6.3.2   Material Effects

Nonlinear material behavior is associated with a non-linear stress-strain relationship. Above a certain stress limit the behavior of the material changes from linear-elastic to nonlinear. Figure 6.3 shows a typical stress-strain relationship for a structural steel (not realistic proportions) in tension. For small strain rates and up to a certain stress level (called the proportional limit) the stress-strain relationship is linear. Beyond this point, the strain increases considerably for no noticeable increase in applied outer force. After a yielding region (in the figure the region from point B to C) the steel starts to strain harden. This is due to changes in the atomic and crystalline structure of the loaded material. After the yielding region, a further increase of the resistance in the material is seen up to the point of ultimate stress.
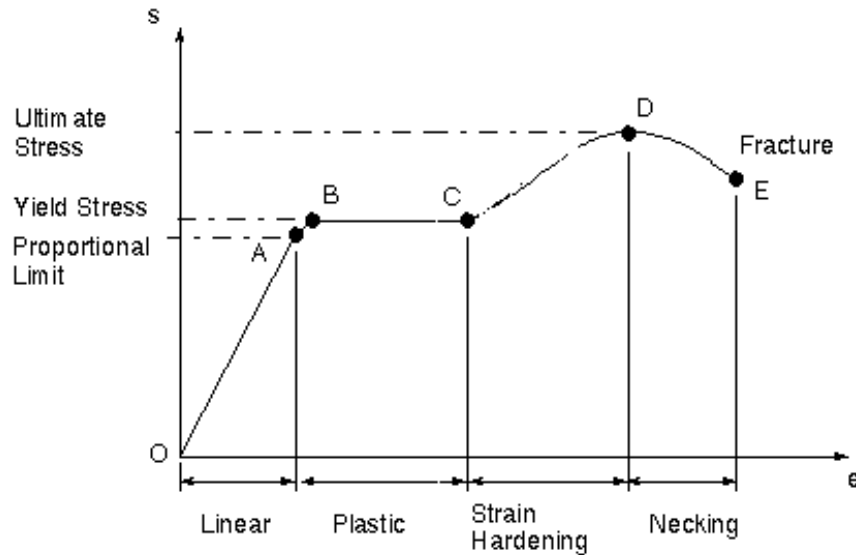
Figure 6.3: Material nonlinear effects (Abaqus, 2014).

6.3.3   Boundary Condition Effects

When two surfaces come into or out of contact the contact areas and pressures will change. This change is not linear dependent on the applied load. Figure 6.4 shows a cantilever beam with a point load. As the beam deflects due to the loading, the tip of the beam will come in contact with the box-shaped object. This sudden change in the boundary condition will prevent any further deflection at the beam tip. This leads to a sudden change in the response of the beam which is not any longer linear dependent on the load.
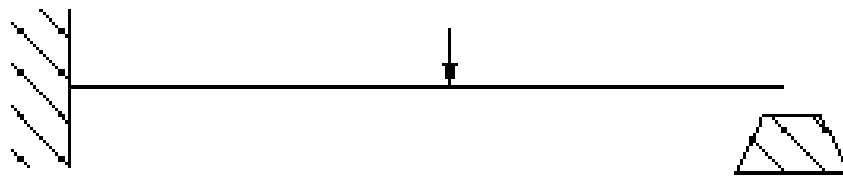
Figure 6.4: Boundary condition nonlinear effects (Abaqus, 2014).

6.4   Numerical Integration

Numerical integration is used to approximate solutions of integrals that may be difficult to solve analytically. Abaqus solves such integrals either by using the Gaussian quadrature rule or the Simpson rule. By default, Gauss rule will be used for integration of shells. Where the Simpson rule uses equally spaced integration points, Gauss offers the choice of changing intervals between the steps. The Gauss quadrature can provide greater accuracy than Simpson's rule for the

same number of integration points by choosing better locations for the integration points. A two-dimensional integral can be computed numerically from

$$I = \int_{-1}^{1} \int_{-1}^{1} f(\xi, \eta) d\xi d\eta \approx \sum_i \sum_j w_i w_j f(\xi_i, \eta_j) \tag{6.6}$$

where the function $f(\xi_i, \eta_j)$ is the value of the integrated function at location (ξ_i, η_j) and w_i and w_j are weight functions. The computational effort depends on the number of integration points. Figure 6.5 shows the integration points in a 2 by 2 integration rule over a square domain.

Figure 6.5: Integration points over a square domain (Moan, 2003a).

Abaqus offers elements which use reduced integration. This means that the element is integrated with a rule of less than full order. Using reduced integration softens the behavior of the element. A full order integration rule ensures an exact solution of the integral, as long as the element is undistorted. Thus, a redu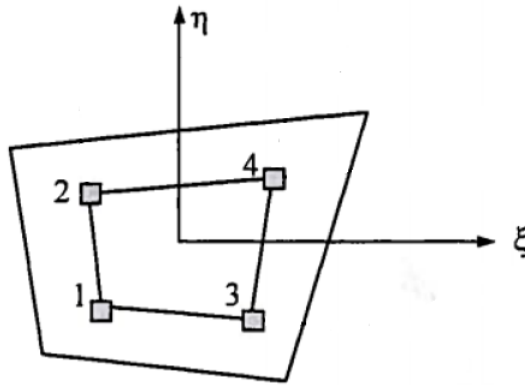ced integration rule is desired if the element subjected to with large bending (full integration will assume a to stiff displacement field). In addition to this, the computational time will be lower due to fewer points. An other advantage of using reduced integrations is that the elements are less prone to locking effects (called shear locking) than fully integrated elements. However, reduced integration elements may produce zero energy modes (called hourglassing) which may lead to individual elements being severely deformed due to lack of bending resistance in certain bending modes. Abaqus deals with this problem by introducing artificial stiffness to the hourglass deformation modes.

6.5   Solution Techniques

When solving a nonlinear problem, the solution can not be found by solving a single system of equations (which is done in a linear analysis). This is due to the fact that the load-displacement curve not any longer will be linear. To account for this, the solutions needs to be approached stepwise such that nonlinear effects are taken into account in the solving process. The stiffness, K, will then be dependent on the displacement, r. The system equation given in equation 6.2 is on incremental form given

$$K_I(r)\Delta r = \Delta R \tag{6.7}$$

where ΔR is the load increment and Δr is the displacement increment. Various techniques for solving nonlinear problems exist. These can be divided into three main groups: incremental (or stepwise), iterative and combined methods.

6.5.1   Load Incremental Methods

Load incremental methods finds a solution of a non-linear problem by applying the external loading stepwise. For each load step, R_{m+1}, a displacement increment Δr_{m+1} is found. The total displacement is found by summing all increments. The incremental stiffness, K_I, is found as a function of the displacement before applying the new load increment. The solution is found by the following set of equations.

$$
\begin{aligned}
\Delta R_{m+1} &= R_{m+1} - R_m \\
\Delta r_{m+1} &= K_I(r_m)^{-1}\Delta R_{m+1} \\
r_{m+1} &= r_m + \Delta r_{m+1} \\
r_0 &= 0
\end{aligned}
\tag{6.8}
$$

The Euler-Cauchy incremental method is illustrated in figure 6.6. It is seen that the solution found deviates from the exact solution and total equilibrium will therefore not be fulfilled. The accuracy can be improved by reducing the size of the load increments. In addition to this, an improvement to the method is achieved be enforcing total equilibrium after each incremental step. This can be achieved by adding the unbalanced forces, R_{eq}, to the next increment, reducing the external forces and thus restoring global equilibrium. The method is expressed with the following set of equations

$$
\begin{aligned}
\Delta R_{m+1} &= R_{m+1} - R_m \\
R_{eq} &= R_m - R_{int}(r_m) \\
r_{m+1} &= K_I(r_m)^{-1}(\Delta R_{m+1} + R_{eq}) \\
r_{m+1} &= r_m + \Delta r_{m+1}
\end{aligned}
\tag{6.9}
$$

where $R_{int}(r_m)$ is the internal force vector which needs to be calculated for each step. The method is illustrated in figure 6.7.
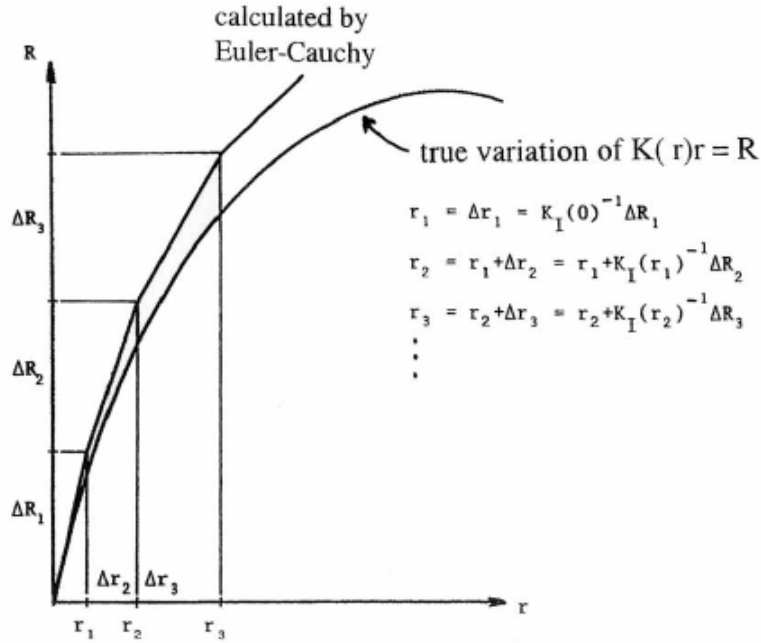
Figure 6.6: Euler-Cauchy incrementing procedure (Moan, 2003b).
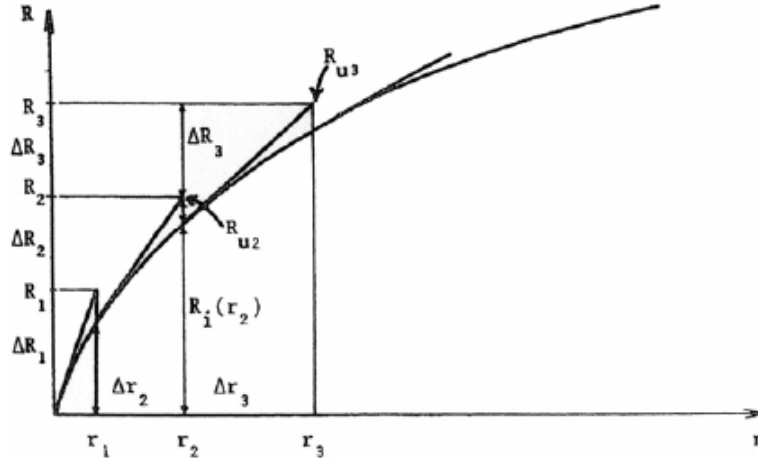
Figure 6.7: Euler-Cauchy incrementing procedure with equilibrium correction (Moan, 2003b).

6.5.2 Iterative Methods

In iterative methods it is the displacements which is applied stepwise, and not the load which is the case in load incremental methods. The stiffness used is kept constant during each step but needs to be updated during the analysis. Doing this for each time step would be really time consuming so methods were this is done less frequently are more common. The most used

iterative method is the Newton-Raphson method. The relationship between the stress and stain increments is found by the iteration formula given by the expression

$$r_{n+1} = r_n - K_I^{-1}(r_n)(R_{int} - R) \tag{6.10}$$

The method requires that K_I is established and that the displacement increment for the next iteration, r_{n+1}, is found from

$$R - R_{int} = K_{I(n)} \Delta r_{n+1} \tag{6.11}$$

The iteration is stopped when the accuracy is acceptable. The criterion for convergence may be expressed on the form

$$\| r_{n+1} - r_n \| < e \tag{6.12}$$

where e is a small, positive number. The Newton-Raphson method is illustrated in figure 6.8. In the specific example, K_I is updated after each step. Since this is time-consuming an option is to update K_I less frequently. This is called a modified Newton-Raphson method and will, if done in a good way, only give a limited loss in rate of convergence.
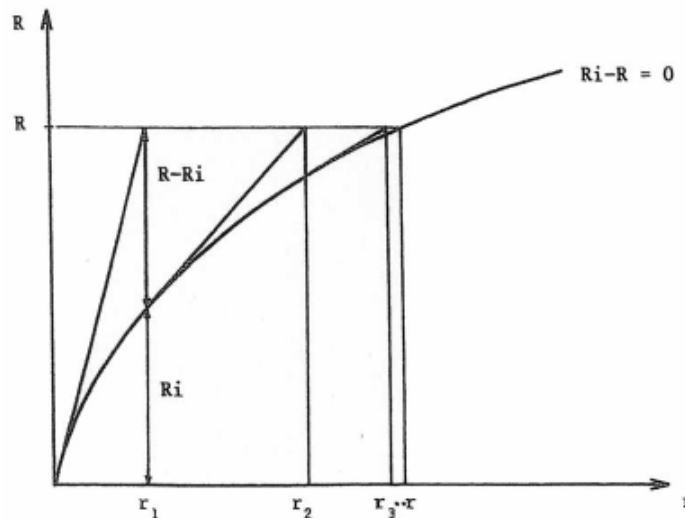
Figure 6.8: Newton-Raphson iteration procedure (Moan, 2003b).

6.5.3 Combined Methods

Abaqus solves nonlinear problems by using a combination og incremental and iterative methods. Such a combination of methods is often applied in computational programs. The load is then applied in increments, and for each step equilibrium is achieved by an iterative process.

Figure 6.9 illustrates a combination of Euler-Cauchy incrementation and a modified Newton-Raphson method. The solution is in this case found by applying the load according to the Euler-Cauchy procedure described in equation 6.8, followed by an iteration after each load increment by using equation 6.10.
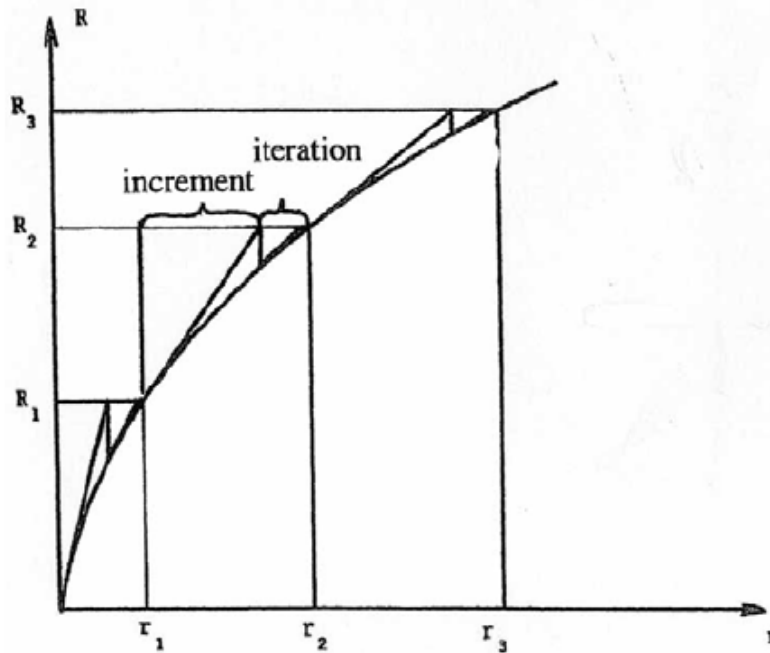
Figure 6.9: Combination of incremental and iterative procedures (Moan, 2003b).

Chapter 7

Modeling and Setup of Analyses

The models used in the analyses were created in Abaqus. Alternatively, a design software like SolidWorks or Catia could have been used. However, to avoid the process of importing and exporting files between different softwares, Abaqus was used both for the modeling part and the analyses.

Three models will be considered. The main model (here called the local model) is a model of 1/16 (or 22.5 degrees) of the outer wall of the Sevan Arctic MODU. From this model, a submodel is extracted, which is used when small areas are investigated. Finally, a larger model (here called the global model) is made as an assembly of three identical local models.

7.1 Local Model

The local model is a model of 1/16 (or 22.5 degrees) of the outer wall of the Sevan Arctic MODU. It is modeled based on drawings provided by Sevan Marine, taken from Haugen (2014). These are given in appendix B. The drawings do not include many details. Cutouts, small openings and other details which in reality would be found on the structure are not included.

7.1.1 Structural Dimensions

The outer hull plating has a thickness of 34 mm. The thickness of the inner decks and bulkheads are 24 mm. The outer plating is stiffened with T450x18x100x40 stiffeners with a spacing of approximately 400 mm (this value is not constant due to the shape of the hull). The stiffeners used in other parts of the structure have smaller dimensions and a spacing of approximately 800 mm. The local model is given in figure 7.1 and shows the thicknesses of the outer plating, decks and stiffeners. More figures showing details from the same model are given in appendix C.1.

Sections	Color
t 12 mm	
t 15 mm	
t 18 mm	
t 20 mm	
t 24 mm	
t 25 mm	
t 30 mm	
t 34 mm	
t 40 mm	
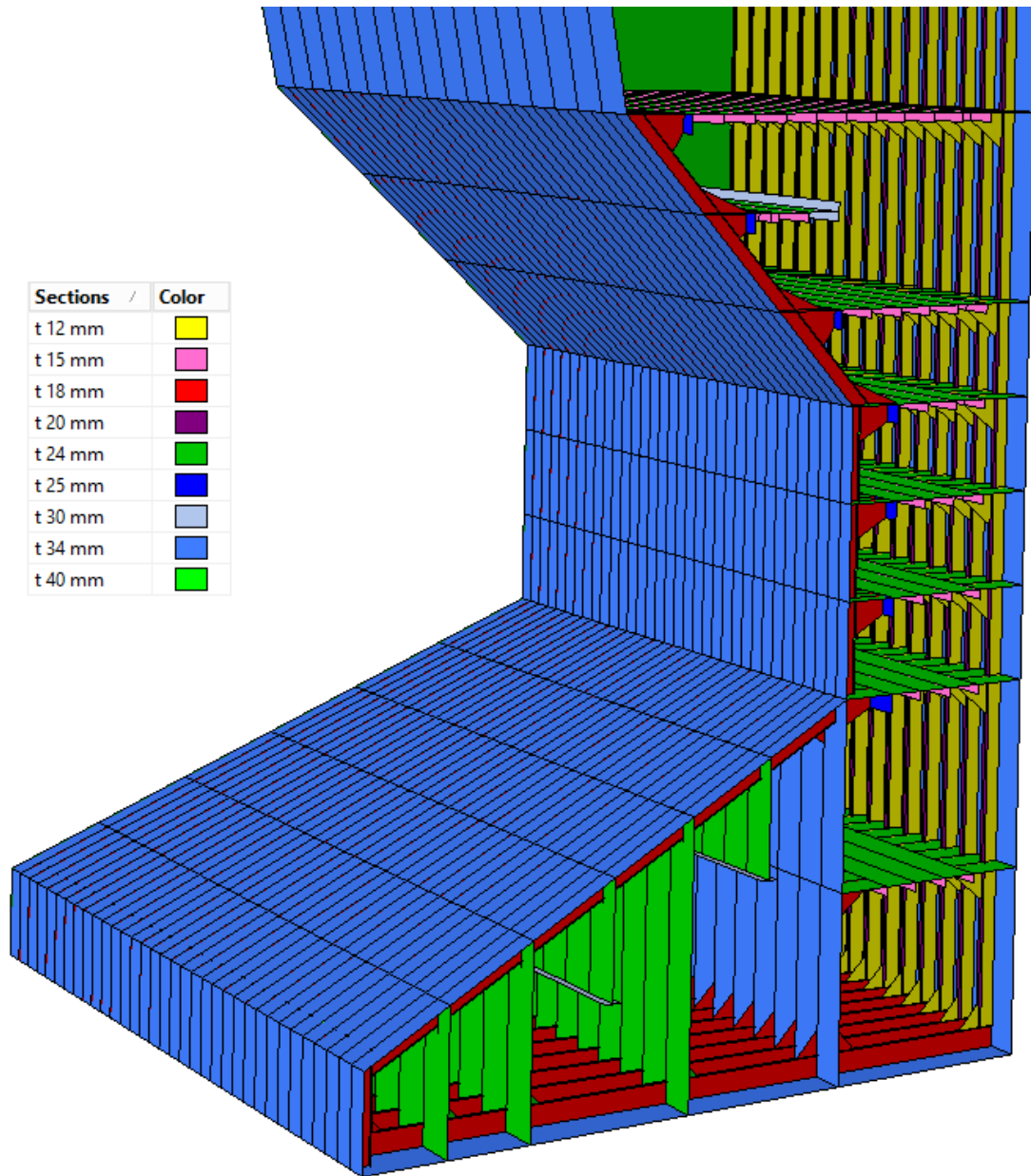
Figure 7.1: Main part of local model, showing thicknesses of plating and stiffener dimensions.

7.1.2 Boundary Conditions

Choosing realistic boundary conditions is essential for assuring accurate results. The boundary conditions used should represent the real condition in a realistic way. When simplifications are introduced (which is almost always the case), it is important to know that this gives results that are accurate or on the safe side (for example that calculated stresses are slightly overestimated). The boundary conditions used with the local model are based on natural structural restraints in the structure. The outer wall sections are separated with bulkheads, as illustrated in figure 7.2. It is assumed that the stiffness from the bulkheads and the adjacent wall sections restrains

the boundaries of the wall section from rotation and translation in all directions. An alternative to this is to allow rotation or translation in one or several directions at the boundaries. The boundary along the inner wall is assumed to be free. A better choice would probably be to set these as totally fixed due to the stiff inner structure. However, the area close to the inner structure is outside the area of main interest. This choice should therefore not have a major influence on the results.
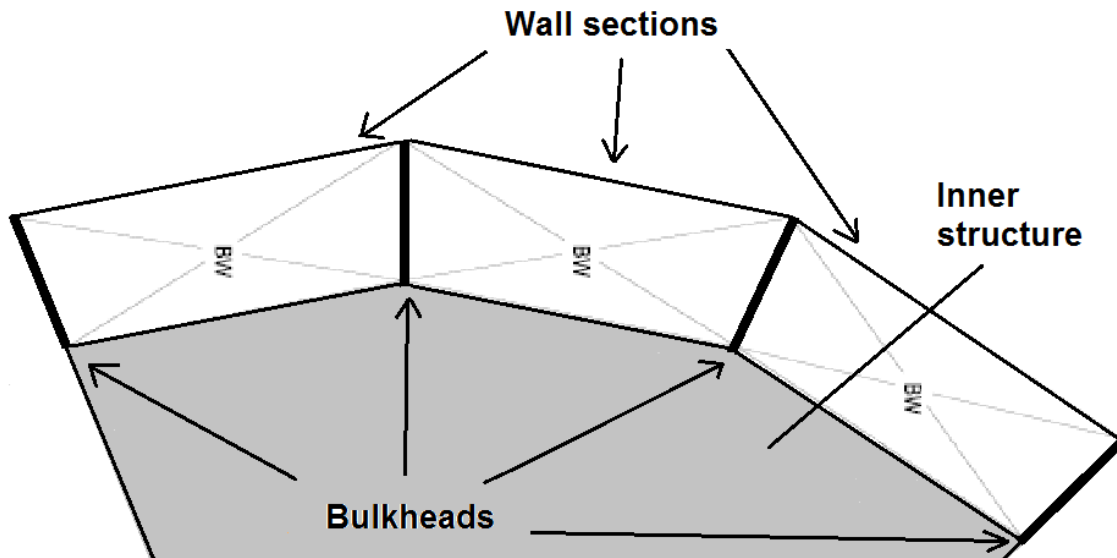

Figure 7.2: Location of local model (seen from above) illustrating the support from the surrounding structure.

7.1.3   Modification of Stiffeners in Decks

Figure 7.1 shows the local model based on the drawings provided by Sevan Marine. In these drawings, the decks are stiffened with stiffeners running perpendicular to the direction of the incoming ice. This will most likely lead to large deformations and stresses in the decks closest to the impact area. A small geometry modification is therefore proposed, where the deck stiffeners are rotated 90 degrees. With this configuration the stiffeners are oriented parallel to the force instead of perpendicular to it. The two different deck configurations are shown in figure 7.3.

An analysis is performed to see how the different deck configurations behave for a typical load condition. Figure 7.4 shows a submodel of the local model presented in figure 7.1. The model is extracted from the local model and includes everything from elevation 8.0 to 20 meters (the elevation of the different decks can be seen in the drawings in appendix B). A submodel is used since this reduces the computational time compared to if the larger local model was being used. In addition to this, the results from this analysis does not need to be very accurate since the goal just is to compare the two configurations. A pressure is applied over an area on the sloping surface of the structure, seen as the red area in figure 7.4. Boundary conditions are applied as described in section 7.1.2.
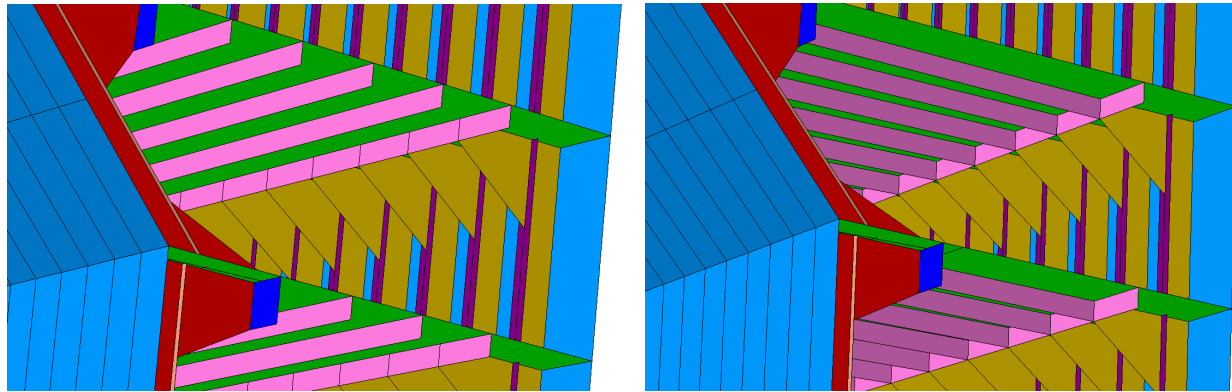
(a) Initial geometry: Stiffeners running perpendicular to the incoming force.

(b) Modified geometry: Stiffeners running parallel to the incoming load.

Figure 7.3: Initial and modified deck configurations.
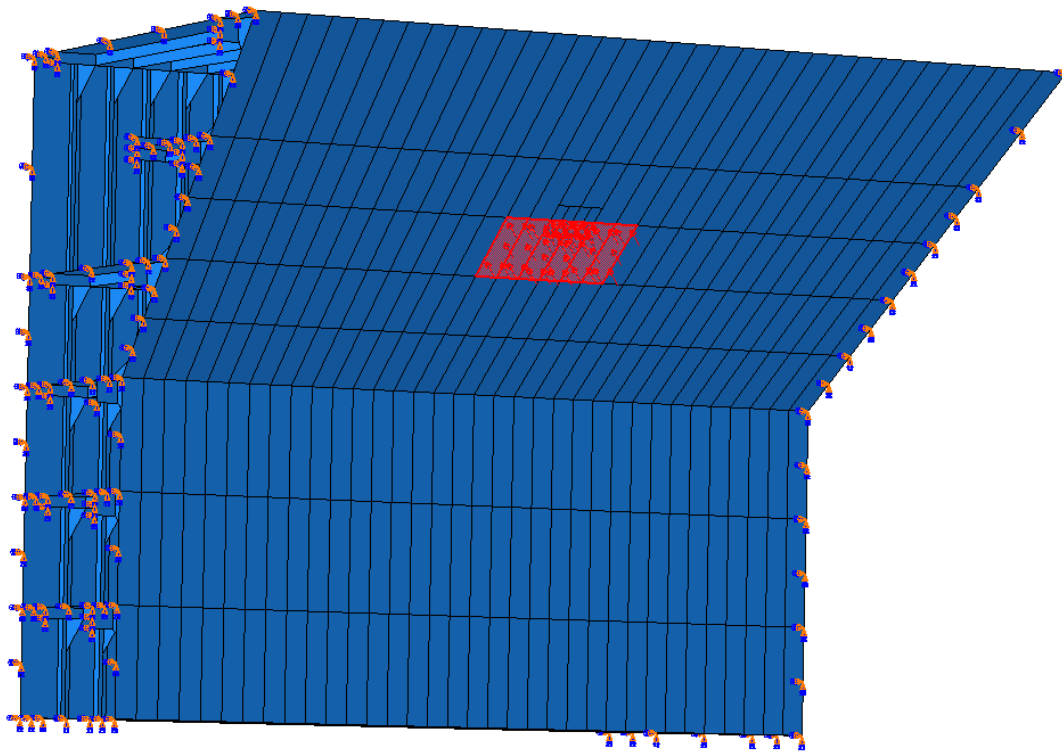
Figure 7.4: Submodel extracted from the local model.

The applied pressure is gradually increased (from zero pressure) up to a level of 8 MPa. A load of 8 MPa does not necessarily represent a realistic loading condition, but the goal is here only to see how the two designs behave for the different magnitudes of applied load. The two designs show similar behavior up to a pressure of around 4 MPa. Up to this point the major part of the forces is dissipated by the plating and stiffeners in the sloping side. When the pressure is increased further, a rapid increase in the deck deflection is seen in the model based on the initial design. This leads to yielding in stiffeners and plating in a large area of the deck. Figures 7.5

and 7.6 show the stress distributions for an applied pressure of 8 MPa for the initial and new design, respectively. Figure 7.5 clearly shows the drawback with the initial design. The stiffeners give little contribution to the stiffening of the deck, resulting in high stresses developing in both the deck plating and the stiffener system. Stress distributions for other load amplitudes can be found in appendix D.2. The modified structure will be used in the analyses since it clearly is an improvement of the initial design.
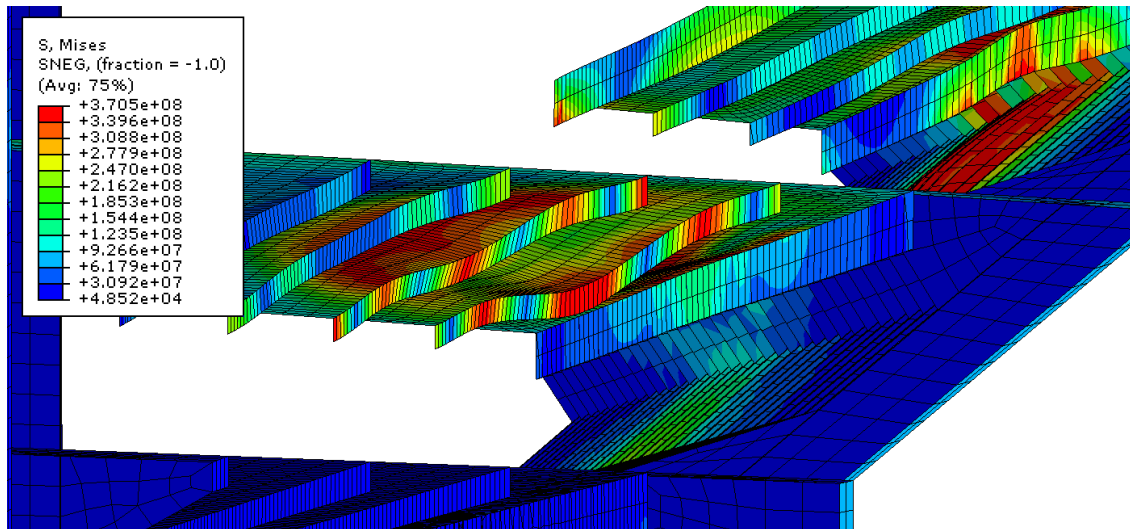

Figure 7.5: Stress distribution for structure with initial deck configuration at an applied pressure of 8 MPa (DSF = 2).
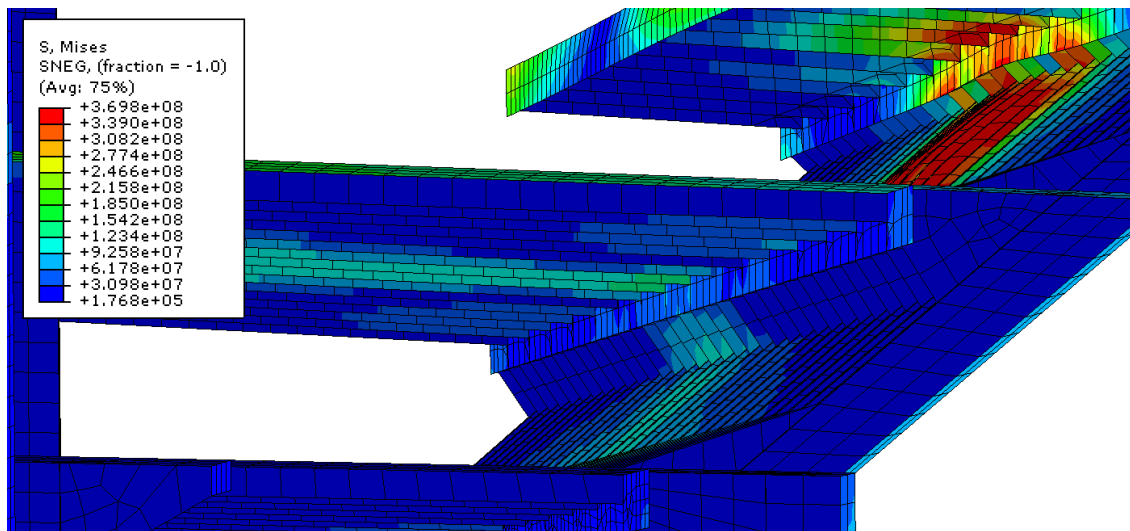
Figure 7.6: Stress distribution for structure with modified deck configuration at an applied pressure of 8 MPa (DSF = 2).

7.2 Global Model

The global model is made by assembling three copies of the local model section shown in figure 7.1. This corresponds to 3/16 (or 67.5 degrees) of the outer wall of the platform. The different sections are separated by vertically bulkheads as illustrated in figure 7.2. Figure 7.7 shows the global model. Figure 7.8 shows the location of the global model in the whole structure.
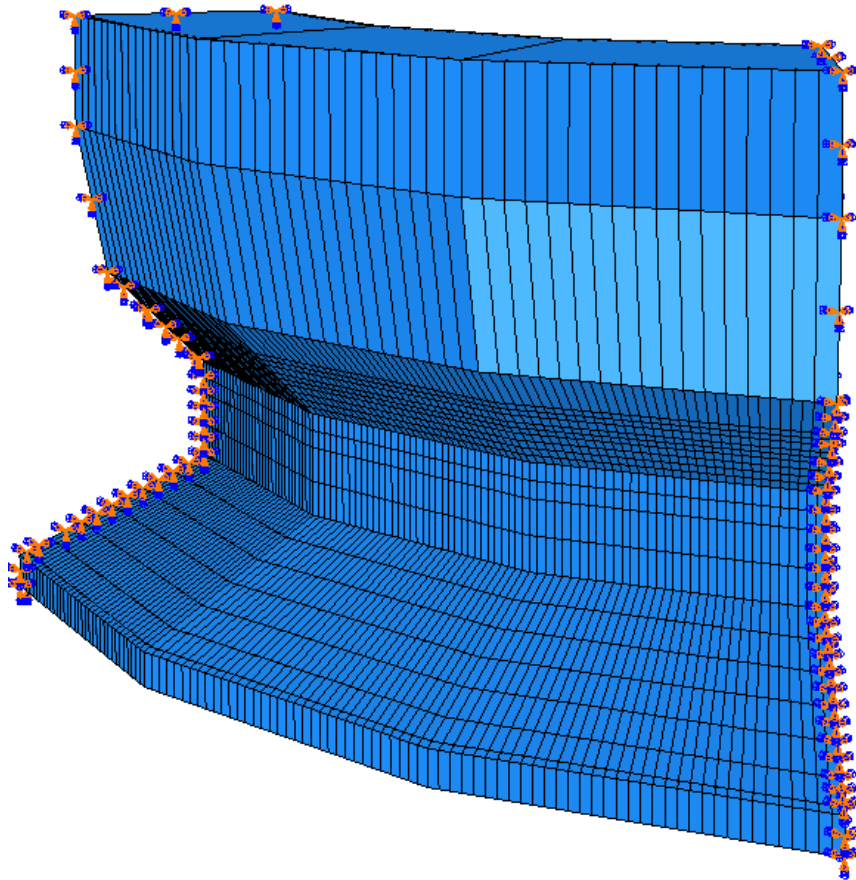
Figure 7.7: Global model.

7.3 Mooring System

The Sevan Arctic MODU is moored with mooring lines divided into four clusters, spread evenly around the hull (see figures 7.9 and 7.10). The unit has the possibility to disconnect, which gives the ability to leave the site when unmanageable ice features approach. Each mooring line has a given rupture capacity. The total load the mooring system can take before it ruptures depends on the direction of incoming ice load. For a scenario where the incoming load has the same direction as of one of the mooring clusters (see figure 7.11b), less offset of the platform from initial position will be seen compared to a scenario where the incoming load direction is different (see
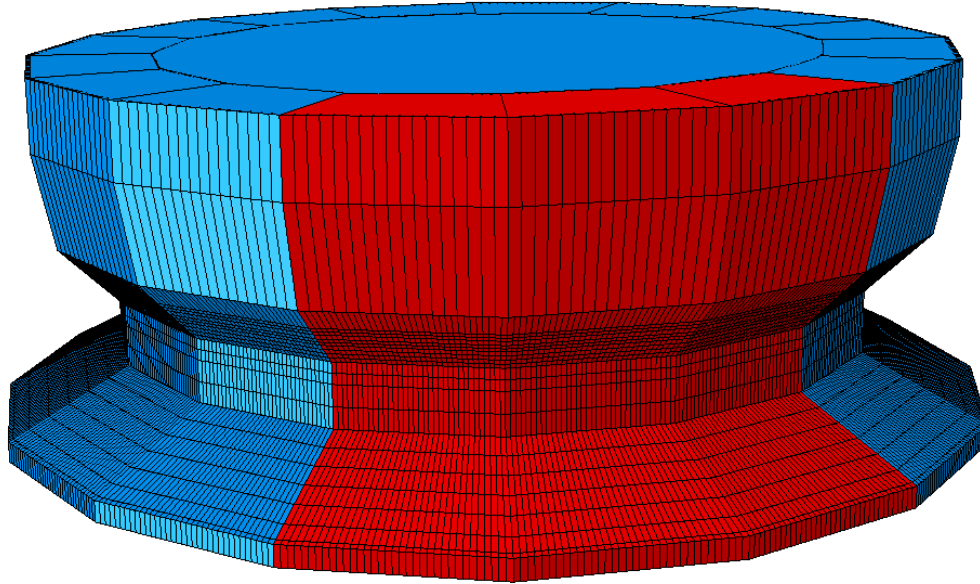
Figure 7.8: Location of global model (red part) in hull structure.

figure 7.11a). The scenario illustrated in figure 7.11b will lead to the largest forces in the mooring system, and therefore rupture at an earlier stage. In an accidental collision this can be favorable since the rupture of the mooring lines may lead to lower force acing on the hull. However, the static holding capacity will in the two scenarios approximately be the same. The difference in the stiffness of the system will mainly be seen in the dynamic of the system. According to Sevan Marine (Glomnes, 2015), a reasonable approximation for the holding capacity is a 45 MN load acting horizontally on the hull.
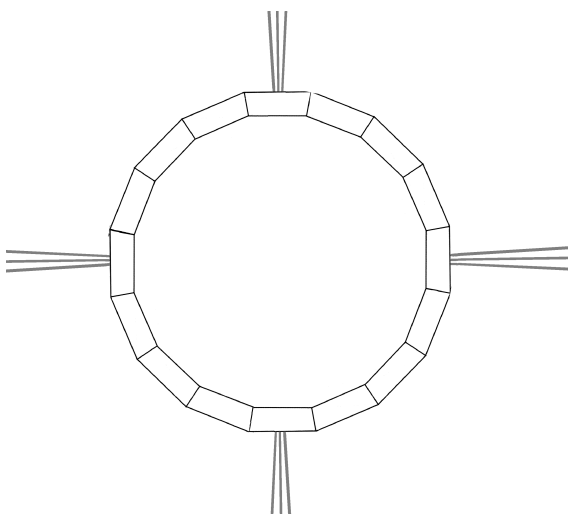
Figure 7.9: Illustration showing mooring system on the Sevan Arctic MODU.
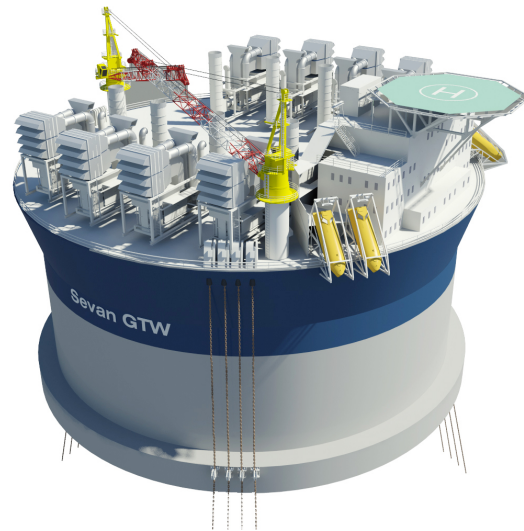
Figure 7.10: Sevan platform showing typical mooring system (sevanmarine.com).

(a) Incoming load not parallel to mooring line cluster.

(b) Incoming load parallel to mooring line cluster.
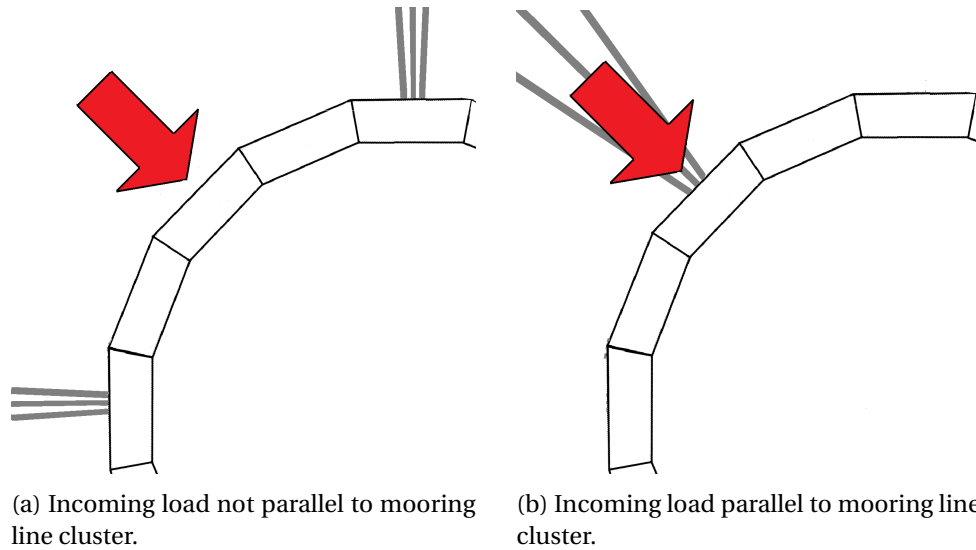
Figure 7.11: Direction of incoming load relative to direction of mooring lines.

7.4 Material Properties

The hull of the structure is to be constructed in S355 carbon steel. This steel grade is commonly applied in the marine industry and has a yield strength $\sigma_{yield} = 355 MPa$. The material is modeled in Abaqus as elastic-plastic. The stress-strain curve is taken from DNV (2013a), which provides recommendations for material properties to use in non-linear FEM analysis. The material data for S355 construction steel is given in table C.1 in appendix C.2. DNV (2013a) recommends to use thickness-dependent curves. A stress-strain curve relevant for plate thicknesses ranging from 16 mm to 40 mm is implemented, since this thickness range covers most parts of the structure.
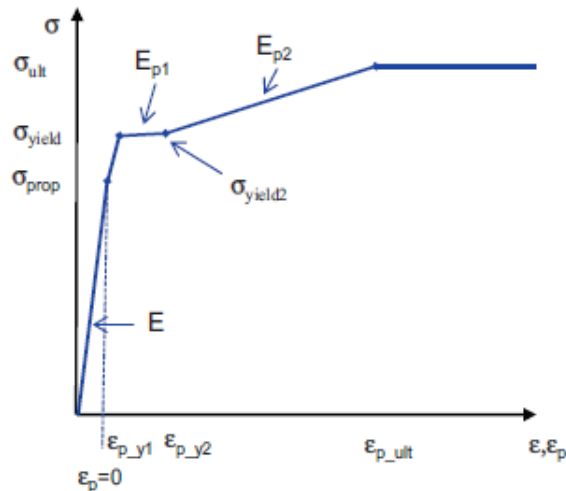
Figure 7.12: Stress-strain relationship for typical steel material (DNV, 2013a).

The material curves given in DNV (2013a) have the shape shown in figure 7.12. It is seen that the shape is significantly simplified compared to a real material curve since few data points are used to define it. Especially is the behavior in the strain hardening region idealized. The curve is based on engineering stress and strain, meaning that the values are calculated based on the initial cross-section of the test specimen used. The following elastic properties are used:

- Young's modulus, $E = 2.1GPa$

- Poisson number, $\nu = 0.3$

- density, $\rho = 7050kg/m^3$

7.5 Convergence Analysis

Convergence test are used to assure that the obtained solutions are within reasonable limit from the correct solution. The computational time and disk space required increases with number of elements in the model and the order of the elements. In FEM, approximations of the strains and stresses are found by applying polynomial functions within each element. In general, a refinement of the mesh will provide convergence of the results. In addition to this, the element type, i.e. the order of the polynomials applied, and the integration rule affect the result. The goal is to find a combination of element type and mesh size that give sufficiently accurate results at a reasonable computational cost. A well designed mesh will give good results and be economical in the sense of computer resources. A bad designed mesh may give inaccurate (and even wrong) results, possibly at a high cost.

When choosing an element type, several factors need to be considered. DNV (2013a) provides a list of points that should be considered when selecting element types for use in nonlinear FEM analysis.

- shell elements or solid elements

- elements based on constant, linear og higher order shape functions

- full vs. reduced vs. hybrid integration points

- number of through thickness integration points

- volumetric locking, membrane locking and transverse shear locking

- hourglas contro/artifical strain energy (for reduced integration elements)

In the following, the effect of using different element shapes (triangular vs. rectangular) and integration rule (fully vs. reduced) will be investigated. The elements considered are presented in section 6.2.3. The element types were chosen because of the difference in shape and integration order. The convergence analysis are performed on four mesh sizes (200, 100, 50 and 25 mm) and for three element types. The mesh is refined by dividing the characteristic length of the elements of the precious mesh in two, which means that the old mesh is contained in new one. This approach should assure a monotonic convergence (Moan, 2003a).

7.5.1 Setup

The convergence test is performed on the submodel shown in figure 7.4. A pressure load with magnitude of 1.5 MPa is applied over the red load area seen in the same figure. The values of the displacement and stress are measured at two points on the model, denoted as *Point A* and *Point B* in figure 7.13. Point A is located at the flange of the middle stiffener where high stresses are expected to occur. Point B is located in the deck at elevation 10 m. The two points are chosen to see if convergence of the results are found both in areas with high and low (relative to the maximum) stresses. It is assumed that convergence of stresses and displacements in the these points indicates that the result converge in general. Ideally there should have been checked for convergence also for higher loads resulting in stresses close to or above the yield limit of the material. This is because higher stresses and stress gradient in general will call for finer mesh to get the same accuracy Abaqus (2014).
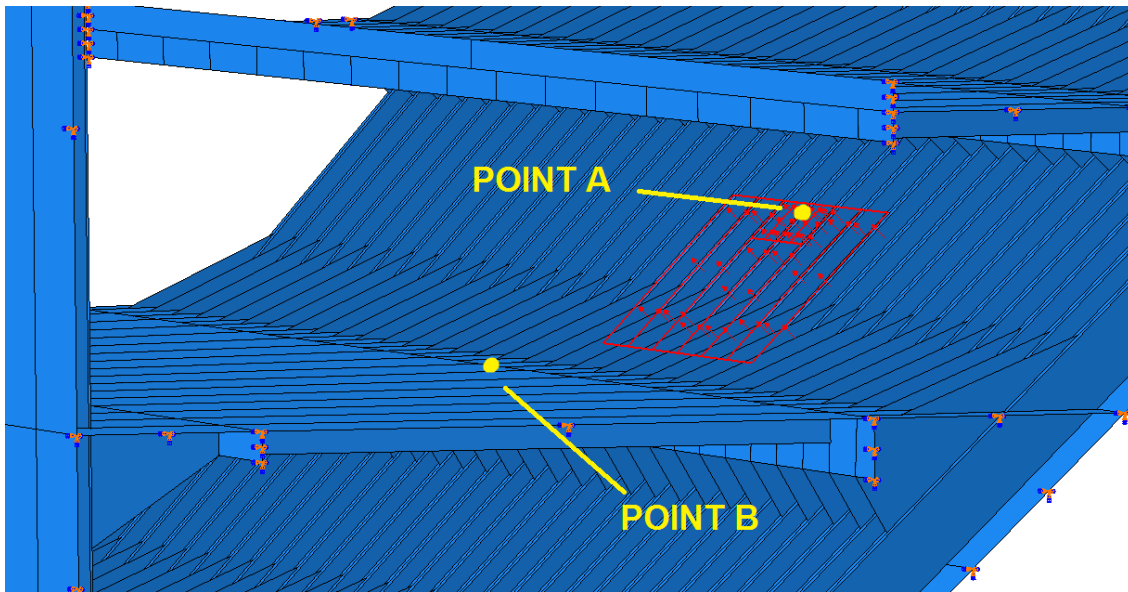
Figure 7.13: Submodel used in convergence analyses showing the points where stress and displacement values are measured.

7.5.2 Results and Conclusion

In figure 7.15 and 7.14 the stress and displacement in point A are plotted against the mesh size. The graphs show that for both the stress and displacement the S4 element, which uses a second order integration rule, converges at a lower mesh size than the elements which uses reduced integration. The drawback with the use of the S4 element is that the analyses are more computational demanding than the S4R and S3R.

The S3R element shows the slowest convergence rate of the three element types tested. This is due to the way the bending and membrane strains are approximated in the element, as mentioned in section 6.2.3. The fact that a finer mesh is required to achieve the same accuracy as the

S4 and S4R elements are therefore expected. The S4R element shows good signs of convergence in stresses and displacements at both point A and B. At a mesh size of about 100 mm the element give good results. The measured values of the stress and displacements are given in table D.1 in appendix D.1. The same appendix also includes the graphs for the stress and displacement measurements at point B. These show similar result as for point A. However, the displacement and stress for the S4R element converges from a low value for point B whereas convergence from a high vale is seen at point A (see figure 7.15 and 7.14). The result for mesh size 200 mm should therefore not be taken as conservative, which seems to be the case when looking at the result at point A.
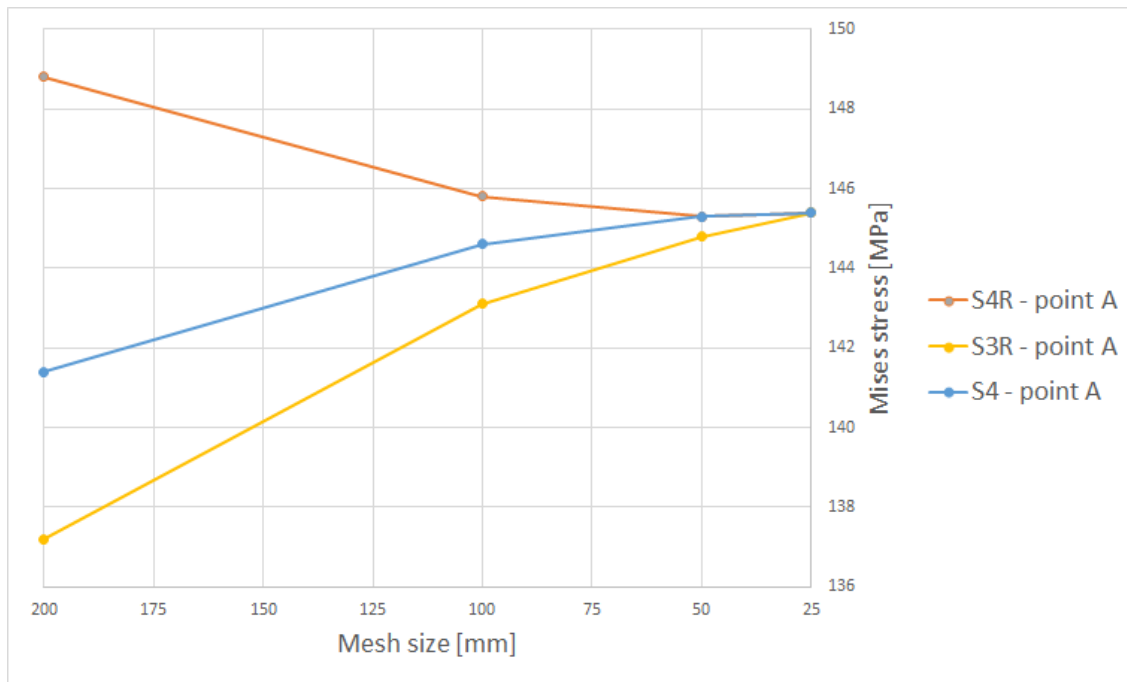
Figure 7.14: Convergence of stresses at point A.

For complex geometries, quadrilateral elements (like the S4 and S4R) have a problem with adapting to the geometry. In such ares triangular elements can be used in combination with quadrilateral shaped elements. The triangular elements are also useful to model transitions between areas with different mesh sizes. In the analyses, the geometry will be meshed with S4R elements with an approximately size of 200 mm. This is because the convergence analysis show that this provides sufficiently accurate results at a reasonable computational cost. S3R elements are applied where appropriate. This is for example the case at brackets, as shown in figure 7.16.
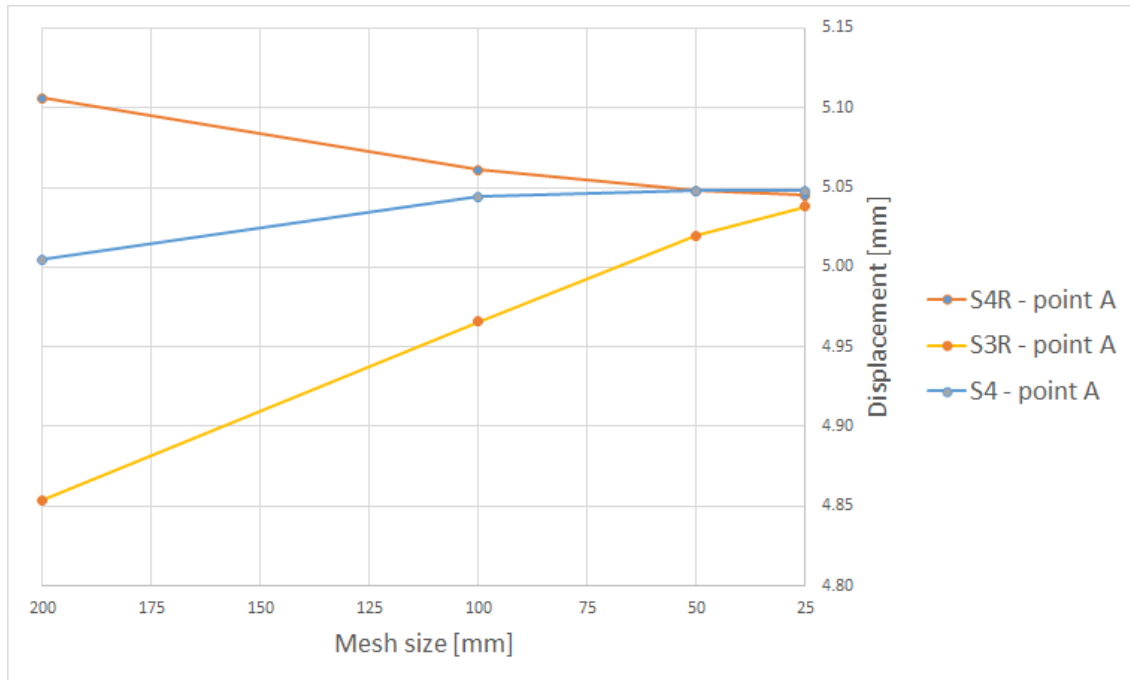
Figure 7.15: Convergence of displacement at point A.

Figure 7.16: Quadrilateral mesh with size of approximately 50 mm.

7.5.3 Singularities at Bracket Toes

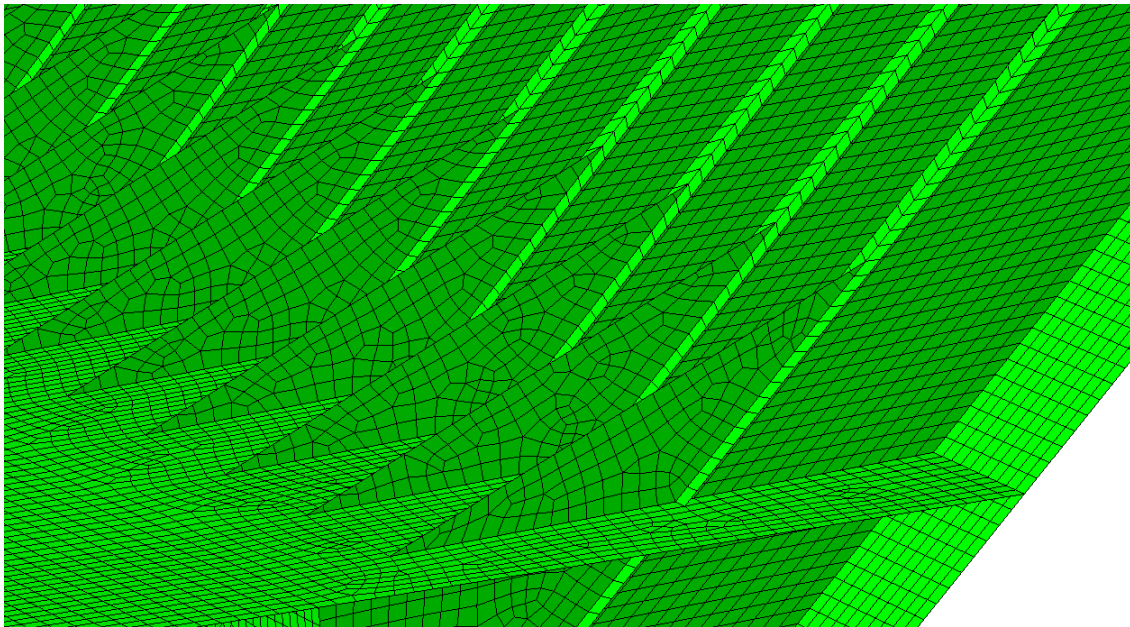From the results of the convergence analysis, a problem with singularities is found to occur at some bracket toes. An example of this is shown in figure 7.17. Brackets are introduced in the structure to reduce or avoid sharp corners in the design. The brackets helps smoothen out

stresses at points where stiffeners or other structural members meet. In the model used in this thesis the brackets are modeled as triangular shapes since these are easier to model. In reality the brackets used are rounded, which can be seen in the drawings in appendix B.

Points of singularity is found at some bracket toes at the stiffeners closest to the applied load. When reducing the mesh size, the extent of the highly stressed areas decreases, but the maximum stresses due to singularity will be higher. No adjustment of the geometry will be done to reduce the spurious stresses found at some locations. Instead, it will be kept in mind when interpreting results from the analyses.
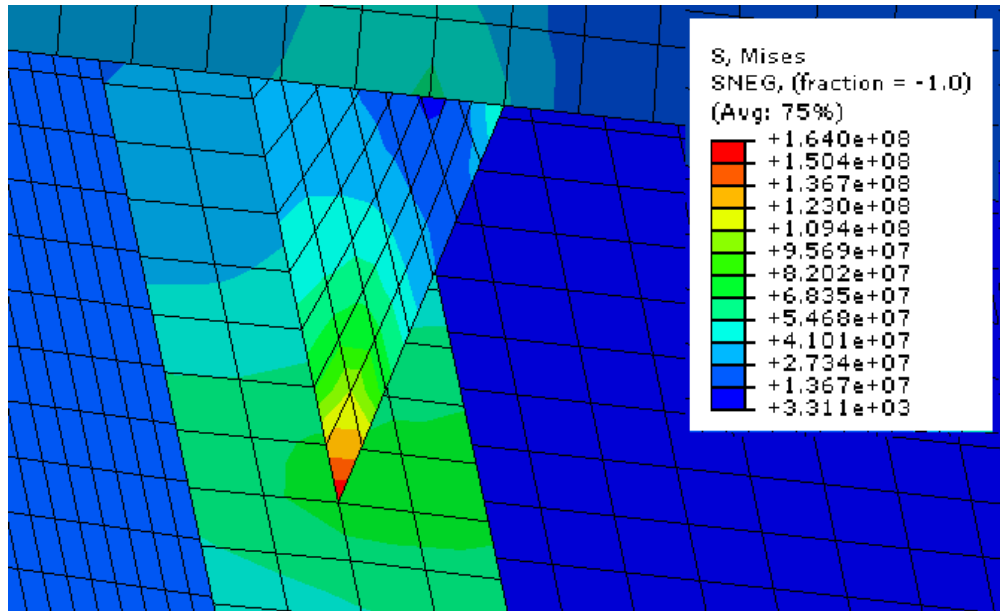
Figure 7.17: Example of singularity point at bracket toe.

7.6 Solution Procedure

The analyses are performed as static and nonlinear. The load is applied as uniform pressures over rectangular load areas. Abaqus uses Newton's method (see section 6.5) to solve nonlinear problems. Abaqus is given the control to choose the necessary size and number of load increments and the number of equilibrium iterations. It will then solve the problem in a way that assures sufficient accuracy at a reasonable computational cost. When using this incrementation rule, Abaqus will contentiously try to increase the size of the applied load increment. This typically leads to a point where the increment get to big for equilibrium to be achieved. The size of the increment is then decreased, and a new attempt is made. For most of the analyzes the necessary size of the increment is found to be in the range of $2*10^{-2}$ to $1*10^{-1}$ s when total solution time is set to 1.0 s.

7.7 Failure Criteria

7.7.1 The von Mises Yield Criterion

The yield condition of a material defines the limit of purely elastic behavior under any combination of stresses. The von Mises yield criterion is the most used design limit state for steel materials. For plane stress problems, i.e. a 2D stress condition with $\sigma_3 = 0$, the von Mises stress is given as

$$\sigma_{mises} = \sqrt{\sigma_1^2 + \sigma_2^2 - \sigma_1\sigma_2 + 3\tau_{12}^2} \tag{7.1}$$

where σ_1 and σ_2 are the in-plane stresses and τ_{12} the shear stress. The criterion states that the material yield if

$$\sigma_{mises} > \sigma_y \tag{7.2}$$

where σ_y is the uniaxial yield strength of the material.

7.7.2 Fracture

For most metals, fracture relates to the formation of microvoids which grow and eventually make a larger void. These voids often form in areas with flaws or in areas where large deformations occur. The rate of which the voids grow is controlled by the deformation and the stress triaxiality in the material at the area. When voids coalesces small cracks eventually form, and the material have reached the state where fracture is initiated. The stress triaxiality, T, is defined as

$$T = \frac{\sigma_{mises}}{\sigma_h} \tag{7.3}$$

where σ_h is the hydrostatic stress defined as

$$\sigma_h = \frac{1}{3}(\sigma_1 + \sigma_2 + \sigma_3) \tag{7.4}$$

Growth of cracks is often associated with the damage variable D. Damage initiation defines the starting point of the degradation of the stiffness. Several models for simulation of rupture exist. The easiest is the approach of failure initiation at some critical equivalent strain. This can easily be implemented into FE codes such as Abaqus. However, this completely neglects the stress triaxiality, showing constant ductility for all variations of stress triaxiality. This is seen as unphysical because it will lead to fracture in pure compression as easily as in tension (Alsos and Amdahl, 2007).

A damage model in the form of the RTCL (Rice-Tracey-Cockcroft-Lathem)-criterion is adopted. This model applies a combination of the Cockcroft-Latham damage model and the Rice-Tracey void growth criterion, which both are functions of the hydrostatic stress state. Together they form a damage criterion which cover the full stress triaxiality range. The expression is given as

$$D = \begin{cases} \int \frac{\sigma_1}{\sigma_{mises}} d\varepsilon_{eq} & \text{if } -\frac{1}{3} \leq T \leq \frac{1}{3} \\ \int \frac{1}{C} exp(\frac{3}{2}T) d\varepsilon_{eq} & \text{if } \frac{1}{3} \leq T \end{cases} \tag{7.5}$$

where $d\varepsilon_{eq}$ is the effective plastic strain increment. C is a factor for which a value of 1.65 has shown good behavior of the RTCL model (Alsos and Amdahl, 2007). Figure 7.18 shows the curves for the RTCL damage and equivalent plastic strain criteria as a function of the stress triaxiality, with the failure strain normalized by the critical damage. The curves represent the limit for when fracture is being initiated.
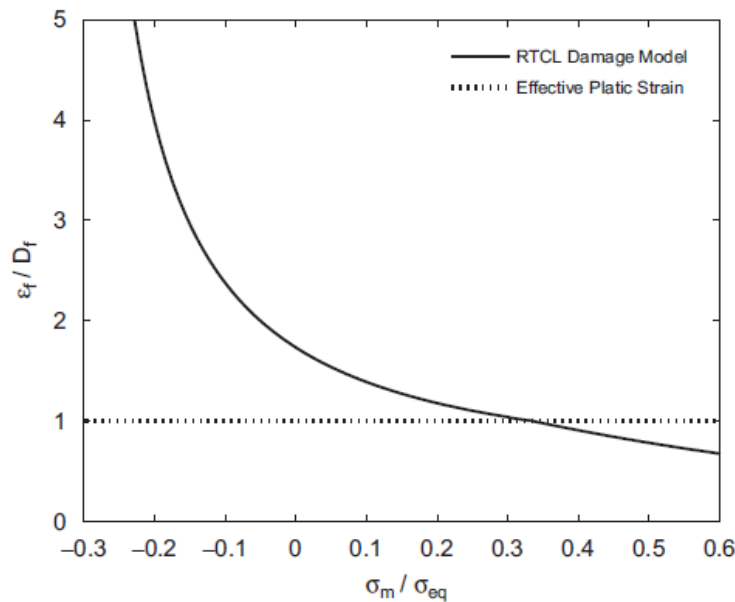

Figure 7.18: Curves for the RTCL damage citerion and the equivalent plastic strain criterion, as functions of the stress triaxiality. Failure strain response is normalized by the critical damage (Alsos and Amdahl, 2007).

Structural elements, and especially shells, are very mesh sensitive close to fracture (Alsos and Amdahl, 2007). This is due to the presence of high stress gradients, which causes the failure to take place at different damage values for different mesh sizes. A way of including the effect of element size is to use mesh sensitivity curves, which can be calculated from tensile test simulations for different mesh sizes. A mesh sensitivity curve for structural steel is given in figure 7.19. Figure 7.20 shows damage strain plotted against triaxiality for mesh sizes 50 mm and 200 mm. The curves are made from the curves in figure 7.18 and 7.19 and plotted for a plate thickness of 34 mm, which is the thickness of the outer plating ot the Sevan Arctic MODU. The data points for the curves are given in table C.2 in appendix C.2.
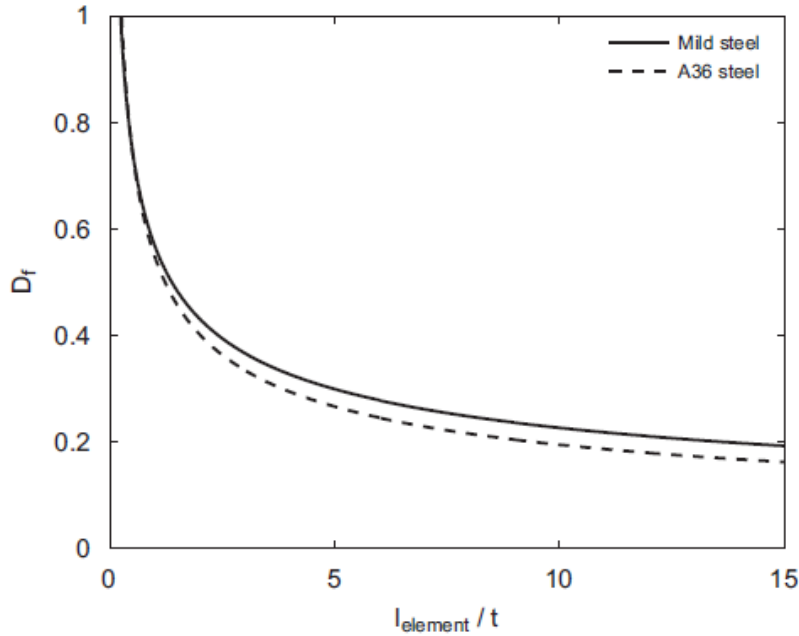
Figure 7.19: RTCL damage scaling. The scaling is a function of the element size (Alsos and Amdahl, 2007).
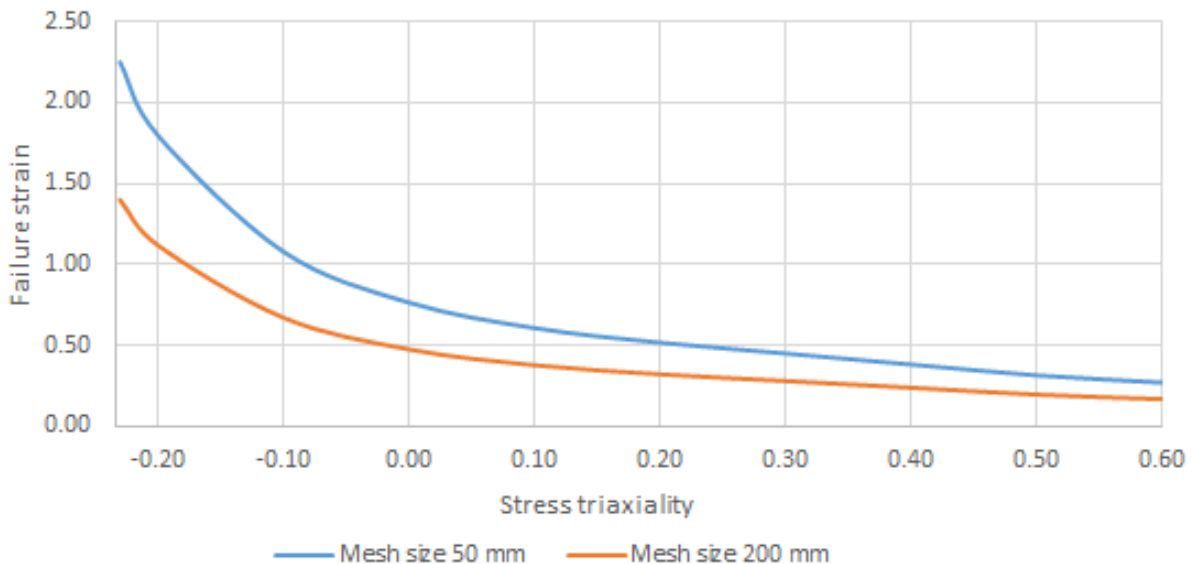
Figure 7.20: RTCL damage scaling. The scaling is a function of the element size.

Abaqus offers the possibility for modeling progressive damage and failure in a structure. The RTCL criterion is implemented as a ductile damage model, which uses equivalent strain and stress triaxiality to calculate the initiation of damage. If the response after a eventual damage initiation is of interest, then additional information is needed. In this thesis, it is seen as sufficient to see if fracture occurs or not, and not to investigate the structures behavior after an eventual damage initiation.

Chapter 8

Main Results

This chapter will present the result from the main analyses performed. The different loading cases are chosen to investigate some relevant loading conditions. In all the cases investigated, the load is applied as static pressures, applied normal onto the surfaces they work on. The following analyses have been performed:

- 8.1: IACS design load condition, including load condition where frame load pressure is applied over stiffener design area.

- 8.2: Capacity analysis for stiffener design area, performed for sloping and vertical section of the hull.

- 8.3: Area dependent loading condition applying the Masterson pressure-area relationship for determining the loads.

8.1   IACS Design Load Condition

The Sevan Arcti MODU is designed according to IACS PC 4, which is described in section 4.3.1. Based on the hull geometry given for the specific class, the design load pressure is calculated as 6.71 MPa. This load is to be applied over a rectangular area of 2.83 m^2. This gives a total force of 18.98 MN acting normal onto the hull. This is a significant load, but it is within the limit of what the structure can handle in terms of holding capacity of the mooring system (see section 7.3). In figure 8.1 this load area is shown as the red and yellow areas. The load is applied normal onto the sloping face. In the case of ice loads from level ice and small incoming ice features, the load would be working parallel with the waterline.

Figure 8.2 shows the Mises stress distribution in the stiffeners at the applied load. Several of the stiffeners are yielding, The maximum stress is 345.5 MPa, found in the center stiffener. The maximum stress in the plating is approximately 250 MPa, found in the center of the load patch (in the location of the yellow load patch in figue 8.1). The extent of the yielded area is significant. However, the magnitude of the stresses in the area is not too large. The design load is used

to determine necessary scantlings of structural members (higher calculated design loads yields larger dimensions). The calculated load should therefore represent the maximum load scenario for the given class. It is also noted that a design according to the requirements given in IACS (2011) allows some plastic deformations. The result from the analysis it therefore considered reasonable.
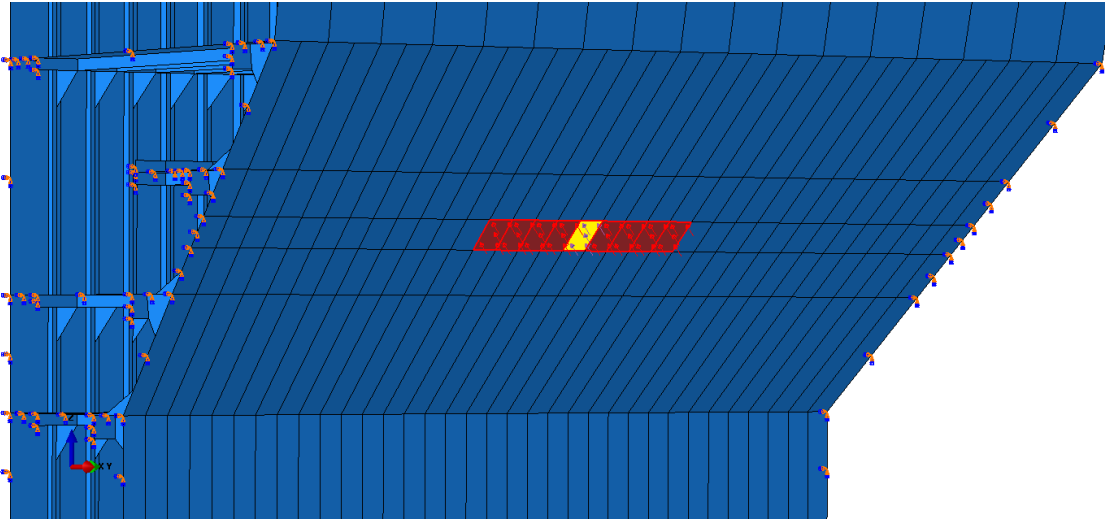

Figure 8.1: IACS PC 4 design load patch. The yellow area is the stiffener design load area. The total design load area is the combination of the yellow and red rectangular areas.
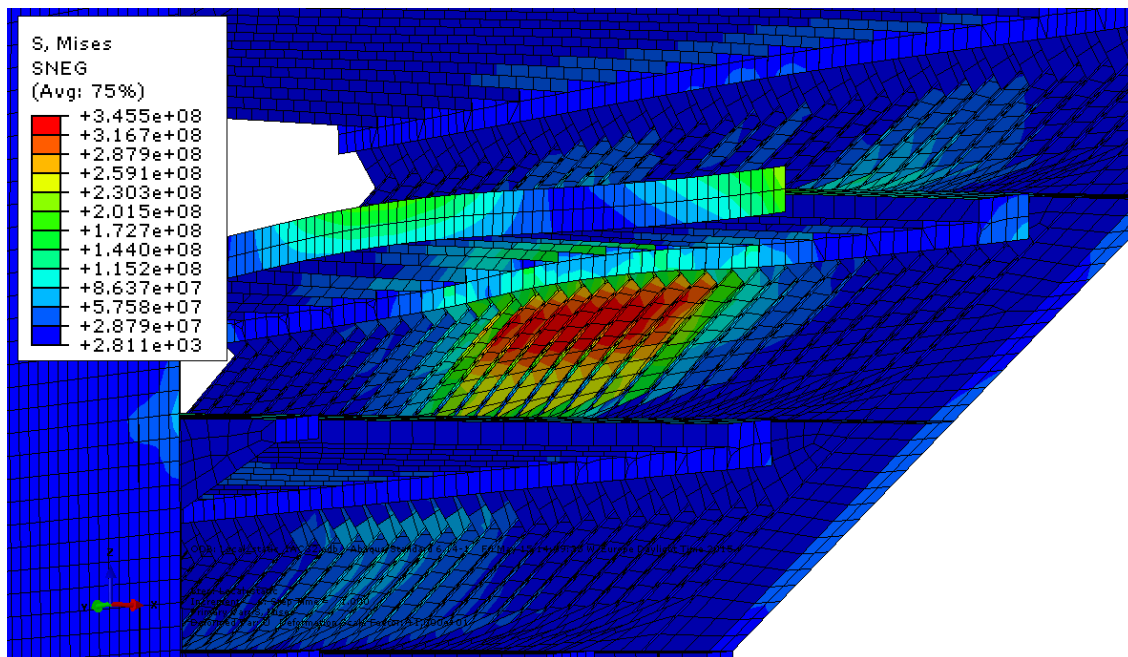

Figure 8.2: Stess distribution for IACS design load condition.

The structure is also checked for a pressure load when the stiffener design load is applied in combination with the design pressure (6.71 MPa) used above. This load is calculated to be 9.39

MPa (see section 4.3.1 for calculations), and is to be applied over a stiffener design area which has a width defined by the spacing of the stiffeners (see figure 4.4 in section 4.3.1). For the Sevan Arctic MODU the stiffener spacing in the ice draft area is 400 mm. The stiffener design loads is shown as the yellow rectangle in figure 8.1. For this loading condition the maximum stress is 345.7 MPa. This is similar to what was found when a pressure of 6.71 MPa was applied over the whole design area (see figure 8.2).

The results from the two load cases presented above are compared in terms of plastic strains. Figure 8.3 and 8.4 shows the plastic strains in the stiffeners for the two cases. In both the cases the plastic deformations are limited to the stiffeners that are in direct contact with the loaded plate area. It is seen that the effect of including the stiffener design pressure only give a small increase in the extent of plastic deformations. Instead, the magnitude of the plastic strains already present in the first case increases.
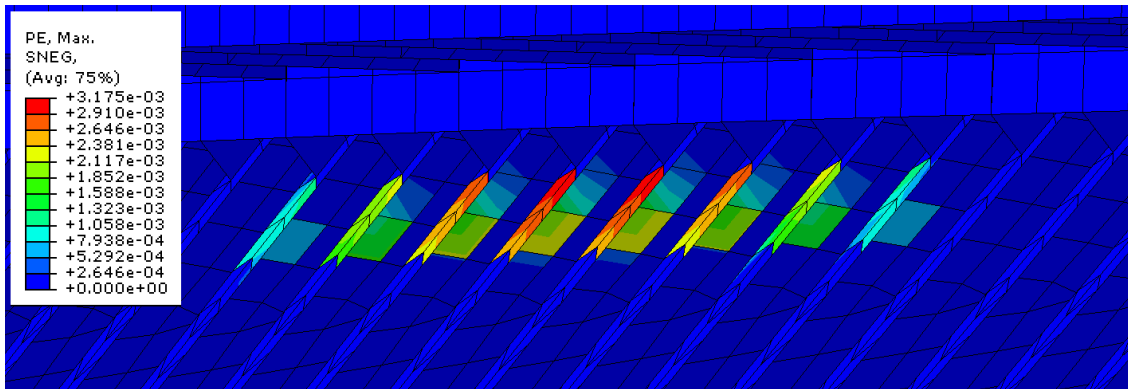

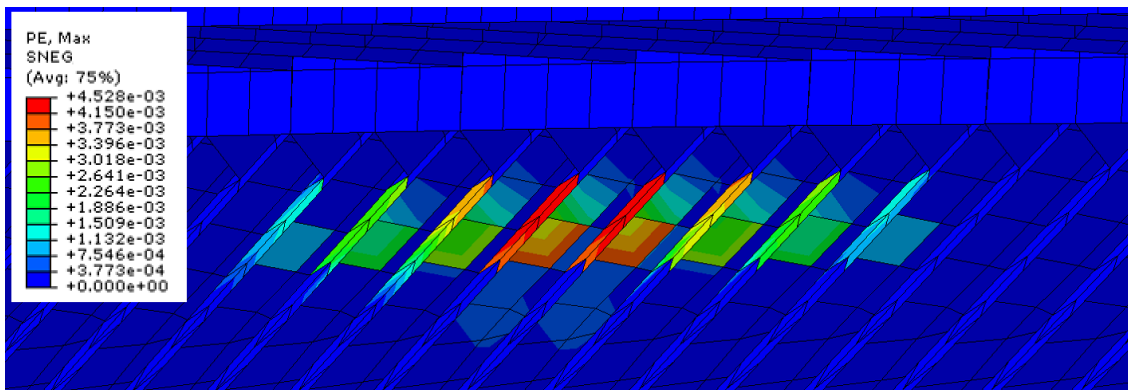Figure 8.3: Plastic strains in stiffeners for IACS design load.

Figure 8.4: Plastic strains in stiffeners for IACS design load in combination with stiffener design load.

8.2　Capacity Analysis

In a collision between an iceberg and a structure, ice within the contact area undergoes confinement and compression. This leads to HPZs where ice pressures may be as high as 70 MPa (Liu et al., 2010). It is therefore interesting to see how the different areas of the Sevan Arctic MODU are able to handle such concentrated pressure loads.

For the loading scenario where an iceberg collides with the platform, the magnitude of the force acting on the structure will be limited by the crushing failure mode. This means that the positive effect of having a sloped surface in the ice draft is strongly reduced (since the benefit of this form is to initiate failure of ice in bending, an thus reducing the forces acting on the hull). The highly randomness of sizes and shapes of icebergs also make it relevant to investigate how different areas of the structure respond to high compressive loads. This is illustrated in figure 4.4.

The following two load areas are considered:

- Impact location A: Pressure load applied over design area on the sloping surface.

- Impact location B: Pressure load applied over design area on the vertical part of the structure.

For both of the cases, the load area is chosen based on the dimensions found for the IACS stiffener load design. This is a rectangular area of approximately 0.3 m^2 (for calculation, see section 4.3.1). The load patches applied for the sloping side (impact location A) and vertical side (impact location B) are shown in figure 8.6a and 8.6b, respectively.
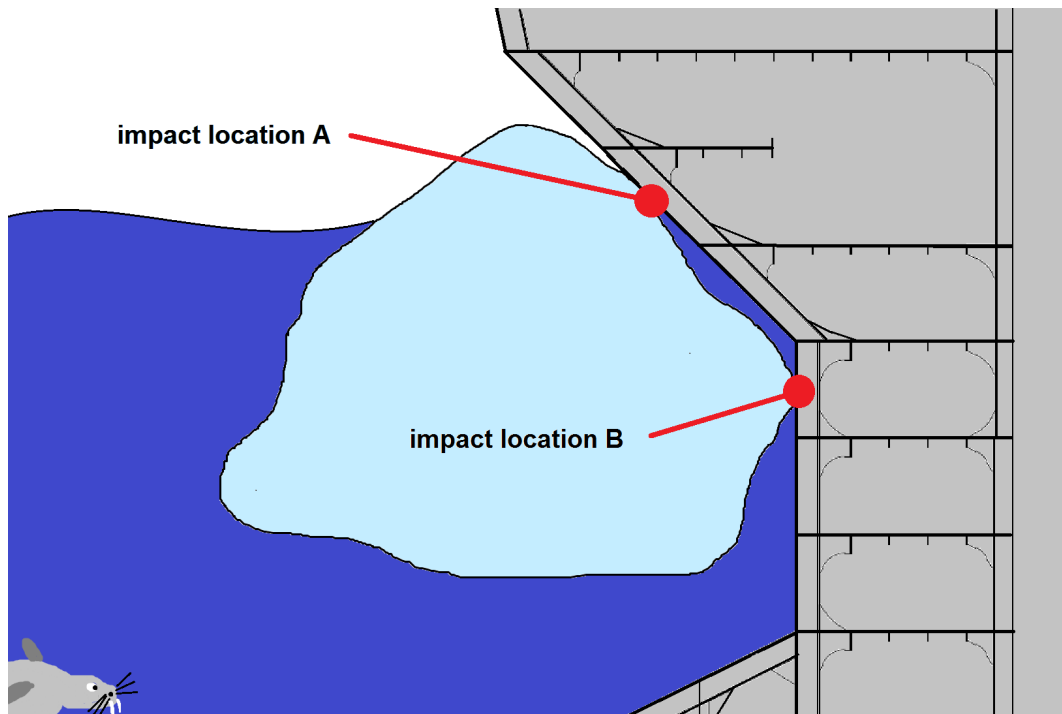

Figure 8.5: Impact locations in iceberg collision scenario.

(a) Impact location A.   (b) Impact location B.
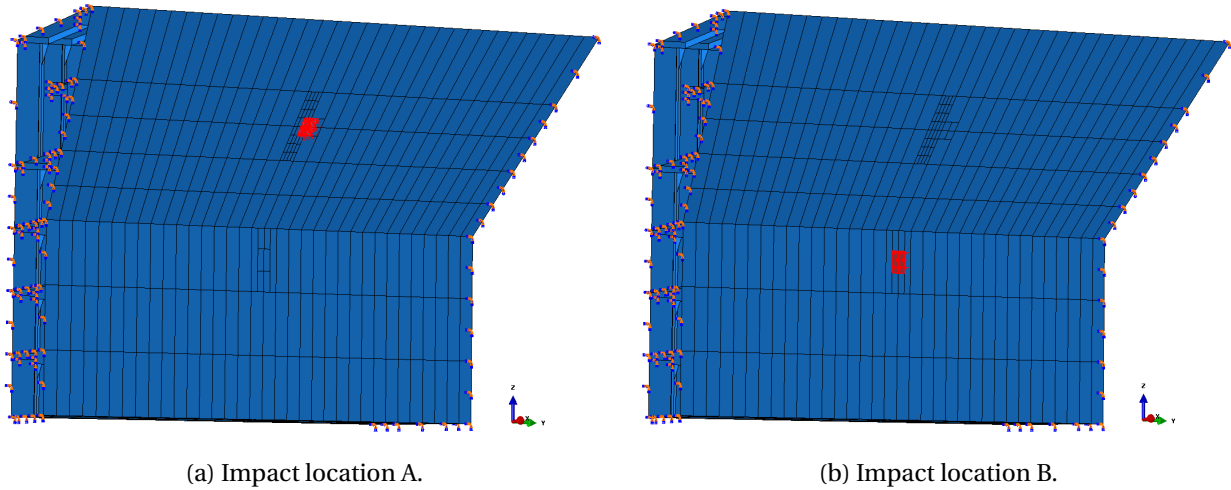
Figure 8.6: Load patches used in capacity analysis.

In the present analysis, stress concentrations and high stress gradients are expected to occur due to the high and concentrated loading. This will typically call for a refinement of the mesh for obtaining the same accuracy as for lower load amplitudes. The mesh is therefore refined. A mesh size of 50 mm is applied in the area surrounding the load patch. This is shown if figure 8.7.
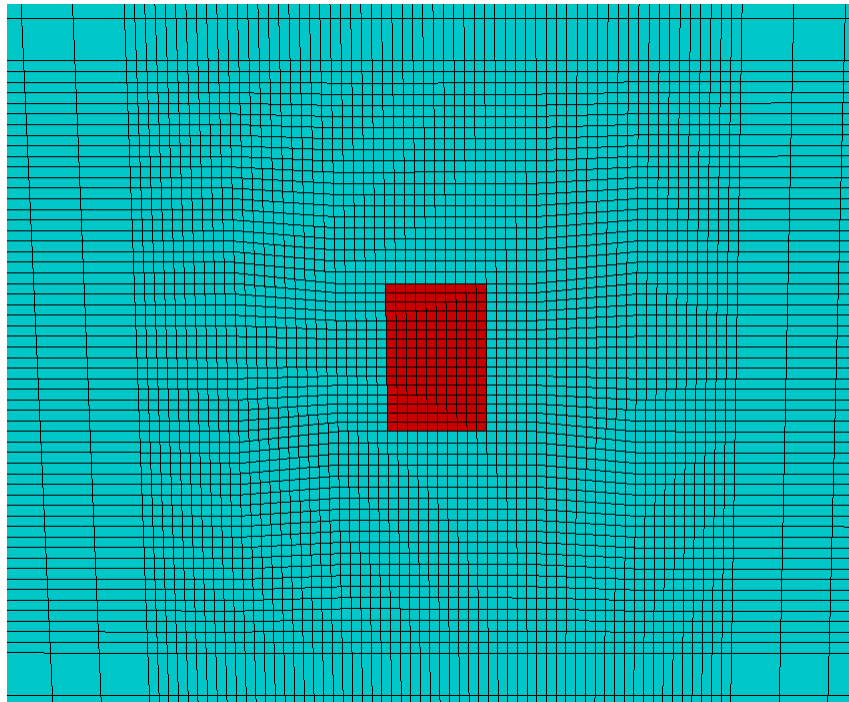

Figure 8.7: Refined mesh in load area. The load patch area is shown as the red rectangle.

8.2.1 Impact Location A

The graph in figure 8.8 show the maximum stress in the stiffener and plating for an increasing pressure load. The same graph show the maximum deflection in the outer plating. Figure D.5 and D.6 in appendix D.3 show the stress distributions for progressive increase of loading for the plate and stiffeners, respectively. The plate and stiffeners both start to yield at a pressure of about 10 MPa. A further increase of the applied pressure gives a rapid increase in extent of yield area in the plate. For the stiffeners, the stresses are more concentrated in just the stiffener directly connected to the loaded area. In an ALS condition, the stiffeners should preferably be allowed to yield, allowing beneficial membrane stresses to develop over a substantial area.

A further increase in the stresses are not seen until the pressure load is about 17.5 MPa. From this point, a rapid increase in the stresses are seen in both the plate and stiffeners. At a pressure of around 28.8 MPa, stress in the stiffener reaches the ultimate strength of the material (which is 470 MPa, see section 7.4). This is occurring in the middle stiffener, seen as the red area in figure 8.9b. For the specific load scenario, this is seen as the ultimate capacity since no fracture, buckling or other damage have been initiated onto this point. However, collapse of a stiffener is not necessarily seen as collapse of the plate field. The plate and adjacent stiffeners possesses substantial resistance provided that fracture does not occur. Figure 8.9a show the plastic strains. It is seen that plastic deformations are limited to the single stiffener.
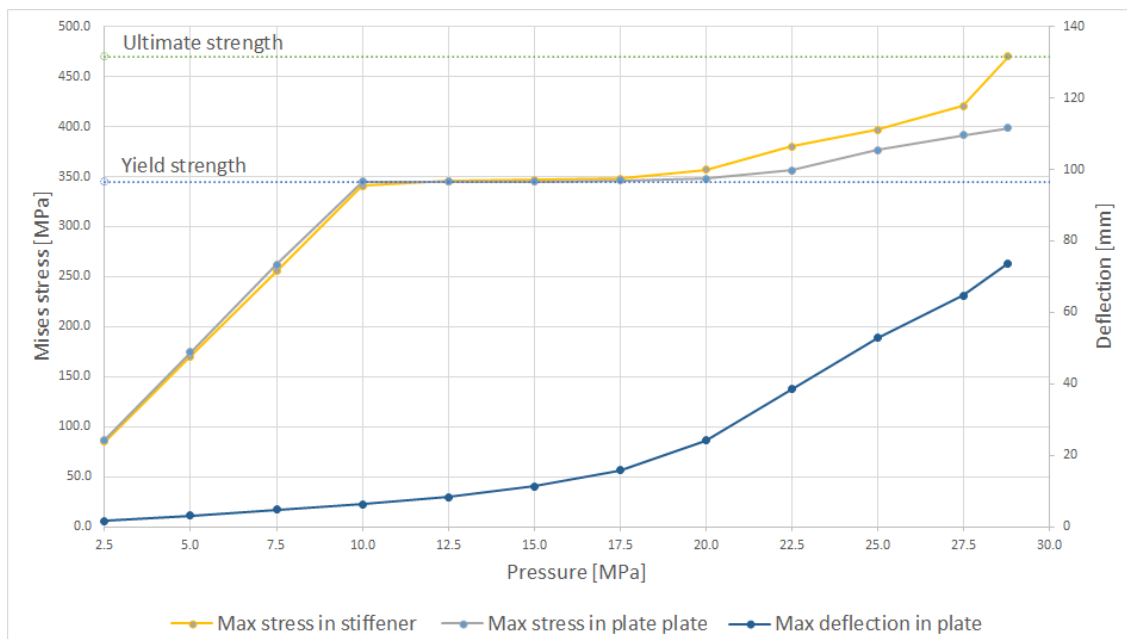

Figure 8.8: Maximum stress and displacement plottet against load pressure for applied loading at impact location A.

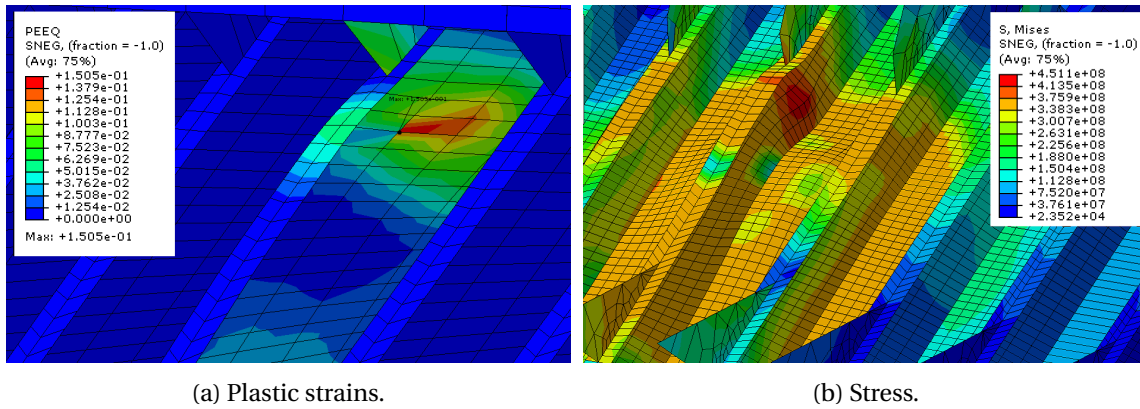(a) Plastic strains.   (b) Stress.

Figure 8.9: Plastic strains and stresses in stiffeners at an applied pressure of 28.8 MPa.

In the results presented above, the membrane stresses developing in the plating is clearly visible (figure D.5 in appendix D.3 show the stress in the plate for various pressure loads). Stiffeners are less likely to benefit from this effect since this will require substantial deformations. Consequently, stiffeners prone to collapse prior to plating in ALS events (Amdahl, 2009). Table D.2 gives the values for the stresses and plate displacement for the various pressure load amplitudes.

8.2.2   Impact Location B

In the case of loading at impact location B (see figure 8.5 and 8.6b) the first yielding is found at a pressure of 15 MPa. The graph in figure 8.12 shows how the stresses and displacement in the plate and stiffeners develop for an increasing pressure force. Compared to the impact location A, the pressure needed for the structure to yield is increased with 50 %. A further increase in the stresses is found from around 22.5 MPa pressure. Final failure, in terms of stresses in the material reaching the ultimate capacity of 470 MPa, is found at a pressure of 45 MPa. The maximum stress is in this case found in the plate. This is different from impact location A, where the largest stress is found in the center stiffener. Figure D.9 and D.7 in appendix D.3 show the stress distributions for progressive loading for the plate and stiffeners, respectively.

The shape of the outer hull should not have a big effect on the result when comparing the results from the two impact locations since the pressure load in both cases is applied normal onto the surface. The main difference between impact location A and B is the span of the loaded stiffeners. For the load case A this is about 2.8 m while the same is 2.0 m at impact location B. In figure 8.10 the stress distribution in the stiffeners for the two cases is shown. The figures also show how the stiffeners deflect. In the case of impact location B (see figure 8.10a) it is seen that the stiffener is twisted. At impact location B (see figure 8.10a) the stiffener is bent inwards (i.e., in the direction of the applied load). The twisting of the stiffener at location B allows the plate to deform much more, increasing the beneficial membrane effect in the plate. Figure 8.11 shows the stress distributions in the plate for the two impact locations. It is seen that the stresses at location B (figure 8.11b) are significantly larger.
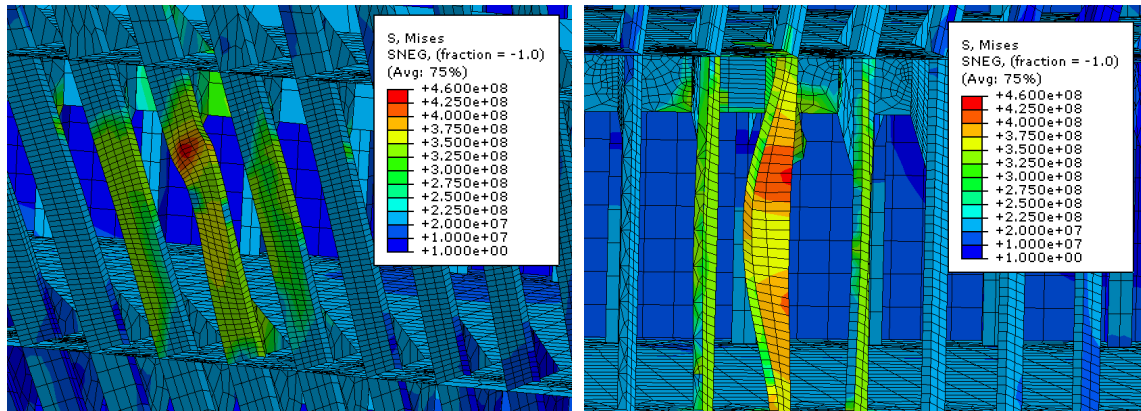
(a) Impact location A, pressure 28.8 MPa.   (b) Impact location B, pressure 45 MPa.

Figure 8.10: Stress distribution in stiffeners at point of failure (DSF = 2).
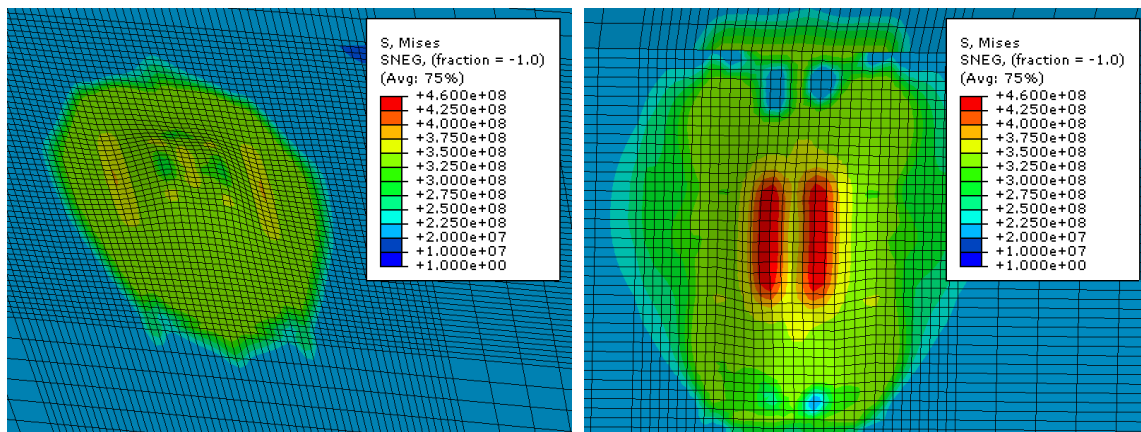
(a) Impact location A, at pressure 28.8 MPa.   (b) Impact location B, at pressure 45 MPa.

Figure 8.11: Stress distribution in plate at point of failure (DSF = 2).

From the plot in figure 8.12 it is seen that a rapid increase in the plate stress and maximum deflection occurs at a pressure of about 26 MPa. At this pressure, the bracket at the upper side of the center stiffener buckles. Figure 8.13 shows the displacement magnitude of the bracket before and after buckling. The horizontal displacement and stress at the mid point of the bracket (marked with a white circle in figure 8.13a) are plotted against the applied pressure. The graph is given in figure 8.14. Buckling of a bracket is not necessarily a critical damage for the structure. However, it is seen from the graph in 8.12 that the stress in the plate from this point increases rapidly.
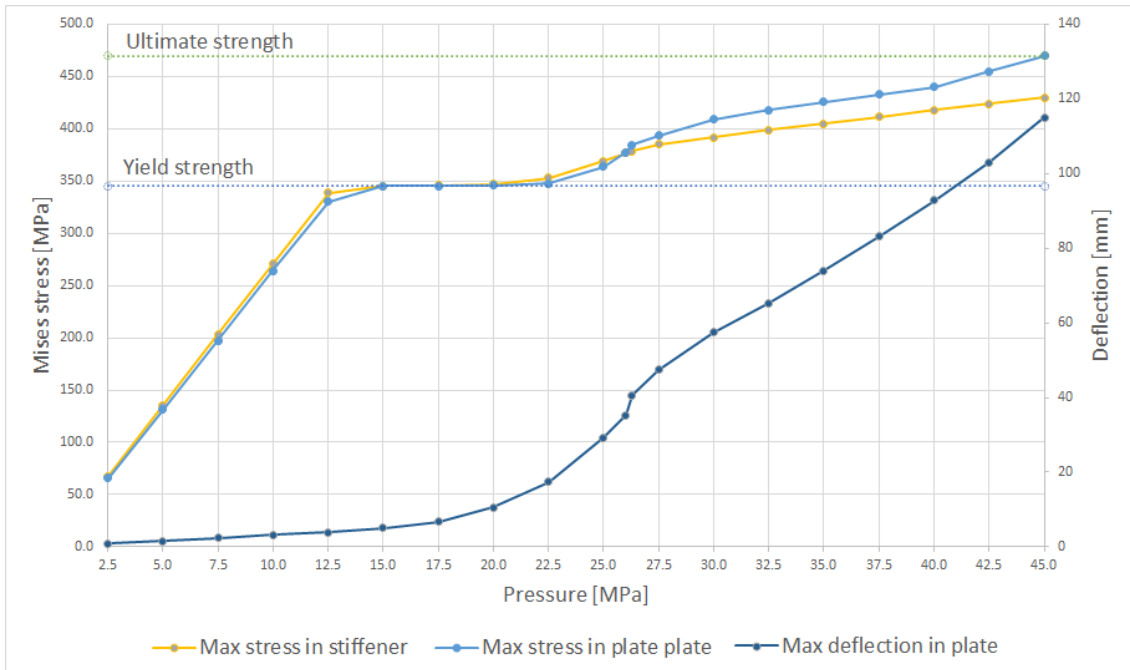
Figure 8.12: Maximum stress and displacement plottet against load pressure for applied loading at impact location B.

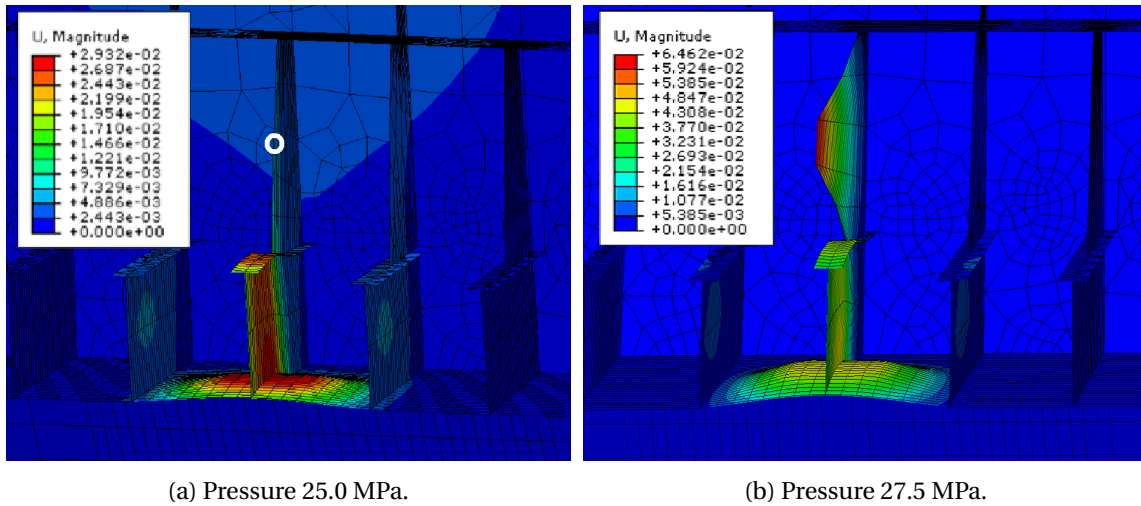

(a) Pressure 25.0 MPa.   (b) Pressure 27.5 MPa.

Figure 8.13: Buckling of stiffener bracket.

8.3 Pressure-Area Dependent Loading

A way of describing the mechanics of an iceberg impact is, as described in section 4.1, by using a pressure-area relationship. In section 5.4.3 the forces acting on the hull of a stationary structure at a head-on collision with an iceberg is calculated. For the case of a spherical iceberg with a radius of 10 m, an effective mass of 6409 tons and a velocity of 2.0 m/s, most of the kinetic collision energy is seen to be dissipated as strain energy in the ice. It is therefore assumed that
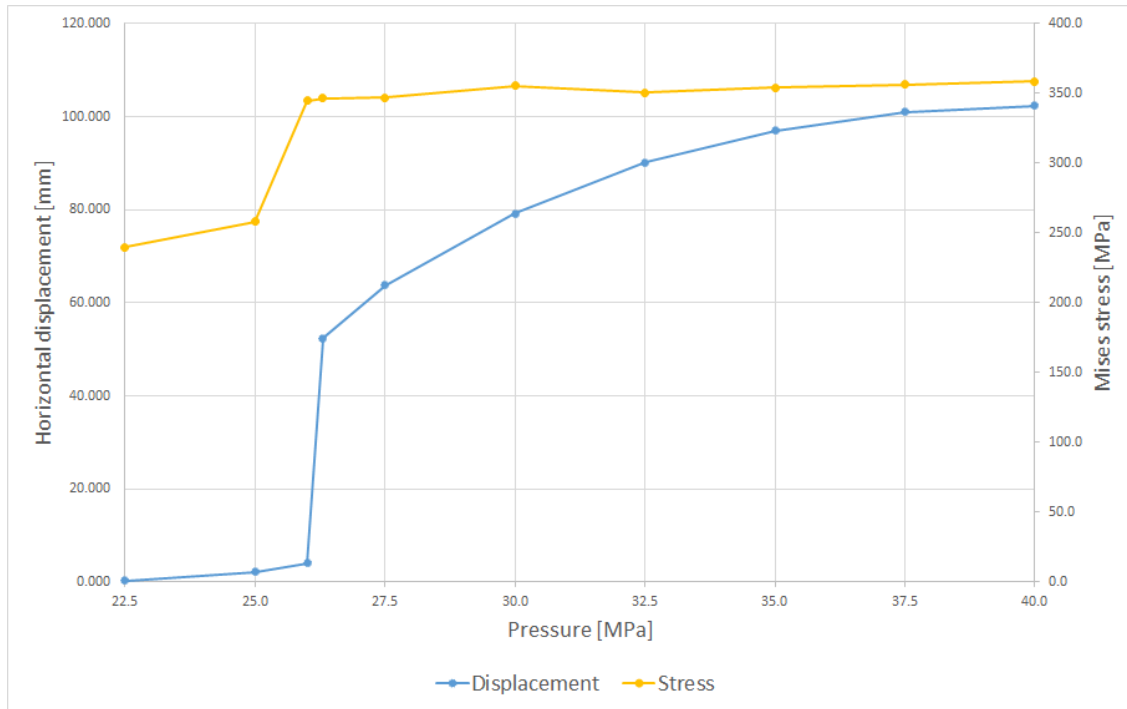
Figure 8.14: Load patch calculated from

the structure will remain stationary during the collision, and the global dynamic of the system will not be considered. For the specific size and velocity of the iceberg, the maximum force is found to be 25.72 MN and the maximum impact area 60.38 m^2 (see table 5.2). When the contact area becomes large, the pressure calculated is small. In Brown and Daley (1999), the expression $P(A) = P_0 A^{ex}$ (which is the same expression as in equation 5.5) is used to calculate the pressures for all contact areas, depending on the size. This means that the calculated pressures will be really small for large contact areas. Because of this, ISO (2010) uses the constant value of pressure 1.48 MPa for thick, massive ice features when the contact area exceeds 10 m^2. This is done because global effects are assumed to be dominant for larger areas.

The collision scenario above is simulated with static load pressures. The area is stepwise increased from 0.33 to around 60 m^2. The pressures for each contact area is determined from the pressure-area relationship in equation 4.1. The relationsship is given in figure 8.15 where it is plotted with logarithmic scales (as it presented by Masterson et al. (2007)). The total contact force from the ice is plotted in the same figure (yellow line). The stippled yellow and blue lines indicate how the total force and pressure develop if the pressure-area relationship given in equation 5.5 is used also after the contact area 10 exceeds 10 m^2.
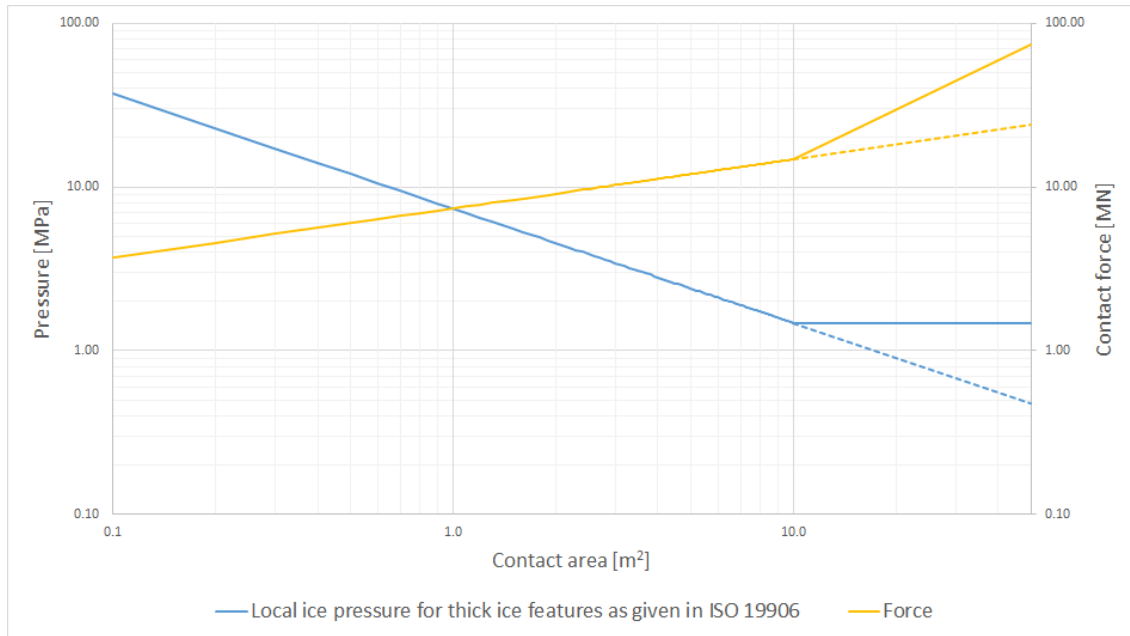
Figure 8.15: Load patch calculated from

In table 8.1, the contact areas and corresponding pressures used in the analyses are listed. The total normal contact force and horizontal force are also given. The total normal force is found as the product of the contact area and the applied pressure. The horizontal force is calculated as the force component of the normal force which is working in the horizontal direction. This value is of interest since the maximum load exerted on the structure is assumed limited by the capacity of the mooring system. This is, as presented in section 7.3, 45 MN working in the horizontal direction. The contact areas applied on the structure are given in figure D.13 in appendix D.4. These areas are made close to quadratic, with a position on the hull determined from what could be expected when an iceberg is crushing against the unit. Due to the density of ice, the major part of the contact area will be below the waterline. This means, as seen from figure D.13g, D.13h and D.13i, that also the vertical part of the structure will be affected.

Table 8.1: Pressures-area combinations and corresponding total normal force and total horizontal force.

Contact Area	Pressure	Normal Force	Horizontal Force
0.33	16.08	5.31	3.81
0.67	9.79	6.56	4.64
1.16	6.67	7.74	5.52
2.50	3.90	9.74	6.90
5.85	2.15	12.57	8.93
12.35	1.48	18.28	12.98
24.42	1.48	36.14	25.66
35.06	1.48	51.89	40.12
58.60	1.48	86.73	68.13

The graph in figure 8.16 present the results from the analysis in form of maximum stresses in the stiffeners and plating plotted against the total applied contact force. For the smallest contact area (A = 0.33 m^2) the applied pressure is 16.08 MPa. It is seen that it is for this area-pressure combination that the largest stresses are found. The stresses are just slightly above the yield strength of the material. For an increasing load area (and thus a decreasing pressure) the stresses are seen to drop significantly in both stiffeners and the outer plate. At a certain level of force (around 40 MN) the stress level in the stiffeners stabilizes at approximately 270 MPa. The stresses in the plate increases slowly from a minimum value of around 100 MPa found at a an applied normal contact force of 18.28 MN (which is found for a contact area of 12.35 m^2, see table 8.1). The result presented in figure 8.16 are also given in table D.4 in appendix D.4.

When pressure forces are applied over an increasingly size of the contact area, high stresses are seen to develop along the boundaries of the local model. When the boundary conditions for the local model were chosen, it was assumed that applying fixed boundaries along the edges of the local model were a good choice as long as the model boundaries are at a adequate distance from the loaded area. When the areas get large (as seen from the largest load patches in figure D.13), this choice does not seem to give good results anymore. It is therefore of relevance to apply the global model for these cases. This, which is presented in section 7.2, is as earlier described made up by three identical local models which are separated by vertical bulkheads.
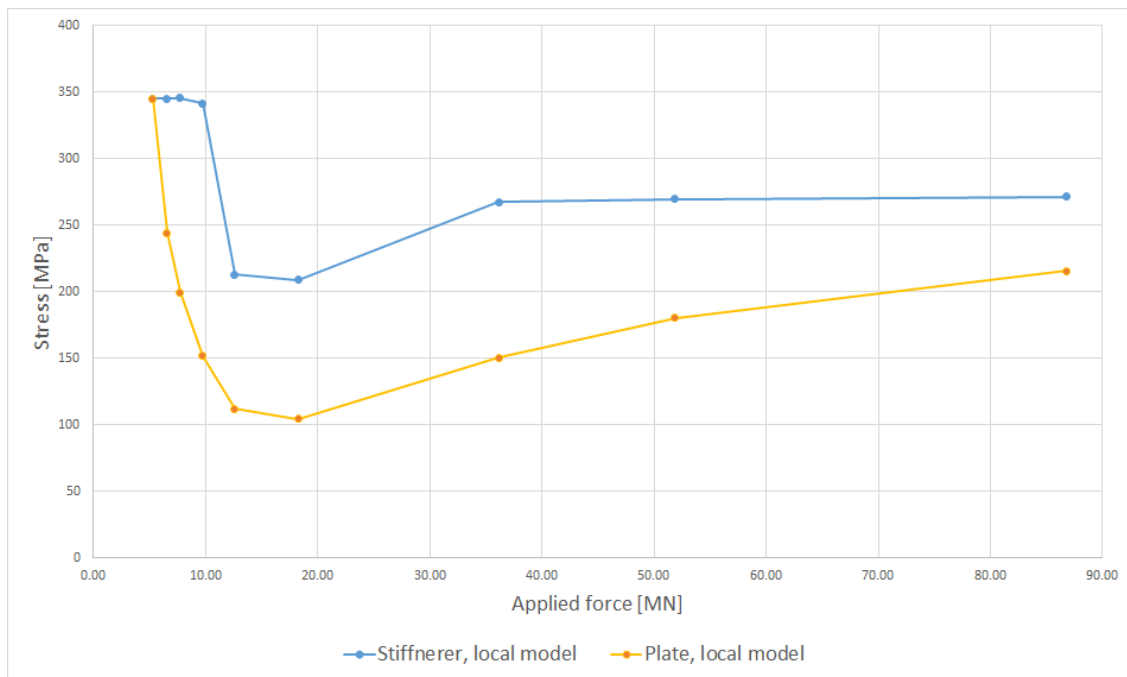

Figure 8.16: Stresses in plate and stiffeners at different magnitudes of applied force.

The stress distributions for the case with the largest contact area (given in figure D.13i in appendix D.4) when applying the local and global models are used are given in figure 8.18 and 8.19, respectively. The stress patterns are quite similar. However, in the local model stress concentrations are found to occur along the boundaries of the model. It is in these areas (marked

by the circles in figure 8.18) that the maximum stresses are found. The same analysis when applying the global model gives significantly higher stresses in the plate field (see circled area in figure 8.19) compared to the local model. In addition to this, the problem with stress concentrations along the boundary is reduced. Figure 8.20 and 8.21 show the displacement pattern on the outer hull for the same two load cases. Comparing the two patterns, the effect of including the response of the adjacent structure becomes apparent. The maximum deflection in the plate field when applying the local model is 17 mm, while the same is close to 30 mm in the case where the global model is used.
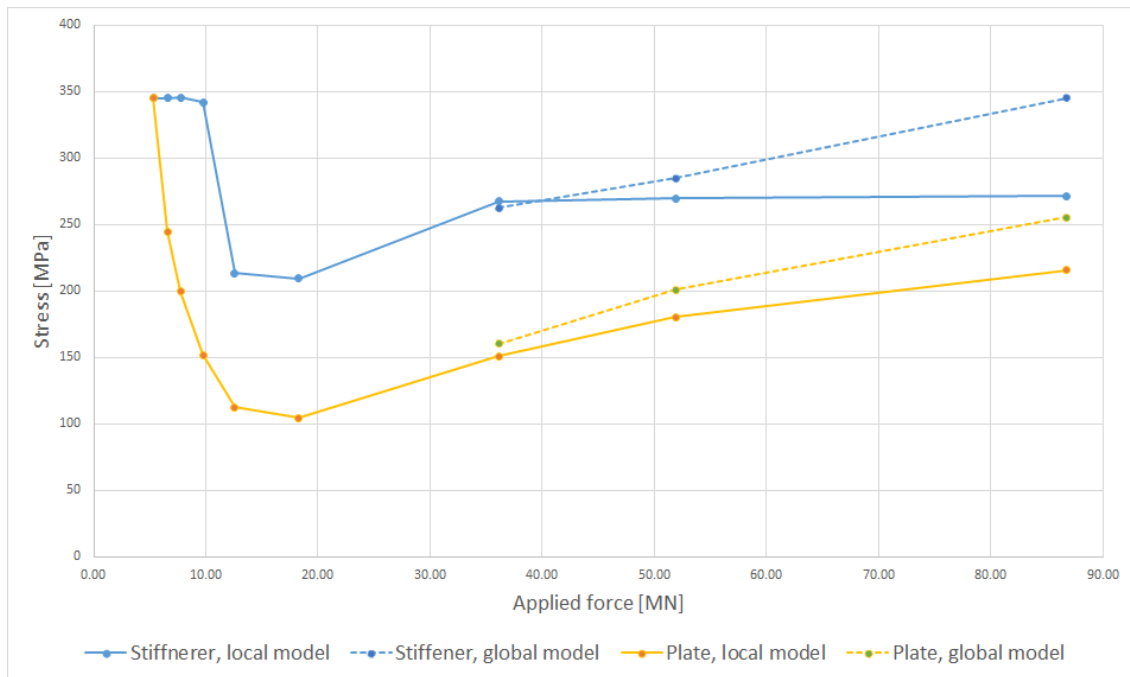

Figure 8.17: Stresses in plate and stiffeners at different magnitudes of applied force.

The analyses applying the three largest contact areas (see table 8.1) are rerun using the global model. The results are in figure 8.17 plotted together with the result obtained from the analyses from the local model. The blue and yellow stippled lines in the graph show the maximum stress found in the stiffeners and plating, respectively, from the results with the global model. The result presented in figure 8.17 are also given in table D.5 in appendix D.4. Based on these results, it may seem that including global effects becomes important when the applied total force exceeds 30 MN. This is not necessarily the case in general since the stresses will depend on the size of the contact area, magnitude of the applied pressures, location of impact etc.
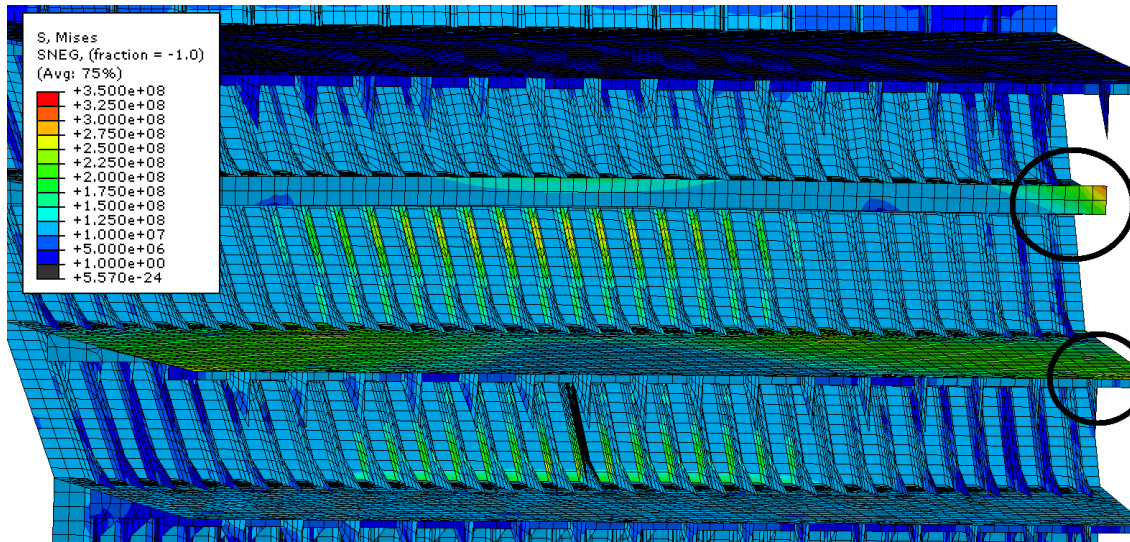
Figure 8.18: Stress distribution in stiffeners at sloping wall for local model at pressure 1.48 MPa applied over load area of 58.60 m^2.

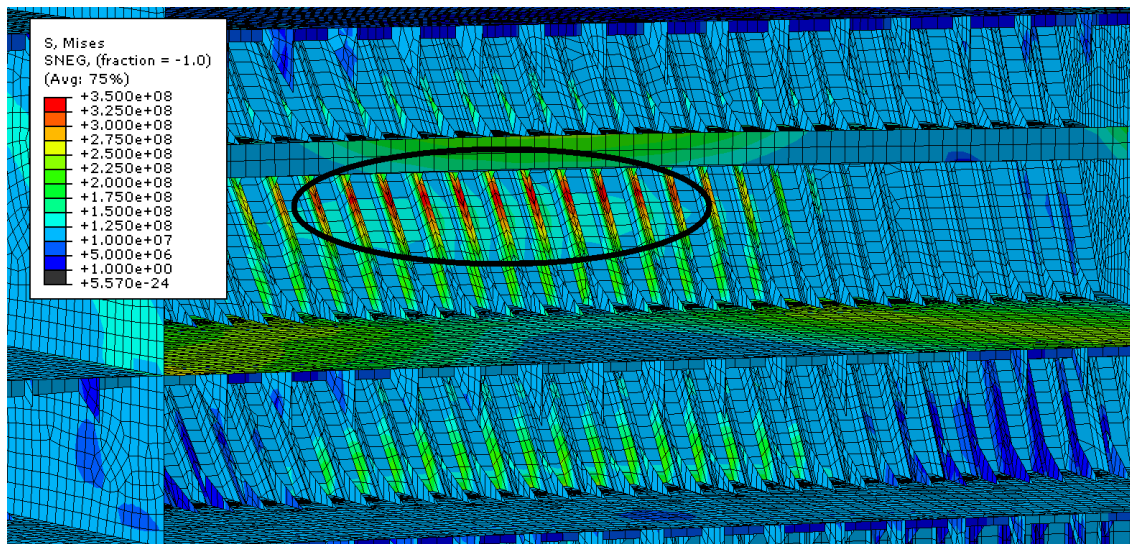
Figure 8.19: Stress distribution in stiffeners at sloping wall for global model at pressure 1.48 MPa applied over load area of 58.60 m^2.
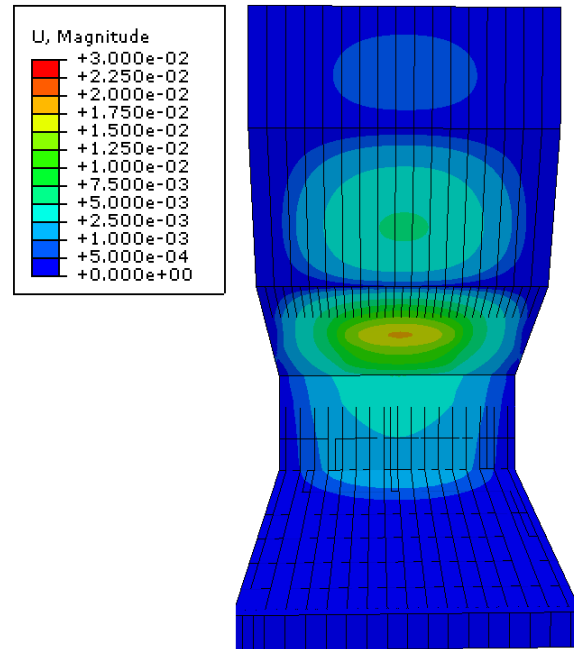
Figure 8.20: Displacement pattern for local model at pressure 1.48 MPa applied over load area of 58.60 m^2.
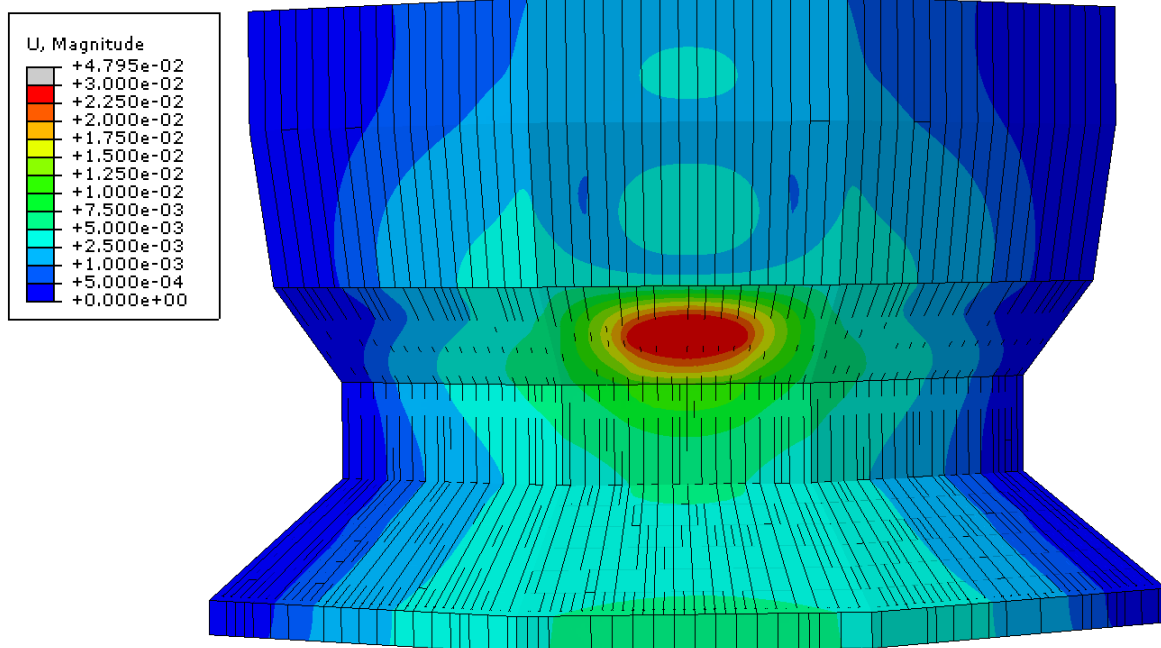

Figure 8.21: Displacement pattern for global model at pressure 1.48 MPa applied over load area of 58.60 m^2.

Chapter 9

General Conclusions

This thesis has discussed some relevant load conditions regarding accidental ice loads on the Sevan Arctic MODU, which is a drilling unit concept developed by Sevan Marine intended for operation i Arctic waters. The results from the analyses performed in this thesis are not sufficient to draw any final conclusions on the structures ability to deal with accidental loads. This is due to the simplified load conditions and the limited number of load scenarios assessed.

As discussed in section 4.2 and 4.4, representing an iceberg impact with static pressures loads is not necessary a good approximation. Such an approach will not include the different behaviors between the confined and unconfined areas of the ice. Neither the random and oscillating amplitudes and located HPZs will be included.

The effects of an iceberg collision have been simulated by splitting the scenario into local and global loads. When an iceberg is colliding with the hull of the Sevan Arctic MODU, high pressures in the ice may develop at the impact locations. Due to the varying sizes and random shapes of the icebergs that may be encountered, other parts of the structure besides the ice draft area may be struck by the ice. It was found that the structure are able to take much higher pressure loads than the design loads from which the scantlings of the hull are based upon. The capacity of the outer wall depends on how the load is applied onto the structure. The thick outer plating possesses substantial resistance provided that fracture does not occur. In this sense the stiffeners should preferably yield and deform since this allows beneficial plate membrane stresses to develop over a substantial area.

Global loads from the iceberg collision were simulated by applying a pressure-area relationship to calculate the pressure loads and contact areas. It was found that the first period of the impact is most critical, when high pressure forces are working over small areas. In a real collision, areas of high pressure will be present also for larger contact areas. An analysis where local and global loads are combined will therefore be required to get a realistic representation of the collision.

Chapter 10

Recommendations for Further Work

The work presented in this thesis only considers a limited number of aspects connected to collision scenarios. To be able to draw any final conclusions for the structures ability to handle accidental loads more work need to be done. Instead of giving any final answers, the thesis may serve as a basis for further work concerning the topic.

The models used in the analyses were made based on drawings containing a limited amount of details. Information about the hull structure outside the outer wall section is limited. It has been shown that for larger loads, the structure surrounding the area included in the local model is important. This should therefore be modeled more accurate to get better and more reliable results.

In addition to the lack of details in the drawings available, it has come to the authors attention that the drawings are to considered somewhat outdated. For now, the Sevan Arctic MODU still only exist on the drawing board and changes in the design have been made since the drawings used in this thesis was made. For later work the author recommends to use an updated design, if this is accessible.

The mechanics in an collision scenario between a structure and iceberg is dependent on many parameters. Calculation of the ice loads should be based on known data for the specific location of operation. A probabilistic approach can be used to determine relevant loads for different design scenarios. It the case of an assessment of a collision between an iceberg at the platform, dynamic analyses are recommended. If a realistic iceberg model (both in terms of shape, size and mechanical properties of the ice material) is included in the analysis, the local action effects due to the ice behavior are better captured than when applying the load in form of static pressures.

In the scenario of a collision with icebergs of considerable size, a better representation of the mooring system can preferably be included. By doing this, the global response of the structure is better taken into account. This become more relevant as the magnitude of the ice loads increases.

Bibliography

Abaqus (2014). *Abaqus 6.13 Documentation.* Dassault Systemes Simulia Corp. Retrieved Oct. 2014, from http://50.16.176.52/v6.13/.

Alsos, H. S. and Amdahl, J. (2007). On the resistance of tanker bottom structures during stranding. *Marine Structures*, 20:218–237.

Amdahl, J. (2009). On the design of plates and stiffeners against ice action. Presentation of Arctic Offshore Engineering, DNV.

Brown, R. and Daley, C. (1999). *Computer Simulation of Transverse Ship-Ice Collisions.* Faculty of Engineering and Applied Science, Memorial University of Newfoundland.

Croasdale, K. (2001). Local ice load data relevant to grand bank structures. *National Research Council of Canada.*

Daley, C. (2000). *IACS Unified Requirement for Polar Ships. Background Notes to Design Ice Loads.* Memorial University.

Diemand, D. (2001). Icebergs. *Academic Press*, pages 1255–1264.

DNV (2013a). Determination of structural capacity by non-linear fe analysis methods. Recommended practice DNV-RP-C208, Det Norske Veritas.

DNV (2013b). Ships for navigation in ice. Rules for Classification of Ships Part 5, Chapter 1, Det Norske Veritas.

Gagnon, R. (2008). Analysis of data from bergy bit impacts using a novel hull-mounted external impact panel. *Cold Regions Science and Technology*, 52(1):50–66.

Gautier, D. L., Bird, K. J., and Charpentier, R. R. (2009). Assessment of undiscovered and gas in the arctic. *Science*, 324(5931):1175–1179.

Glomnes, E. B. (2015). Personal Communication with Sevan Marine.

Haugen, I. (2014). Analysis of hull structure response for a sevan arctic mobile drilling unit in arctic areas subjected to ice loading. Master's thesis, Norwegian University of Science and Technology, Department of Marine Technology.

IACS (2011). Requirements concerning polar class. Technical report, International Association of Classification Societies, Geneva, Switzerland.

ISO (2010). Petroleum and natural gas industries - arctic offshore structures. ISO 19906, International Organization for Standardization, Geneva, Switzerland.

Kim, E. (2014). *Experimental and numerical studies related to the coupled behaviour of ice mass and steel structures during accidental collisions*. PhD thesis, Department of Marine Technology, Norwegian University of Science and Technology.

Kämärainen, J. (1993). *Studies in Ice Mechanics*. Helsinki University of Technology.

Liu, Z., Amdahl, J., and Løset, S. (2010). Plasticity based material modelling of ice and its application to shipship-ice impacts. *Cold Regions Science and Technology*, 65(3):326–334.

Liu, Z., Amdahl, J., and Løset, S. (2011). Integrated numerical analysis of an iceberg collision with a foreship structure. *Marine Structures*, 24:377–395.

Løset, S., Shkhinek, K. N., Gudmestad, O. T., and Høyland, K. V. (2006). *Actions from ice on arctic offshore and coastal structures*. LAN, St. Petersburg.

Masterson, D. M., Frederking, R. M., Wright, D., and Karna, T. (2007). A revised ice pressure-area curve. *Proceedings of the 19th Inernational Conference on Port and Ocean Engineering under Arctic Conditions*, pages 305–314.

McKenna, R. (2005). Iceberg shape characterization. *Proceedings of the 18th International Conference on Port and Ocean Engineering under Arctic Conditions*, 2:555–564.

McTaggart, K. A. and Isaacson, M. (1990). Probabilistic evaluation of design iceberg collision. *Cold Regions Science and Technology*, 4(2):85–101.

Moan, T. (2003a). *Finite element modelling and analysis of marine structures*. Department of Marine Technology, Norwegian University of Science and Technology, Trondheim.

Moan, T. (2003b). *Finite element modelling and analysis of marine structures, chapter 12: Nonlinear analysis*. Department of Marine Technology, Norwegian University of Science and Technology, Trondheim.

NORSOK (2004). Design of steel structures. NORSOK N-004, Standards, Norway.

Palmer, A. and Croasdale, K. (2012). *Arctic Offshore Engineering*. World Scientific, Singapore.

Raghuvanshi, U. and Ehlers, S. (2015). An assessment of iceberg loads for operations in the north barents sea. *Proceedings of the ASME 2015 34th Inernational Conference on Ocean, Offshore and Arctic Engineering, OMAE2015, Paper OMAE2015-41483*.

sevanmarine.com. Retrieved June 5th 2015, from http://www.sevanmarine.com/technology/design-principles/potential-applications.

Timco, G. and Sudom, D. (2013). Revisiting the sanderson pressure-area curve: Defining parameters that influence ice pressure. *Cold Regions Science and Technology*, 95:53–66.

USGS (2008). Circum-arctic resource appraisal: Estimates of undiscovered oil and gas north of the arctic circle. *USGS Fact Sheet*, 2008-3049.

Appendix A

Polar Class

A.1 Information About the Classes

Table A.1: Polar Class descriptions.

Polar Class	Ice Description (based on WMO Sea Ice Nomenclature)
PC 1	Year-round operation in all Polar waters
PC 2	Year-round operation in moderate multi-year ice conditions
PC 3	Year-round operation in second-year ice which may include multi-year ice inclusions.
PC 4	Year-round operation in thick first-year ice which may include old ice inclusions
PC 5	Year-round operation in medium first-year ice which may include old ice inclusions
PC 6	Summer/autumn operation in medium first-year ice which may include old ice inclusions
PC 7	Summer/autumn operation in thin first-year ice which may include old ice inclusions

Table A.2: Polar Class factors. IACS (2011)

Polar Class	Crushing Failure Class Factor (CF_C)	Flexural Failure Class Factor (CF_F)	Load Patch Dimensions Class Factor (CF_D)	Displacement Class Factor (CF_{DIS})	Longitudinal Strength Class Factor (CF_L)
PC1	17.69	68.60	2.01	250	7.46
PC2	9.89	46.80	1.75	210	5.46
PC3	6.06	21.17	1.53	180	4.17
PC4	4.50	13.48	1.42	130	3.15
PC5	3.10	9.00	1.31	70	2.50
PC6	2.40	5.49	1.17	40	2.37
PC7	1.80	4.06	1.11	22	1.81

A.2   Design Load Calculations

Table A.3: IACS PC 4 design load calculations.

Input values

Symbol	Unit	Value	Description
CF_C	-	4.50	Crushing Failure Class Factor
CF_F	-	13.48	Flexural Failure Class Factor
CF_D	-	1.42	Load Patch Dimensions Class Factor
CF_{DIS}	-	130	Displacement Class Factor
CF_L	-	3.15	Longitudinal Strength Class Factor
β'	deg	45	Normal frame angle at upper ice waterline
α	deg	90	Upper ice waterline angle
L_{wl}	m	81	Ship length measured at ice waterline
x	m	0	Distance from the forward perpendicular to station under consideration
Δ_{tk}	kt	97.4	Ship displacement at ice waterline

Calculated values

Symbol	Unit	Value	Description
$f_{aB,1}$	-	1.10	Shape coefficient, value 1
$f_{aB,2}$	.	0.23	Shape coefficient, value 2
$f_{aB,3}$	-	0.60	Shape coefficient, value 3
f_{aB}	-	0.23	Shape coefficient, taken as minimum of $f_{ai,1}$ $f_{ai,2}$ and $f_{ai,3}$
F_B	MN	19.01	Force
AR_B	-	6.35	Load patch aspect ratio
Q_B	MN/m	4.48	Line load
P_B	Mpa	6.71	Pressure
w_B	m	4.24	Width of design load patch
b_B	m	0.67	Height of design load patch
A_B	m2	2.83	Area of design load patch

Appendix B

Input from Sevan Marine

The following pages contains information about the Sevan Arctic MODU. The pages are taken from the Haugen (2014). Some details are, at the request of Sevan Marine, removed from the structural drawings. Thus, these are slightly different from those found in Haugen (2014).

Memo				SEVAN marine
To:	Ine Haugen	**Date:**	20.01.2014	
Cc:	Otto Skjaastad, Audun Nyhus, Ragnar Thunes	**Doc. Id.:**		
From:	Hans Olav Sele	**Project No.:**		
Approved by:	Ragnar Thunes	**Project Title:**	Project work at NTNU	
Subject:	Sevan Hull exposed to Ice			

Table of Contents

1   BACKGROUND

1.1   Project Work

This memo is written with intention to define a task for analysis by the student in order to understand the design of the circular hull and to define the necessary design loads to be considered in the project work.

It is suggested that the student build up a relevant model for the ice and model the relevant (exposed) parts of the structure in order to quantify the level of deformation and damage to the structure during impact.

The information in this memo may be supplemented with additional computer files etc. available for the design.

2   HULL DESIGN

2.1   Hull Form

Sevan Marine is in the process of designing an arctic intended for oil exploration in the arctic environments. The hull form is characterized by a cylindrical main body extended with a "bilge box" (skirt) at the lower section of the hull. The hull is flared in order to manage ice loads and have the possibility to break ice.There are to two variations of the hull that is considered in the design phase.

1. Downward breaking cone
2. Upward breaking cone

The difference in the hull form should be evalutated in terms of behavior in ice conditions.

Figure 2-1   Hull Form

2.1.1   Arrangement

The hull is a typical plate/beam structure featuring vertical bulkheads, horizontal stringers, decks and frames. Some of the key structural characteristics are summarized below:

- Double side structure, depth 3.5 m
- Horizontal stringers, spacing (typical) 4.0 m
- Horizontal stringers, Ice Belt 2.0 m
- Typical stiffener spacing in panels is typically in the range of 800 mm.
- Stiffener spacing in icebelt (whole side) is 400 mm

Figure 2-2 shows the structural arrangement of the hull.

Figure 2-2 Hull Section View

2.1.2   Materials

The hull will be constructed in carbon steel. The material selection for the FPSO is carbon steel with yield strength of 355 MPa (NV36 – DNV Certified steel in accordance with DNV OS-B101) will be used for plated structure including profiles.

2.1.3   Hull Size

Figure 2-3 Hull Size

Table 2-1 Main Dimensions and Draft

Item		Upward breaking Cone	Downward breaking Cone
Main Hull Diameter	(m)	75.0	
Main Deck Diameter	(m)	113.0	
Double Bottom Height	(m)	3.5	
Double Side Breadth	(m)	5.0	
Main Deck El. (Hull depth)	(m)	24.0	
Draft, Transit	(m)		10.0
Draft, Ice Operation	(m)	12.0	15.0

2.1.4 Structural Arrangement

Stiffener spacings in the side shell:

Figure 2-4 Typical Radial Cross Section

Figure 2-5 Hull Section View, Plates

Figure 2-6 Hull Section View, Profiles

3 ICE LOADS

3.1 General

The hull is designed to take the ice loads from any direction for the ultimate limit state analysis.

The hull will be designed in accordance with Polar Class (DNV or equivalent), PC4. (PC4 rule formulas may be used to determine scantlings.)

The operation will be in typical 1st year ice condition.

The following data should be considered in the design:

Table 3-1 Ice Load Scenarios

Ice feature	Thickness	Comment
Level Ice	1.20 m	Some typical ice data: Density 890 kg/m3 Bending strength 500 kPa Compressive Strength 1.2 MPa Emodulus 3.5 GPa
Managed Ice	1.20 m	Floe size 100 m x 100 m Ice data as above
Ice Ridges		Sail height 9.3 m Keel depth 21 m Consolidated layer thickness 3 m Bending strength consolidated layer 640 kPa Compressive strength consolidated layer: 1.5 MPa

LONGITUDINAL SECTION

HOLD

27°
8000
12000
17000

Open water draft

Ice draft

EL 8000

ICE DRAFT

OPEN WATER DRAFT

HOLD

2000

EL. 20 000

EL. 16 000

EL. 12 000

EL. 8 000

EL. 4 000

B.L
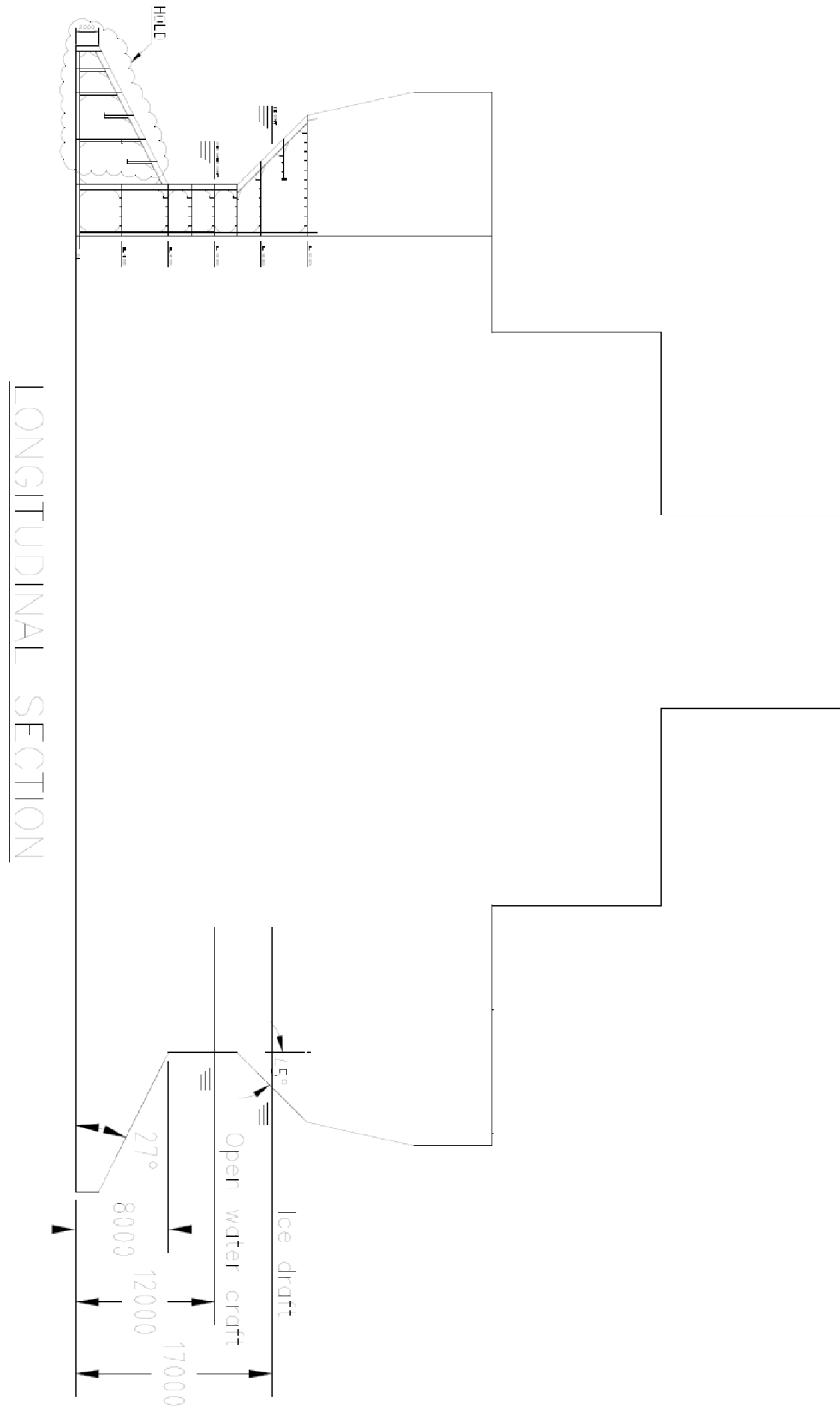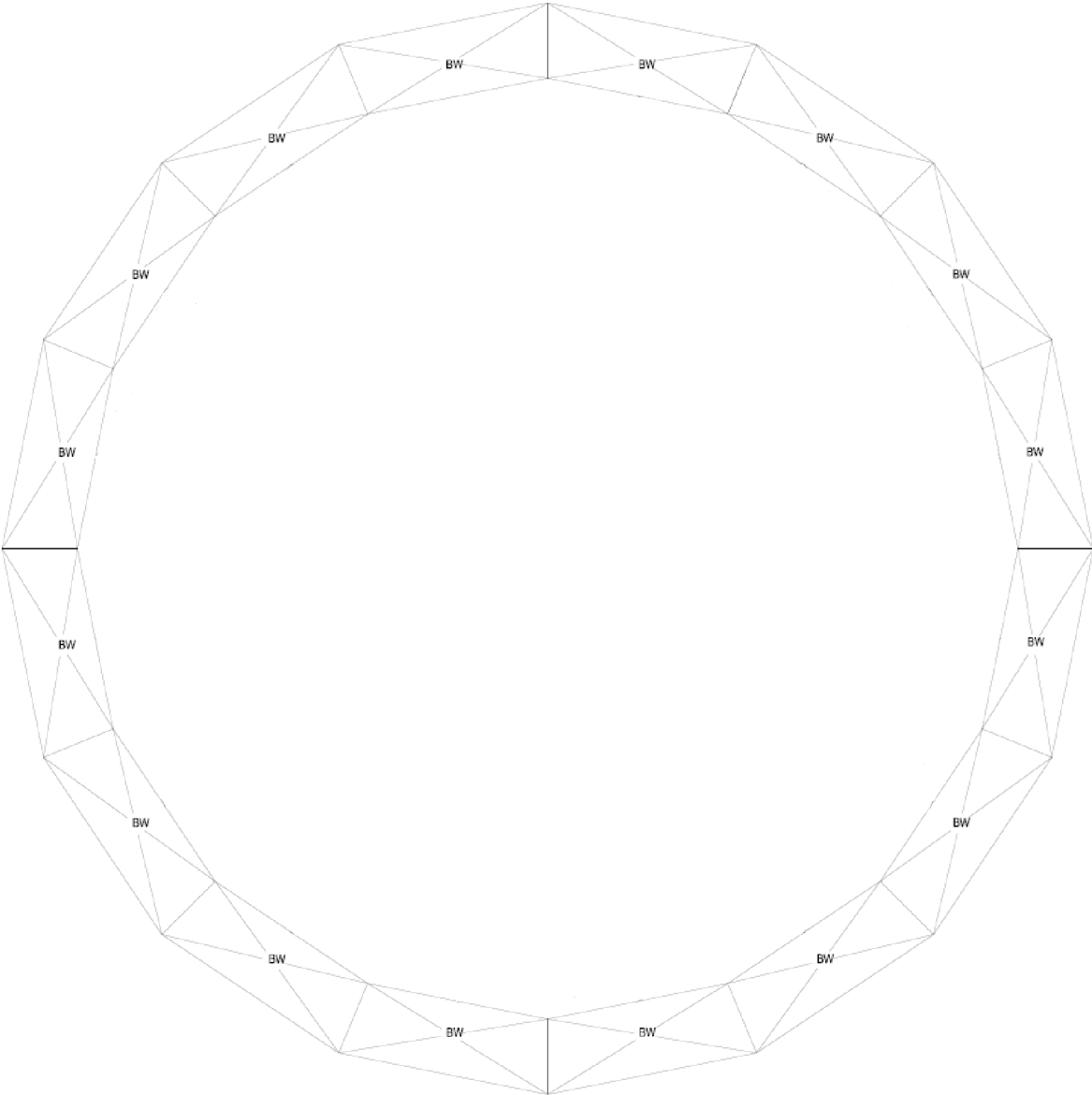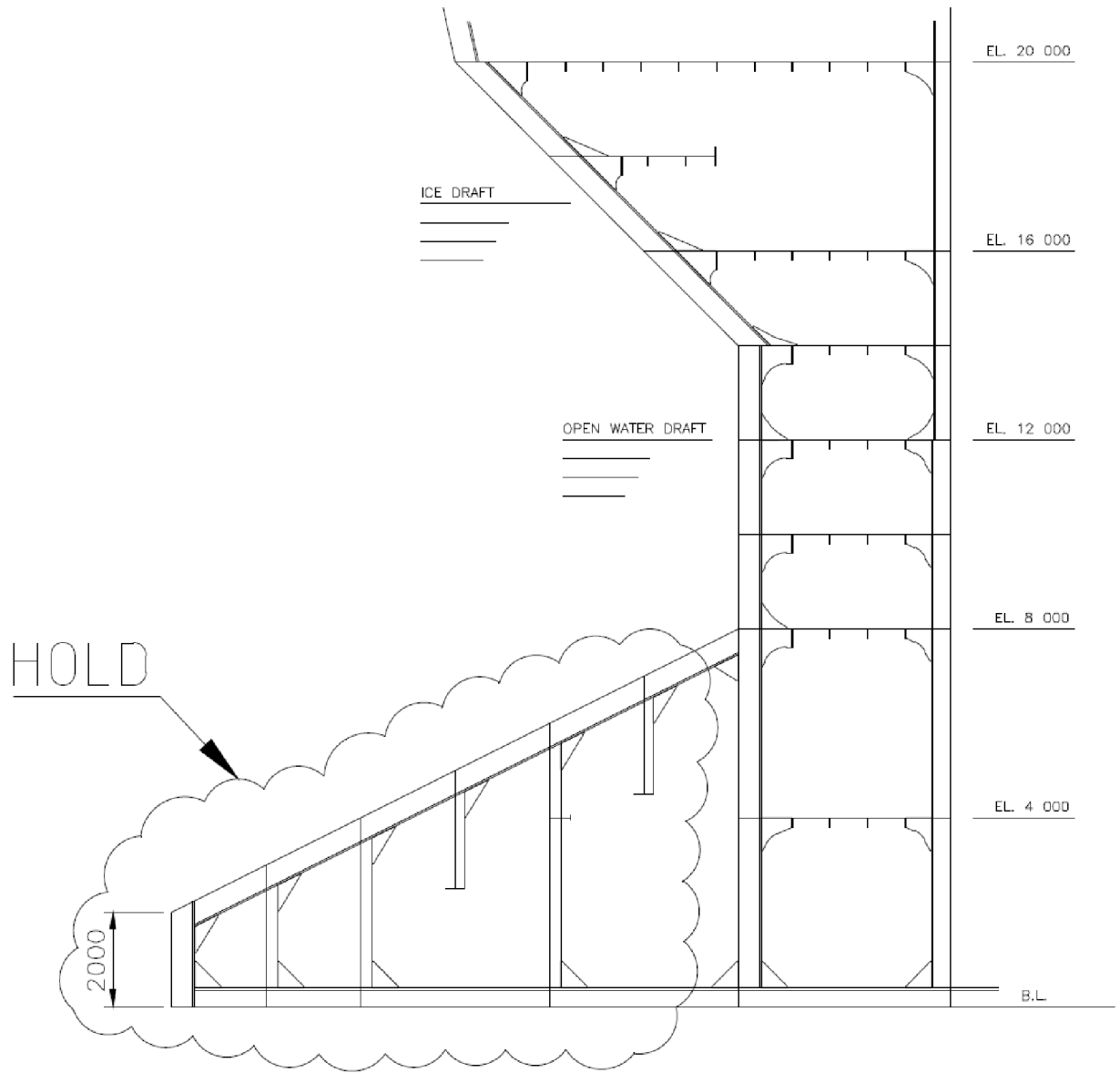
Appendix C

ABAQUS Model

C.1   Model Details
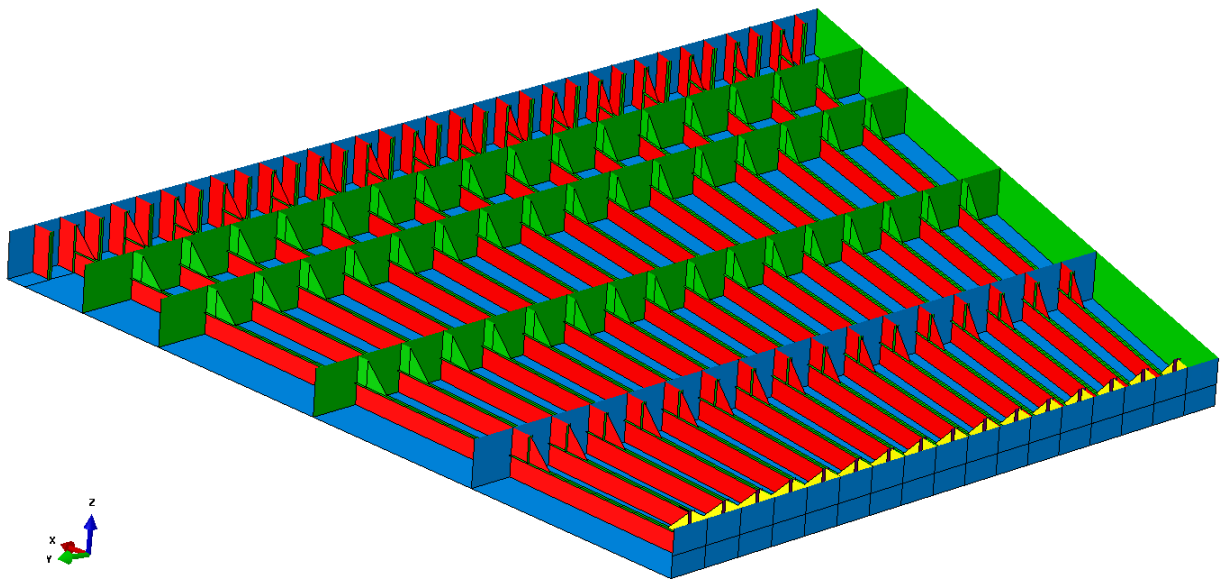
Figure C.1: Stiffener configuration in bottom.
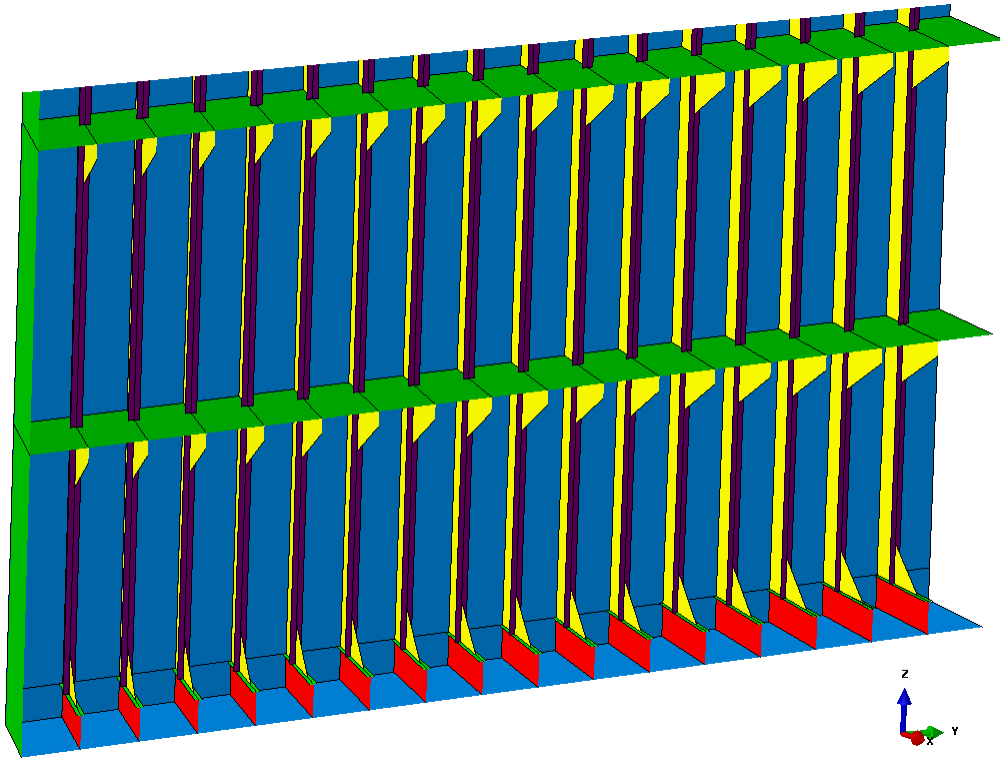
Figure C.2: Stiffener configuration at back wall.
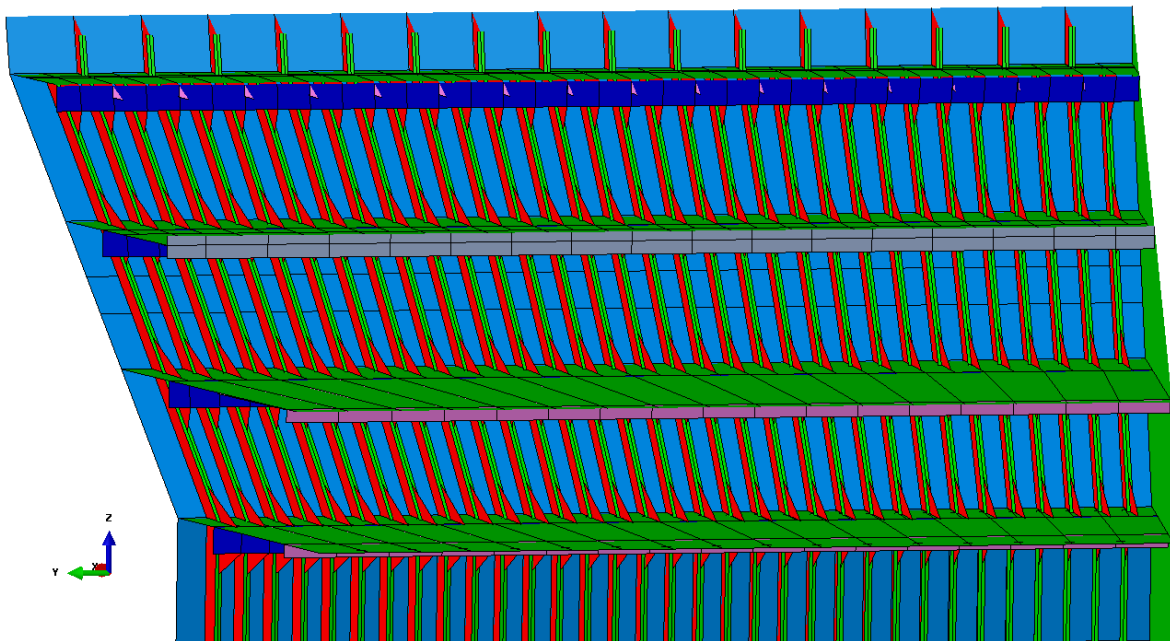
Figure C.3: Stiffener configuration at 45 degrees sloping wall.
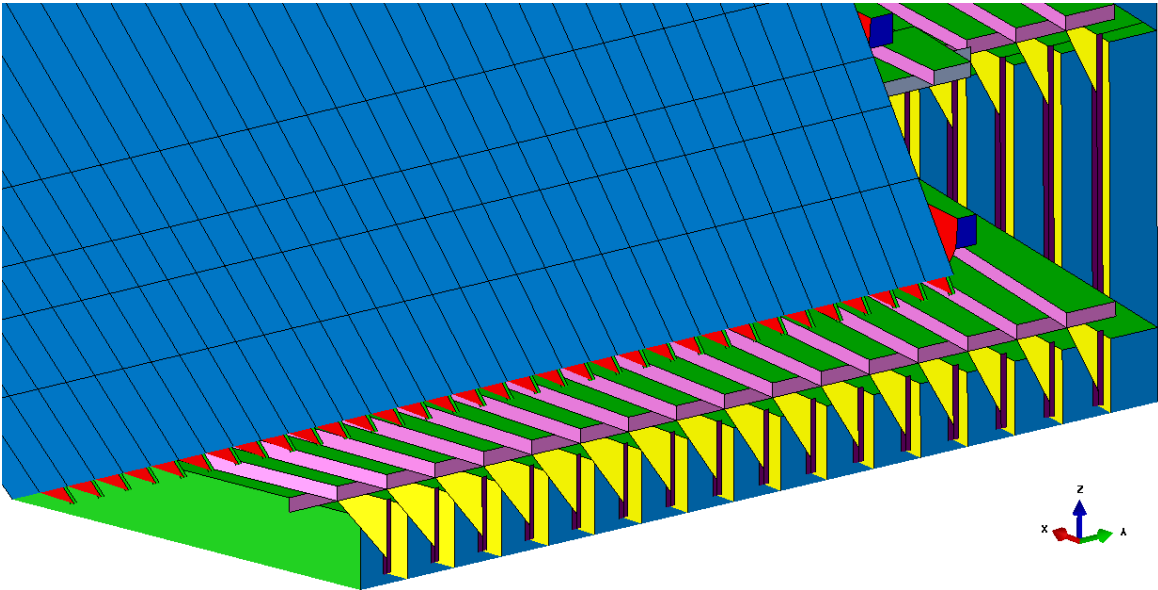
Figure C.4: Stiffener configuration in decks.

C.2 Material Model Input

Table C.1: Material properties for S355 construction steel (DNV, 2013a).

Table 4-3 Proposed non-linear properties for S355 steels (Engineering stress-strain)

	S355		
Thickness [mm]	$t \leq 16$	$16 < t \leq 40$	$40 < t \leq 63$
E [MPa]	210000		
$\sigma_{prop}/\sigma_{yield}$	0.9		
E_{p1}/E	0.001		
σ_{prop} [MPa]	319.5	310.5	301.5
σ_{yield} [MPa]	355	345	335
σ_{yield2} [MPa]	358.4	348.4	338.4
σ_{ult} [MPa]	470	470	450
ε_{p_y1}	0.004		
ε_{p_y2}	0.02		
ε_{p_ult}	0.15		
E_{p2}/E	0.0041	0.0045	0.0041

Table C.2: Input data for RTCL damage model.

Triaxiality	Normalized failure strain	Failure strain	
T	ef/Df	Mesh 50 mm	Mesh 200 mm
-0.23	5.00	2.25	1.40
-0.20	4.00	1.80	1.12
-0.10	2.40	1.08	0.67
0.00	1.70	0.77	0.48
0.10	1.35	0.61	0.38
0.20	1.15	0.52	0.32
0.30	1.00	0.45	0.28
0.40	0.85	0.38	0.24
0.50	0.70	0.32	0.20
0.60	0.60	0.27	0.17

Appendix D

Additional Results

D.1 Convergence Analysis
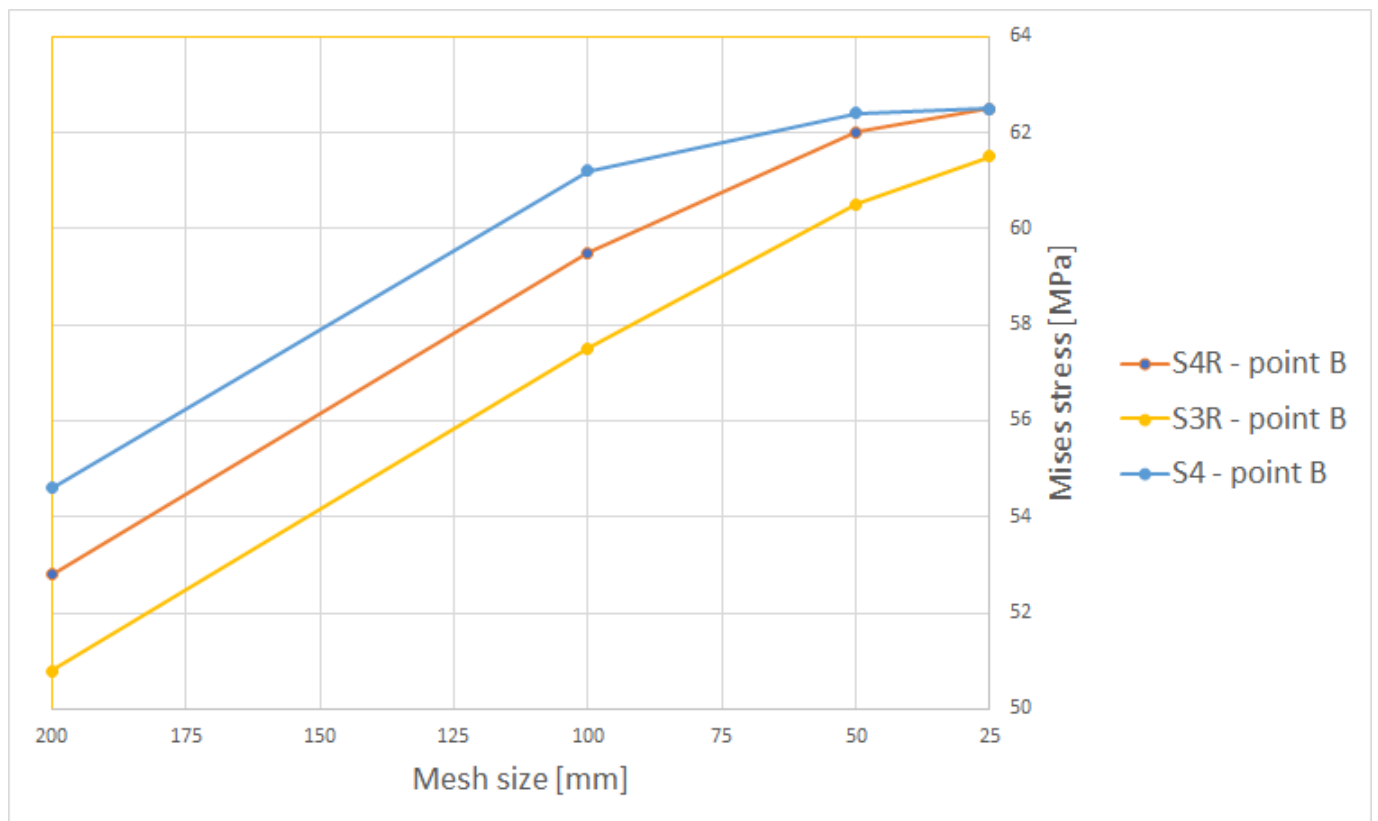
Figure D.1: Convergence of stress at point B.
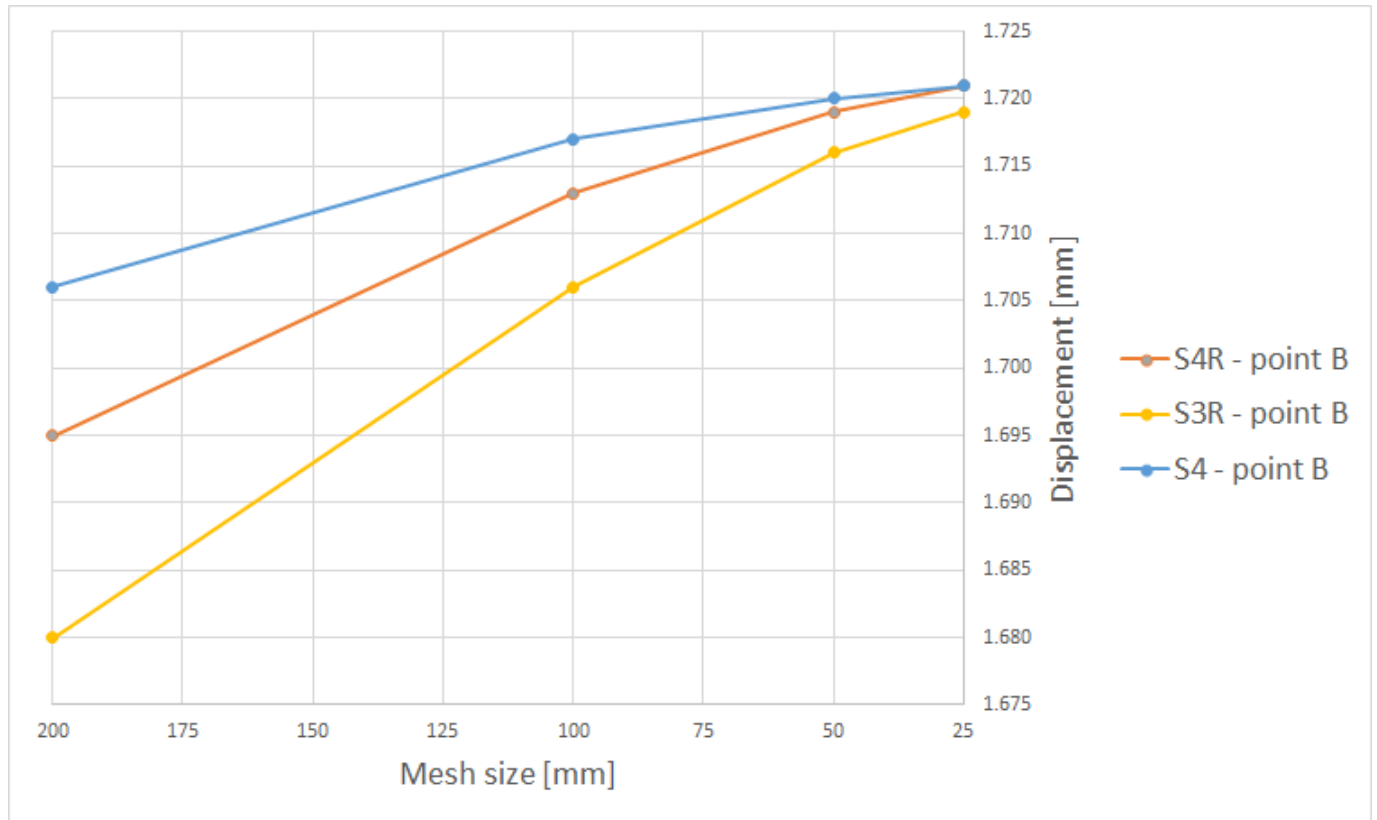
Figure D.2: Convergence of displacement at point B.

Table D.1: Measured stress and displacement values from convergence analysis.

Mises stress [Mpa]

Location	Point A			Location	Point B		
Mesh size		Element		Mesh size		Element	
[mm]	S4R	S3R	S4	[mm]	S4R	S3R	S4
25	145.4	145.4	145.4	25	62.5	61.5	62.5
50	145.3	144.8	145.3	50	62.0	60.5	62.4
100	145.8	143.1	144.6	100	59.5	57.5	61.2
200	148.8	137.2	141.4	200	52.8	50.8	54.6

Displacement magnitude [mm]

Location	Point A			Location	Point B		
Mesh size		Element		Mesh size		Element	
[mm]	S4R	S3R	S4	[mm]	S4R	S3R	S4
25	5.045	5.038	5.048	25	1.721	1.719	1.721
50	5.048	5.020	5.048	50	1.719	1.716	1.720
100	5.061	4.966	5.044	100	1.713	1.706	1.717
200	5.106	4.854	5.005	200	1.695	1.680	1.706

D.2 Deck Stiffener Configuration
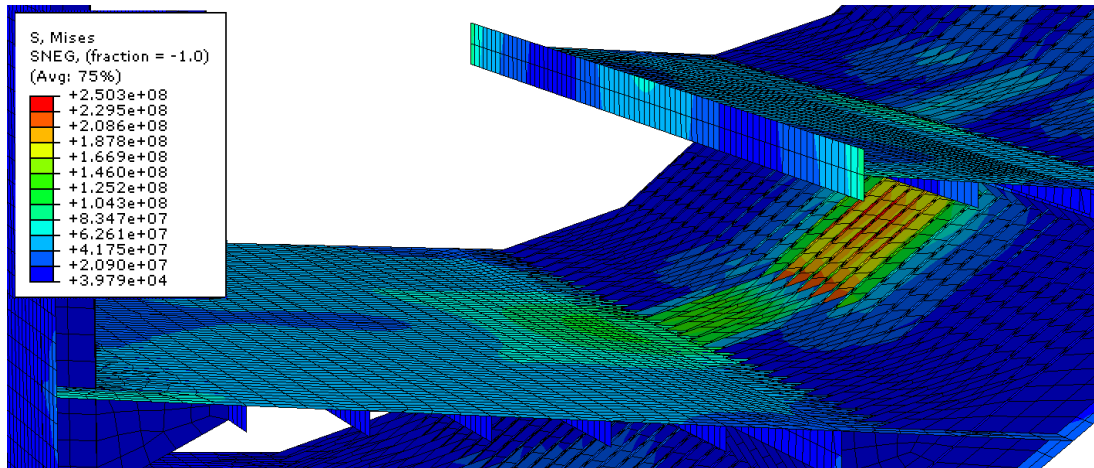
(a) Pressure 3 MPa.
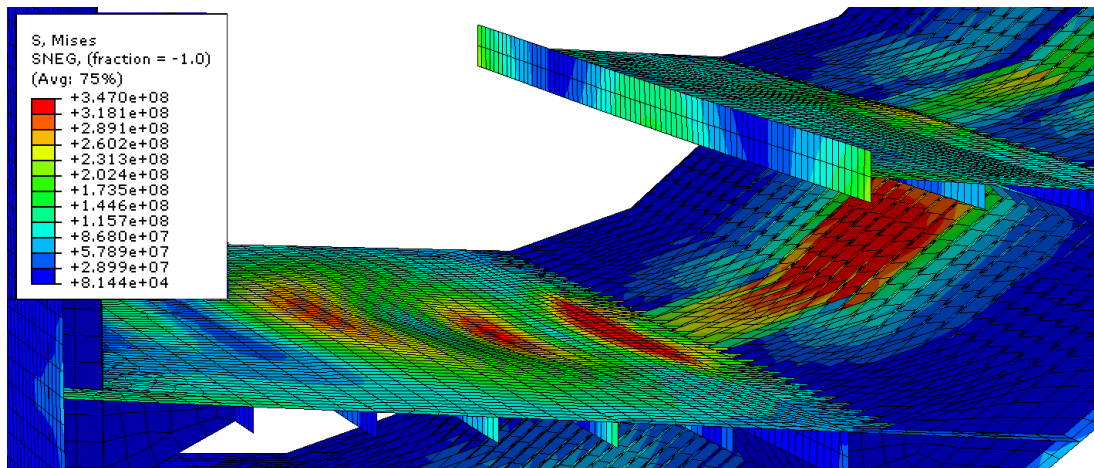
(b) Pressure 6 MPa.
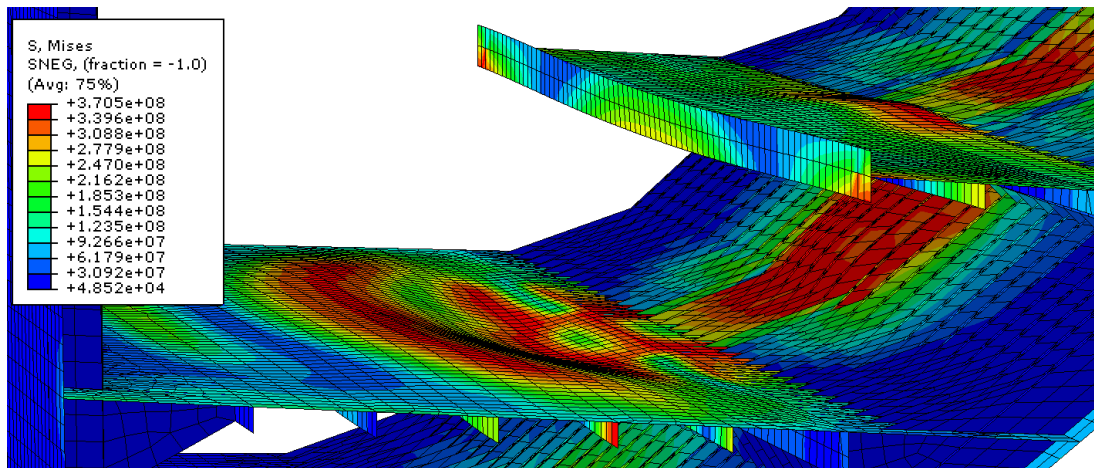
(c) Pressure 8 MPa.

Figure D.3: Stress distribution for initial deck design.
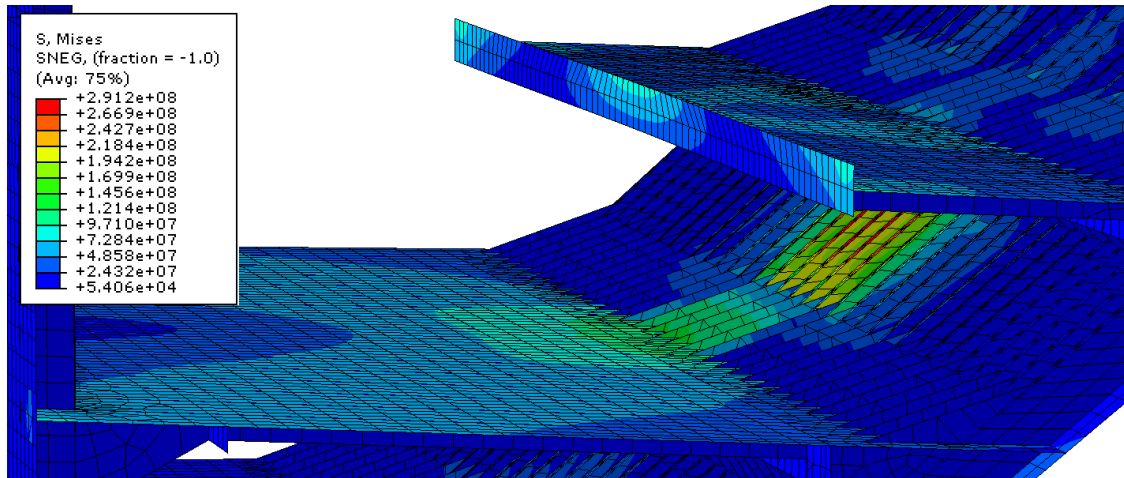
(a) Pressure 3 MPa.
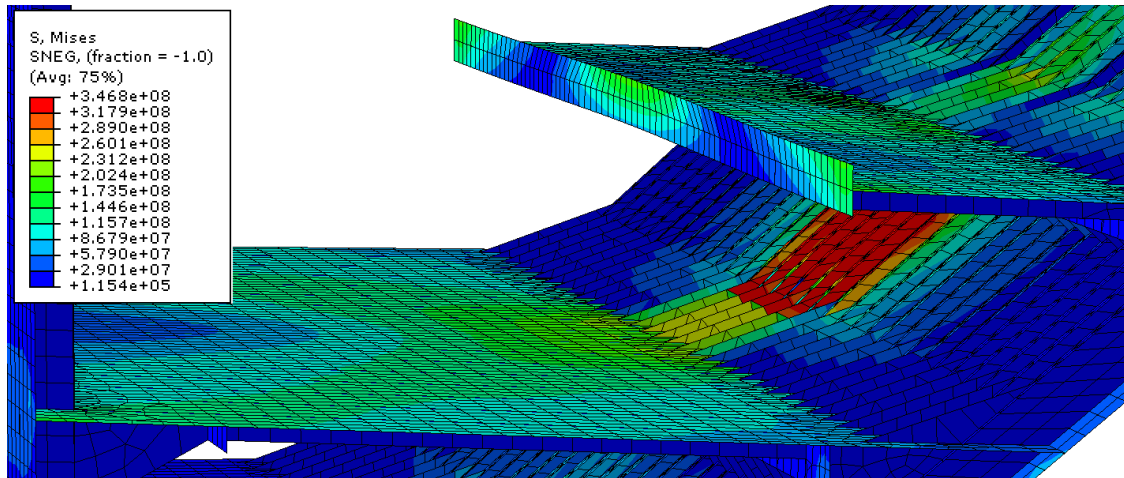
(b) Pressure 6 MPa.
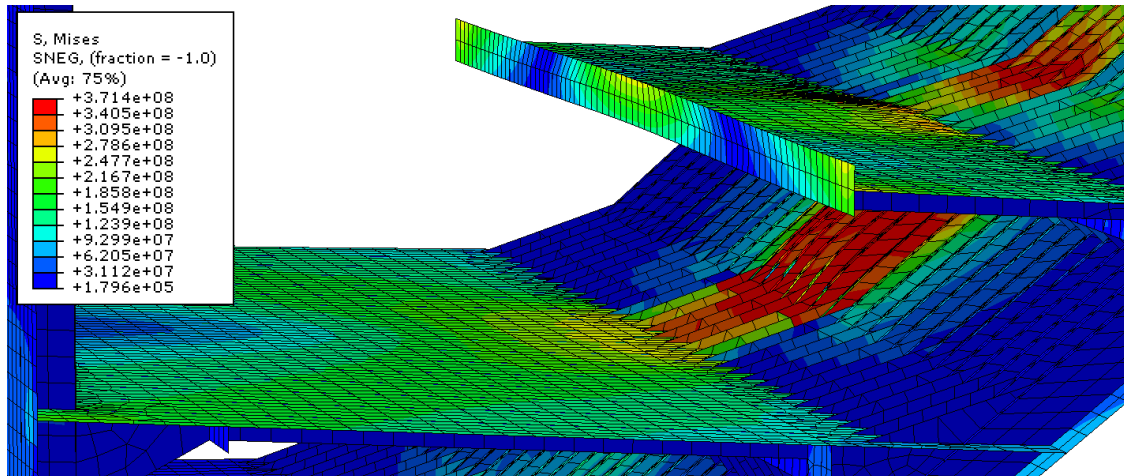
(c) Pressure 8 MPa.

Figure D.4: Stress distribution for modified deck design.

D.3 Capacity Analysis

Table D.2: Results from capacity analysis on sloped side.

Pressure	Mpa	2.5	5.0	7.5	10.0	12.5	15.0
Max deflection in plate	mm	1.59	3.181	4.774	6.367	8.269	11.24
Max stress	Mpa	86.9	174.3	262.3	345.0	345.3	346.3
Max stress in plate	MPa	86.9	174.3	262.3	345.0	345.1	345.2
Max stress in stiffener	MPa	85.2	170.5	255.8	341.0	345.3	346.6

Pressure	Mpa	17.5	20.0	22.5	25.0	27.5	28.8
Max deflection in plate	mm	15.81	24.18	38.45	52.85	64.65	73.71
Max stress	Mpa	347.7	356.9	377.3	396.6	420.6	470.0
Max stress in plate	MPa	346.1	347.9	356.0	376.4	391.4	398.7
Max stress in stiffener	MPa	347.8	356.9	380.1	396.6	420.6	470.0

Table D.3: Results from capacity analysis on vertical side.

Pressure	Mpa	2.5	5.0	7.5	10.0	12.5	15.0
Max deflection in plate	mm	0.786	1.573	2.360	3.147	3.935	4.957
Max stress	Mpa	67.2	135.4	203.2	270.9	338.9	345.3
Max stress in plate	MPa	65.6	131.4	197.6	264.0	330.6	345.1
Max stress in stiffener	MPa	67.2	135.4	203.2	270.9	338.9	345.3

Pressure	Mpa	17.5	20.0	22.5	25.0	27.5	30.0
Max deflection in plate	mm	6.752	10.53	17.42	29.32	47.43	57.40
Max stress	Mpa	346.0	347.3	352.9	369.3	393.8	409.3
Max stress in plate	MPa	345.2	345.8	347.5	363.8	393.8	409.3
Max stress in stiffener	MPa	346.0	347.3	352.9	369.3	385.2	391.8

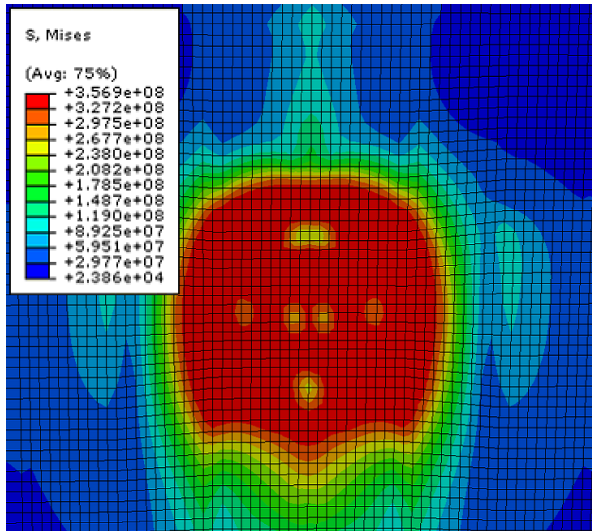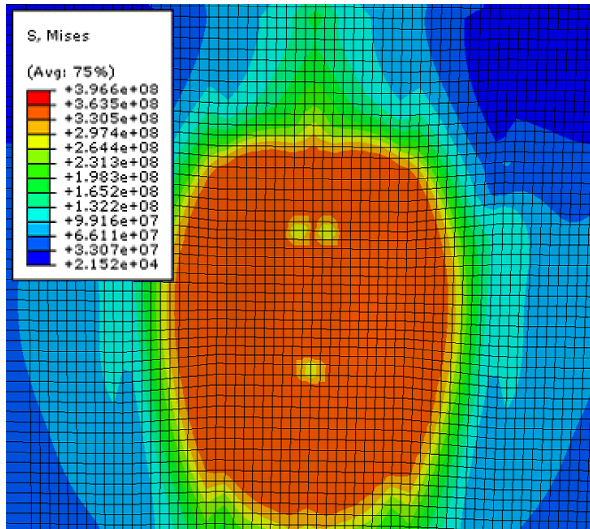| Pressure	Mpa	32.5	35.0	37.5	40.0	42.5	45.0
Max deflection in plate	mm	65.37	73.89	83.17	92.89	103.07	115.10
Max stress	Mpa	417.9	425.9	433.0	439.8	455.0	470.0
Max stress in plate	MPa	417.9	425.9	433.0	439.8	455.0	470.0
Max stress in stiffener	MPa	398.8	404.8	411.6	417.7	423.7	429.9
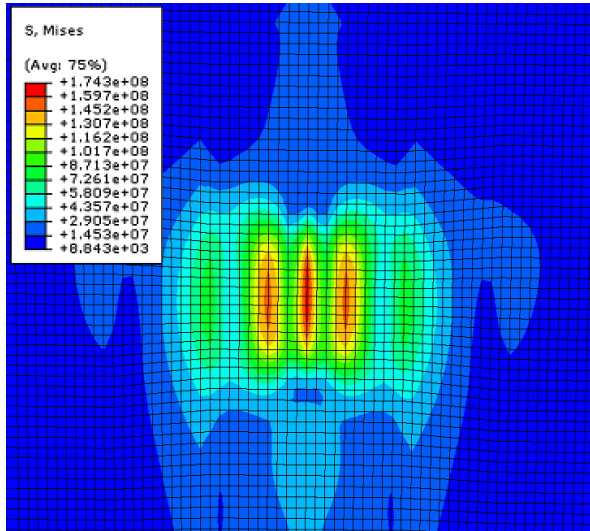
(a) 5 MPa pressure.
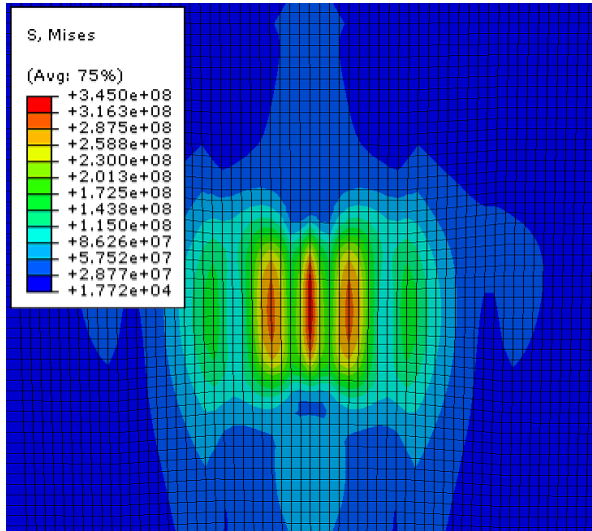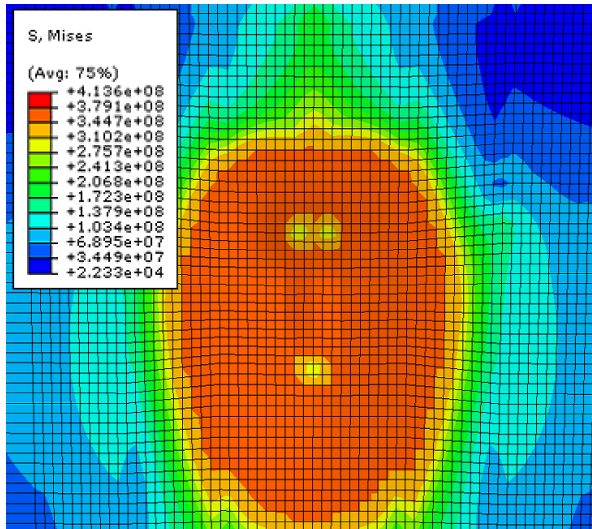
(b) 10 MPa pressure.
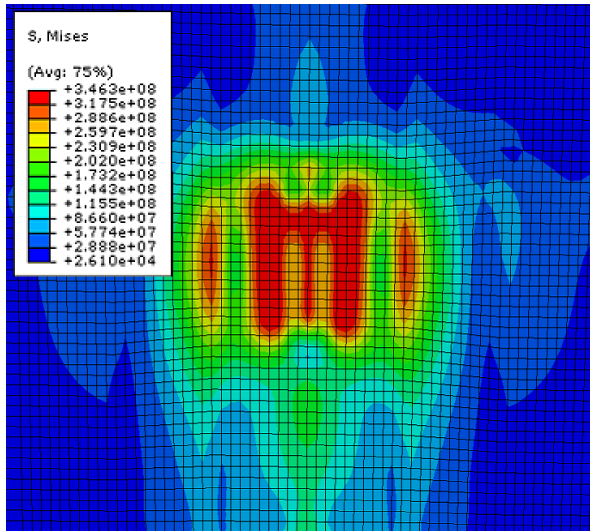
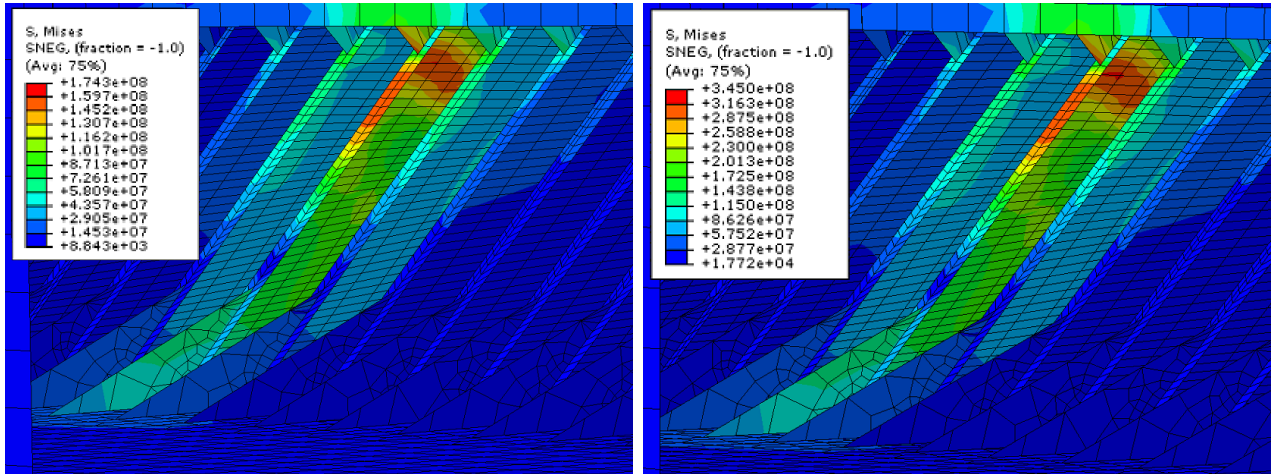(c) 15 MPa pressure.

(d) 20 MPa pressure.
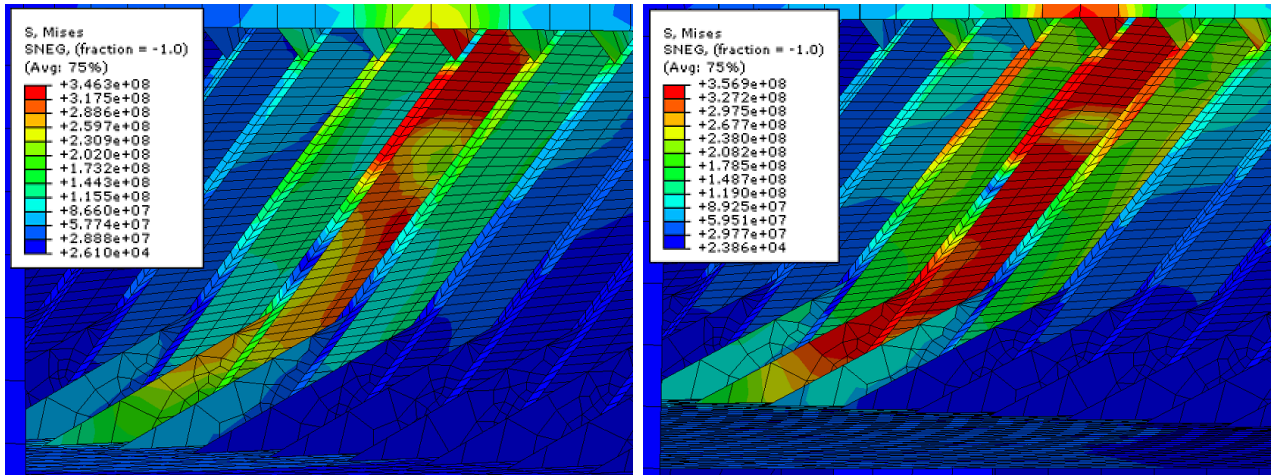
(e) 25 MPa pressure.

(f) 28.8 MPa pressure.

Figure D.5: Stress distribution in outer plate at point A.
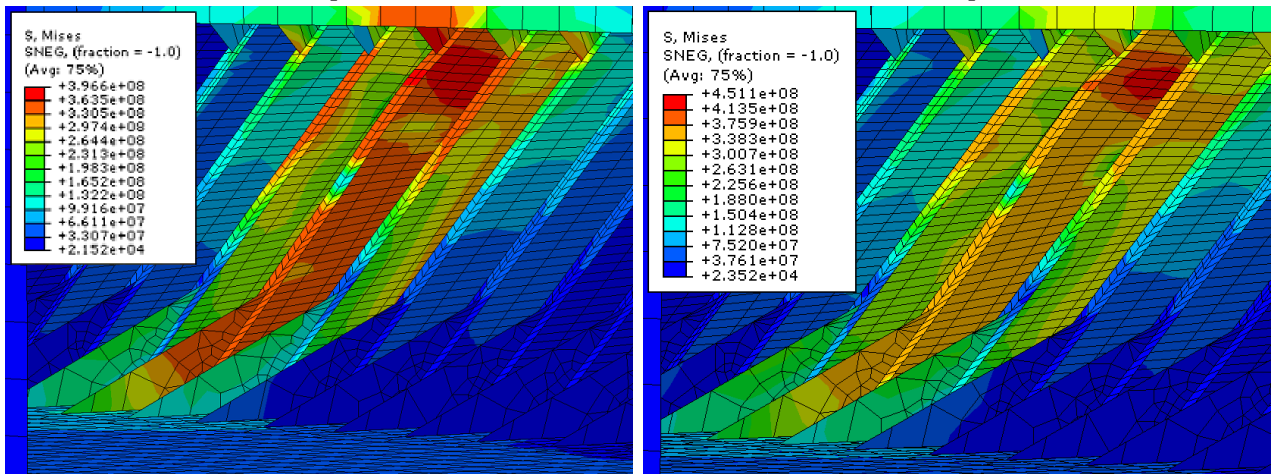
(a) 5 MPa pressure.

(b) 10 MPa pressure.

(c) 15 MPa pressure.

(d) 20 MPa pressure.

(e) 25.0 MPa pressure.

(f) 28.8 MPa pressure.

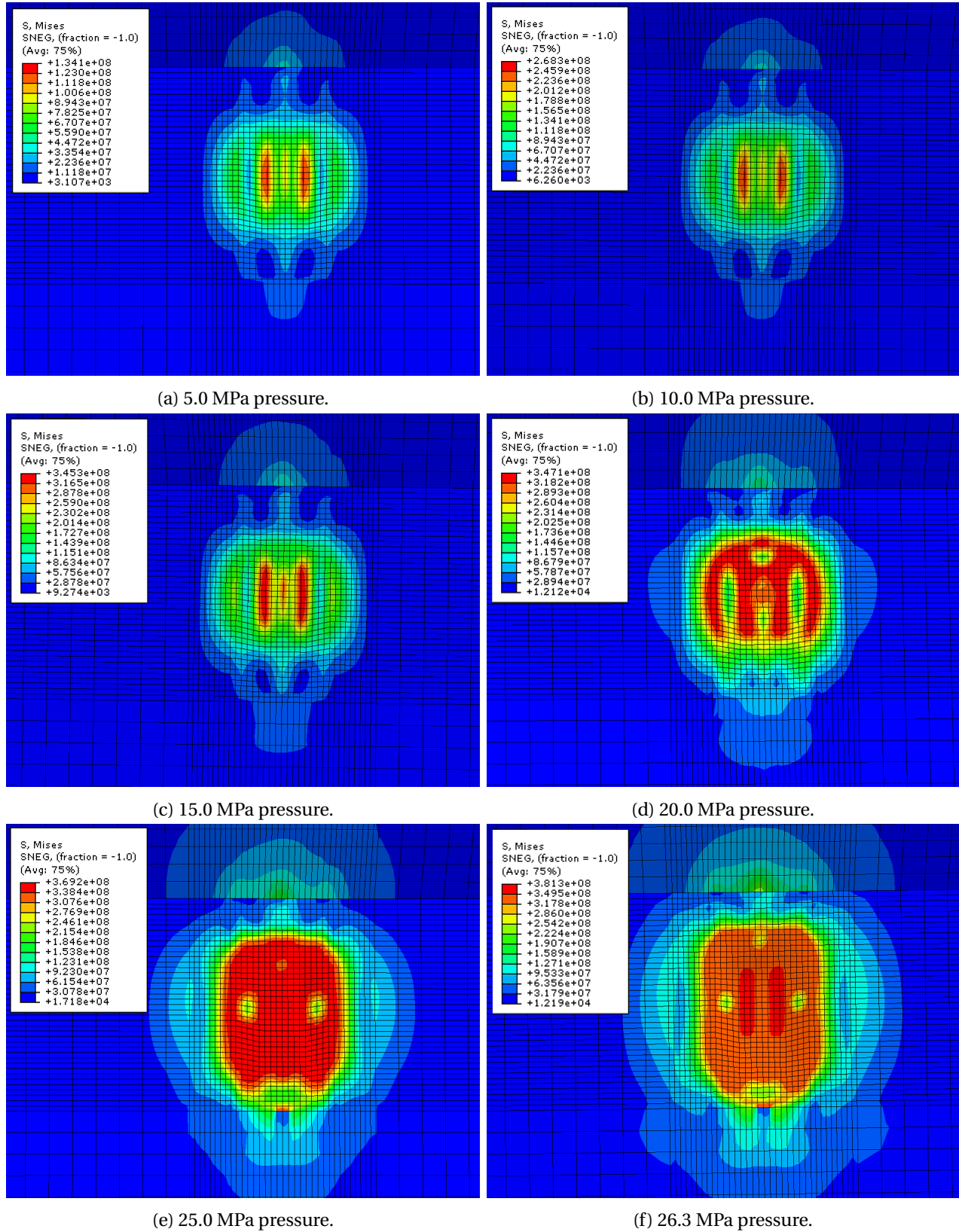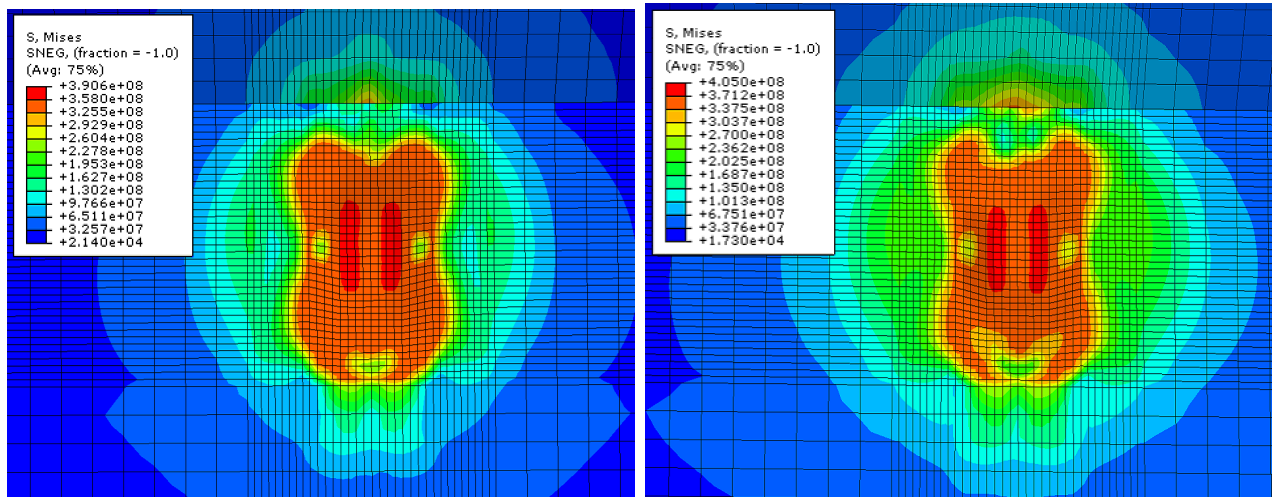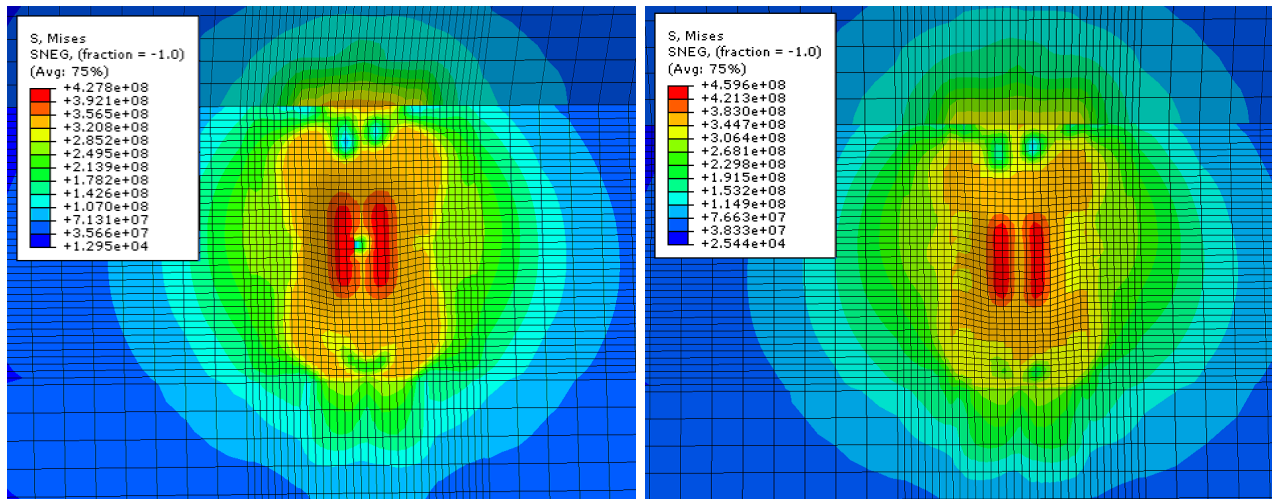Figure D.6: Stress distribution in stiffeners at point A.

(a) 5.0 MPa pressure.

(b) 10.0 MPa pressure.

(c) 15.0 MPa pressure.

(d) 20.0 MPa pressure.

(e) 25.0 MPa pressure.

(f) 26.3 MPa pressure.

Figure D.7: Stress distribution in outer plate at point B (applied pressure ranging from 5-25 MPa).

(a) 30.0 MPa pressure.

(b) 35.0 MPa pressure.

(c) 40.0 MPa pressure.

(d) 45.0 MPa pressure.

Figure D.8: Stress distribution in outer plate at point B (applied pressure ranging from 30-45 MPa).
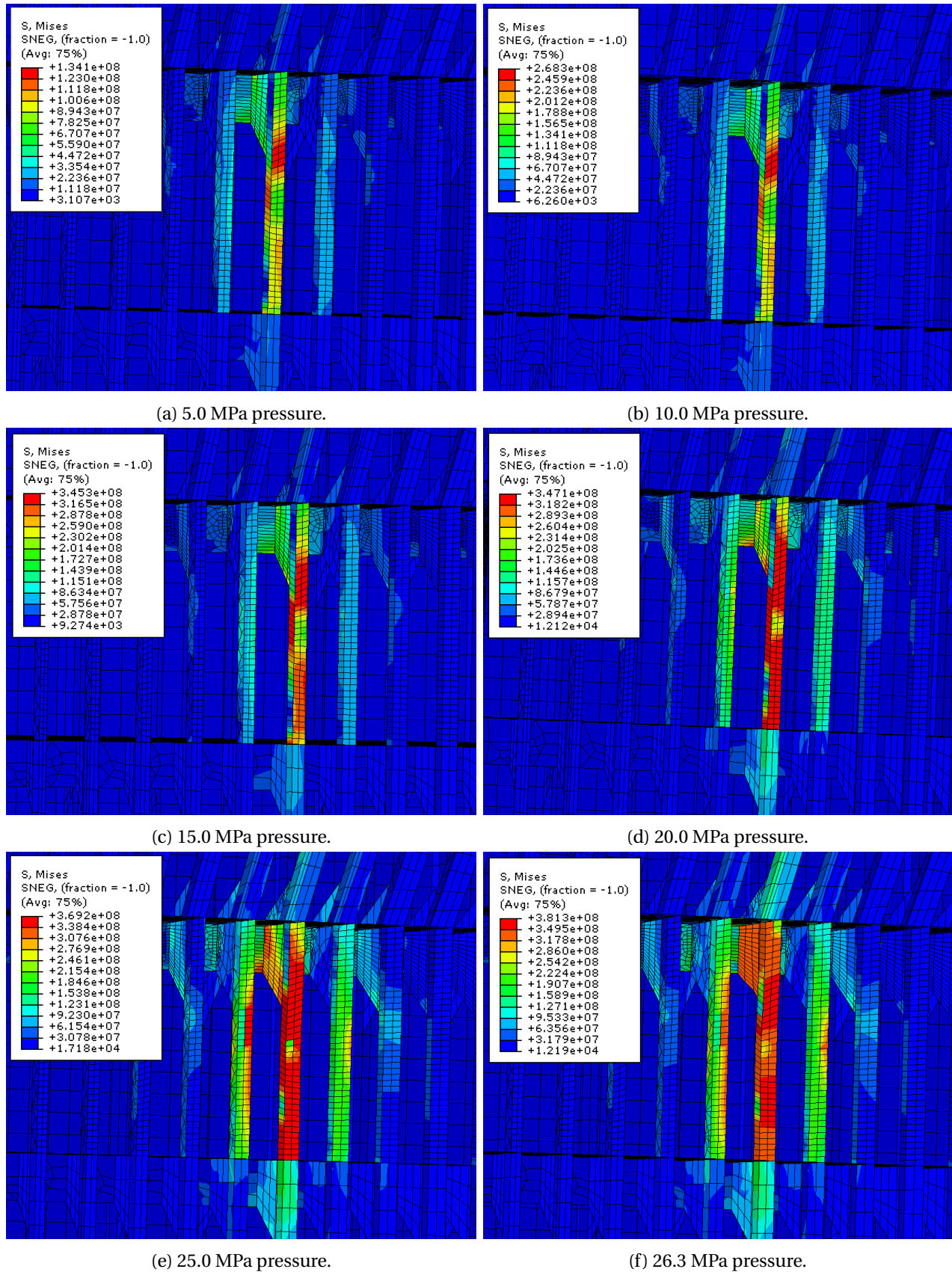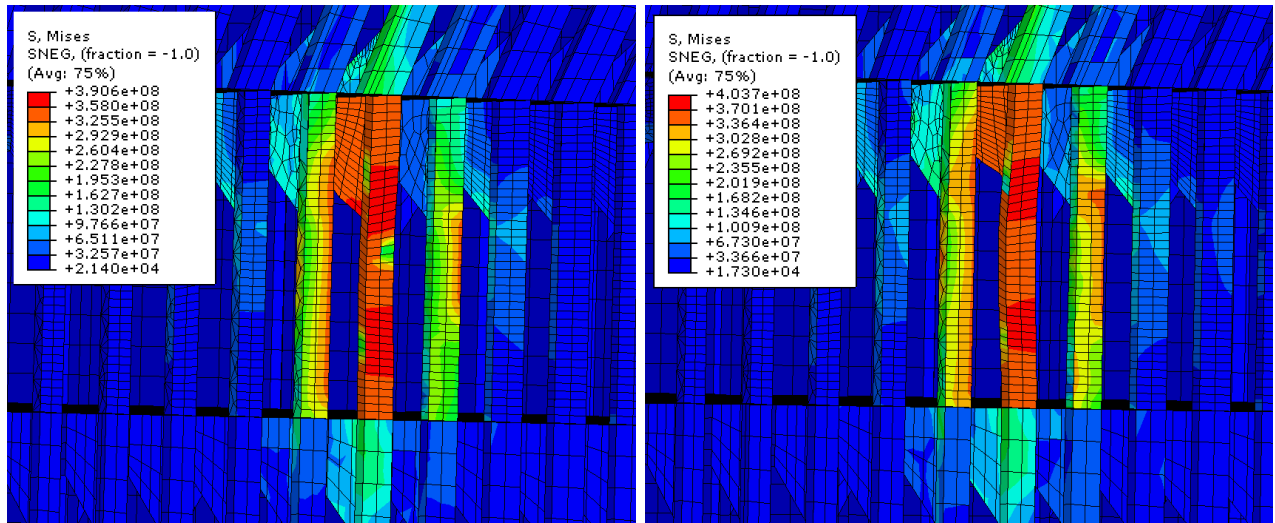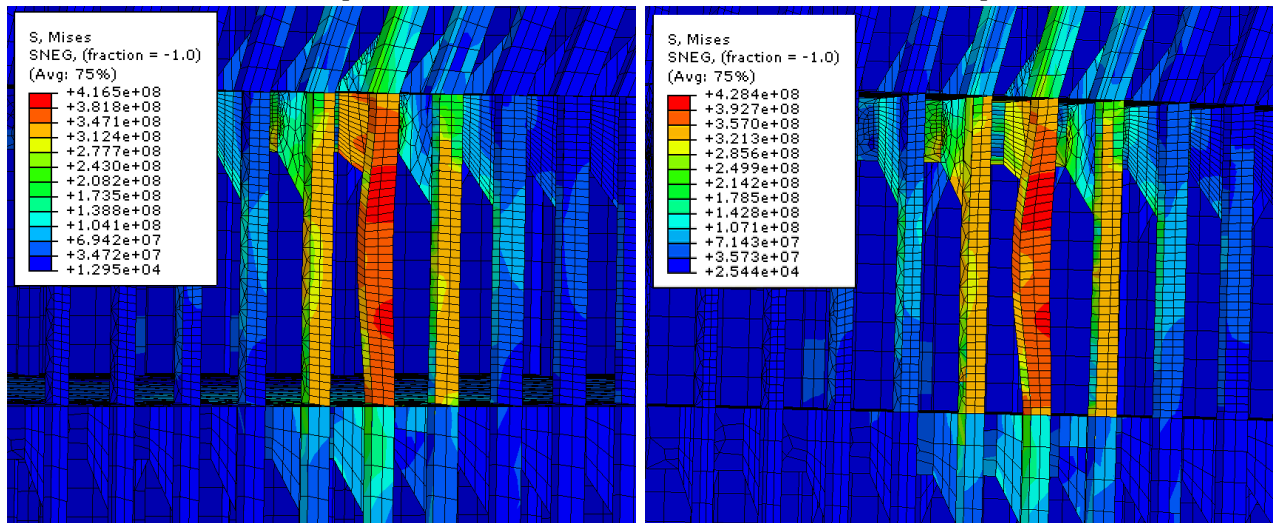
(a) 5.0 MPa pressure.

(b) 10.0 MPa pressure.

(c) 15.0 MPa pressure.

(d) 20.0 MPa pressure.

(e) 25.0 MPa pressure.

(f) 26.3 MPa pressure.

Figure D.9: Stress distribution in stiffeners. Capacity analysis at point B (applied pressure ranging from 5-25 MPa).

(a) 30.0 MPa pressure.

(b) 35.0 MPa pressure.

(c) 40.0 MPa pressure.

(d) 45.0 MPa pressure.

Figure D.10: Stress distribution in stiffeners. Capacity analysis at point B (applied pressure ranging from 30-45 MPa).
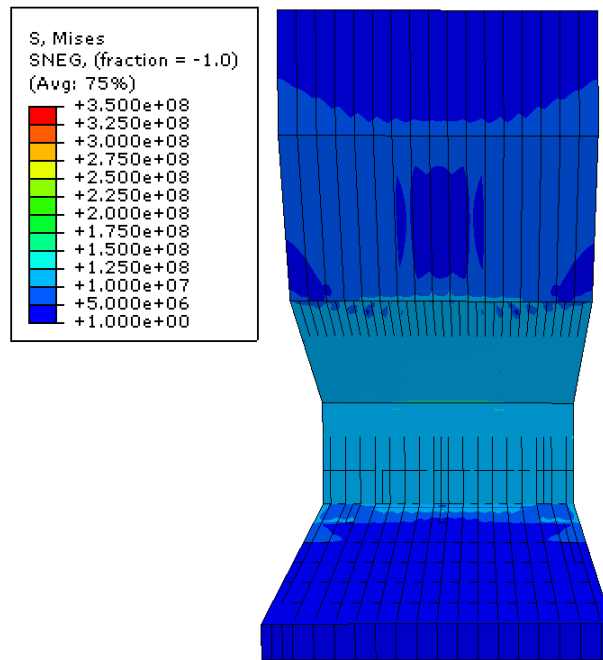
D.4   Pressure-Area Dependent Loading

Figure D.11: Stress distribution for local model at pressure 1.48 MPa applied over load area of $58.60\,\mathrm{m}^2$.
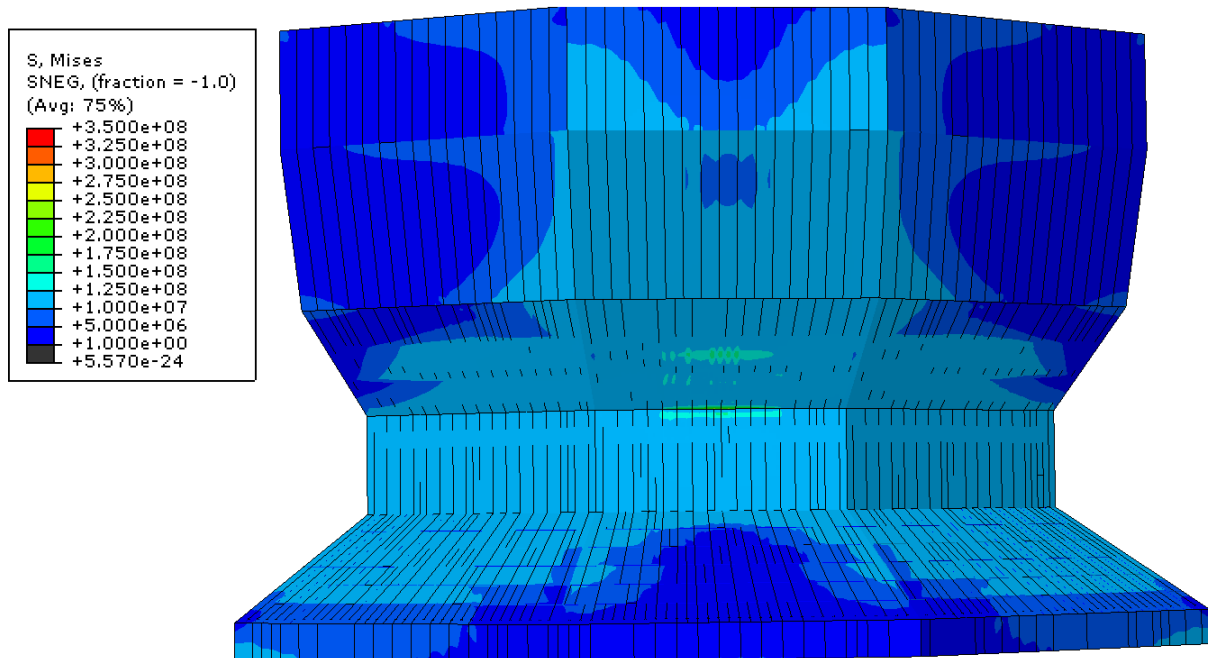

Figure D.12: Stress distribution for global model at pressure 1.48 MPa applied over load area of $58.60\,\mathrm{m}^2$.

Table D.4: Results from analysis with pressure-area dependent loading using local model.

Area	m2	0.33	0.67	1.16	2.50	5.85
Pressure	MPa	16.08	9.79	6.67	3.90	2.15
Normal force	MN	5.31	6.56	7.74	9.74	12.57
Horizontal force	MN	3.81	4.64	5.52	6.90	8.93
Max stress stiffener	MPa	345.1	345.1	345.5	341.6	213.1
Max stress plate	MPa	345.1	244.3	199.4	151.9	112.3
Max deflection plate	mm	11.34	9.84	11.85	10.59	9.56

Area	m2	12.35	24.42	35.06	58.60
Pressure	MPa	1.48	1.48	1.48	1.48
Normal force	MN	18.28	36.14	51.89	86.73
Horizontal force	MN	12.98	25.66	40.12	68.13
Max stress stiffener	MPa	209.1	267.2	269.6	271.2
Max stress plate	MPa	104.4	150.6	180.4	215.7
Max deflection plate	mm	10.87	14.11	15.47	17.70

Table D.5: Results from analysis with pressure-area dependent loading using global model.

Area	m2	24.42	35.06	58.60
Pressure	MPa	1.48	1.48	1.48
Normal force	MN	36.14	51.89	86.73
Horizontal force	MN	25.66	40.12	68.13
Max stress stiffener	MPa	262.4	284.8	345.1
Max stress plate	MPa	160.1	201.0	255.1
Max deflection plate	mm	18.53	21.18	29.73

(a) A-1: 0.33 m^2

(b) A-2: 0.67 m^2

(c) A-3: 1.13 m^2

(d) A-4: 2.50 m^2

(e) A-5: 5.85 m^2

(f) A-6: 12.35 m^2

(g) A-7: 24.42 m^2
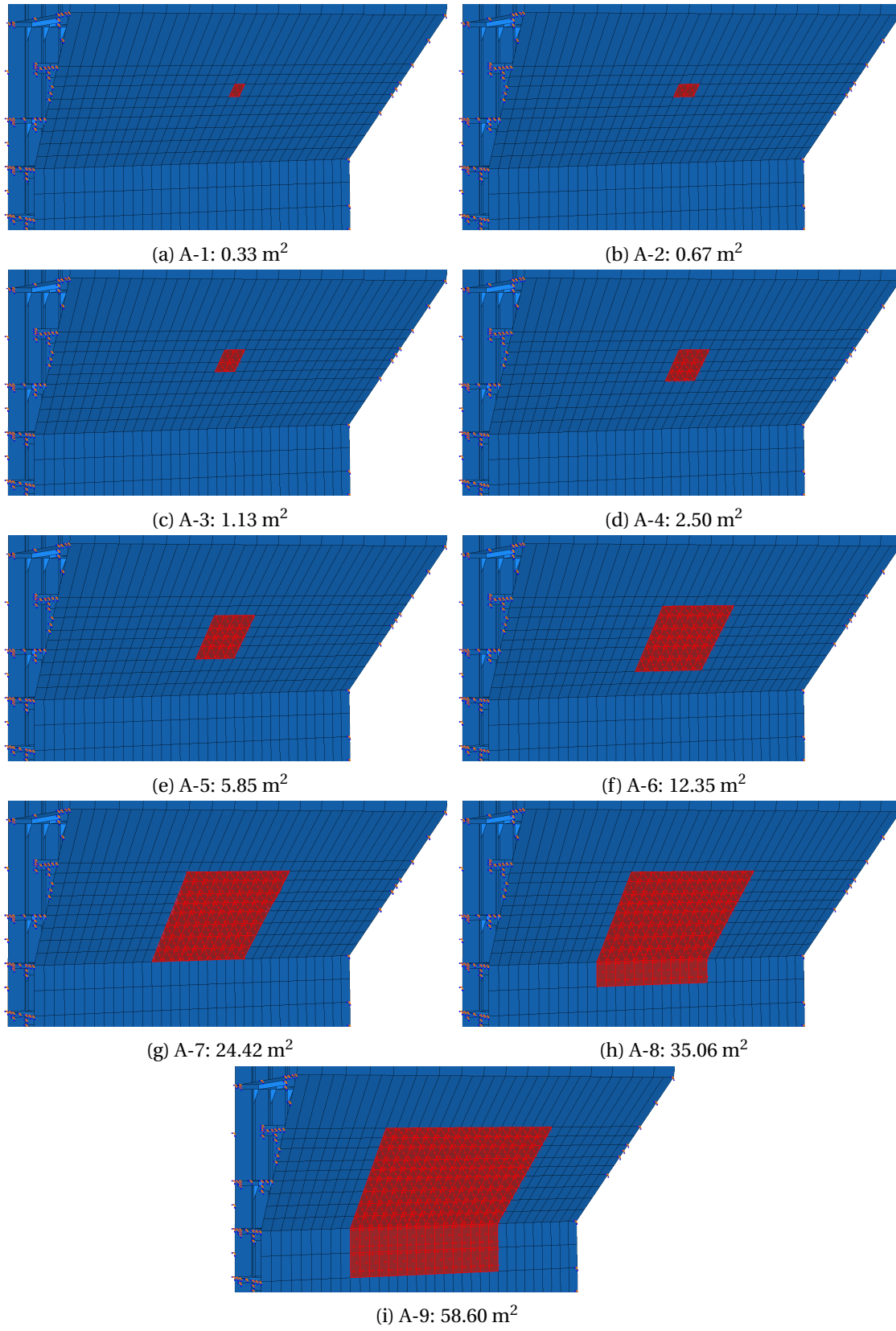
(h) A-8: 35.06 m^2

(i) A-9: 58.60 m^2

Figure D.13: Load patch areas used in analysis with pressure-area dependent loading.